Applications of Surface Acoustic Waves (SAW) for Chemical and Biological Analysis

by

Kumudesh Sritharan

The University of Augsburg

Experimental Physics 1

Augsburg, Germany

D-86159

Referees:

Prof. Dr. Achim Wixforth (Thesis Advisor and Reviewer)

Prof. Dr. Stefan W Schneider (Thesis Reviewer)

Priv. Doz. Dr. Igor Goychuk

Prof. Dr. Wolfgang Brutting

Date of Oral Exam: July 11th 2008

Abstract

The objective of the proposed thesis is to demonstrate the use of surface acoustic wave (SAW) for a chip based microfluidic system. We utilize this unique SAW chip as a nano-pump to move and mix small volumes of liquids in two dimensional and three dimensional channel geometries for both biological and chemical applications. For instance this technique enables us to analyze the complex interplay of the biochemical and physical properties of cells, proteins and chemicals in blood flow conditions. First of all the surface acoustic waves (SAW) are generated using a piezoelectric substrate where metal transducers are deposited to induce an oscillatory deformation on the chip surface. The SAW which is generated hits the solid liquid interface resulting in an acoustic streaming of the liquid. The result is the observation that the SAW can be used to enhance the mixing of parallel fluid streams on a 3-dimensional microchannel which help alleviate the mixing constraints in microfluidic channels, thereby making it a faster process. In a similar study, a thermoresponsive polymer called pluronics was utilized as an electrically switchable valve for SAW driven microfluidic systems to create obstacles in channels to distort fluid flows and to indirectly induce mixing.

Next we utilize a novel SAW driven microfluidic flow chamber to study the physiological conditions of tumor cell adhesion within our blood vessel. Initially, the SAW driven microfluidic flow chamber was successfully utilized to study the mechanical properties of protein stretching in our blood stream. A large glycoprotein complex known as von-Willebrand Factor (VWF) which is involved in triggering the blood clotting cascade was used to demonstrate that upon a critical shear rate ($\geq$1000 s^{-1}) results in conformational changes to VWF increasing its function as an adhesive protein. Although this mechanism is well known to bind platelets, the shear dependent conformational changes to VWF can also promote melanoma cell adhesion is studied using the SAW driven microfluid flow chamber. To develop a more realistic model of our blood vessel,

we were able to develop a cell assay to show VWF secretion from a cultured endothelial cell layer enabling melanoma cell adhesion under hydrodynamic flow. The micropipette aspiration technique is employed to quantify tumor cell adhesion to VWF conformations. The velocity and size measurements of particles (cells, proteins, DNA) were optimized by incorporating a Fourier analysis detection method to the SAW driven microlfuidic chip.

In my thesis, I discuss the successful employment of SAW as unique micromixer and biochip. The size and flexibility of the SAW chip enables us analyze biological and chemical materials in fluids at the microliter and nanoliter scales as well as to tackle complex issues of microfluidics.

Table of contents

Chapter 1

1.1 Introduction

The concept of microfluidics emerged in the 1990's as a way to analyze small volumes of liquids ranging from micrometer to nanometer scales. In order to analyze these small volumes of liquids, a flow has to be generated by micropumping mechanisms to circulate liquids on an artificially constructed channel of various geometries which can then be molded or etched onto a so-called microchip. The size of the channels can be modified to optimize mass transport and thermal transport. The microchips have a size of 2-3 cm square and are typically made of materials such as silicon, glass, quarz or piezoelectric (40). Specific pumping techniques such as electoosmotic or electrokinetic methods have been employed as well as micromixers to mix and move volumes of liquids (14). The advantage of these microsystems is to consolidate a laboratory onto a chip. For example in a chemical or biological lab, the mixing of chemicals which is traditionally done by a chemist or biologist involves pouring two separate chemicals onto a beaker where the mixing by stirring would result in a chemical reaction. However, by using a biochip it would not only reduce the reaction time, so less sample volume is needed but there would be an increased performance of the system.

Recently, surface acoustic waves (SAW) have been employed to move droplets on chemically modified or functionalized piezoelectric substrate. The surface acoustic waves are generated by employing ultrasonic sound waves which are propagated to the surface of the piezoelectric substrate to move water droplets (58). This occurs by exciting the interdigital transducers (IDT's) which are deposited onto the piezoelectric substrate, by applying a certain high frequency voltage to excite the sound waves. The design of the IDT's is the key to the development of the SAW. The surface of the piezoelectric

substrate can be chemically modified to be hydrophobic, so to keep the form of the water droplet intact and can use SAW to manipulate one droplet towards another to induce mixing. This revolutionary discovery by Achim Wixforth and his colleagues have been implemented in the fields of microfluidics and lab on a chip technology. These findings led to the motivation for my thesis, which is to look further into the potential application of surface acoustic waves in microfluidics to pump and mix fluids.

1.2 Microfluidic Valves, Pumps and Mixers

To understand why SAW is such an innovative technique, especially as a pump and mixer for microfluidic systems, the recent developments of microfluidic devices such as valves, pumps and mixers will be discussed.

Valves

Initially, traditional biological and chemical techniques were miniaturized with the aid of microfluidics to enhance the analytical performance of the system. It was first introduced when miniaturizing high performance liquid chromatography (HPLC) where a certain analyte of a mixture to be examined was added to a planar tubular column, on a 5 x 5 mm silicon chip, containing chemical interactions within the stationary phase of the column to separate the components of the mixture as it traverses down the column by an external pump and valve. A detector was also added to the chip to detect the analytes separated (40). The flow rates are controlled by valves which are integrated into the silicon microchip, various passive and active micromixers have been fabricated for such applications. An active microvalve use external devices to control the actuation and it provides energy. An example of an active micromixer would be the use of hydrogels which can polymerize by changing pH or temperature. In microscale dimensions the gelling of the hydrogels can either be controlled by diffusion of the protons or heat convection of the stream layer to regulate the flow autonomously (5). In fig 1 shows a response of a hydrogel to changes in pH conditions as a check valve. Passive

micromixers limit the flow to one direction by using a temporary flow stop device. Passive one way valves can be constructed by silicon or elastomers to direct fluid flow.

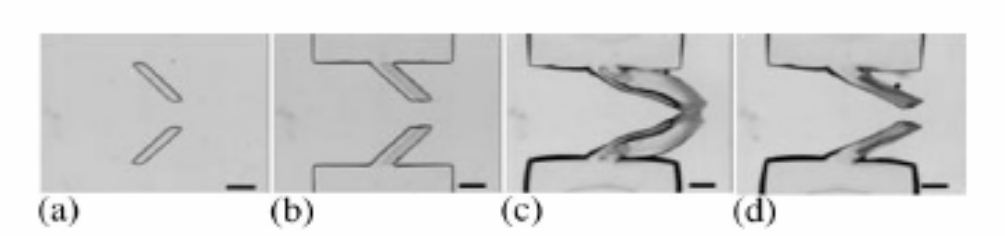

Fig. 1: Fabrication of the bio-mimetic hydrogel check valve. (a) The hydrogel strips are formed by changes to the pH levels. (b) Non-pH anchors are attached to the hydrogel strips for firm support. (c) When exposed to a basic solution the hydrogel strip starts to expand to form a closed valve. (d) As the solution is changed to an acidic environment there is a change in the structure of the valve and becomes deactivated, returning to the open state (D. Bebee et al 2002).

Pumps

Later, pressure driven flows were generated by syringe pumps enabling molecules to be transported in a fluid stream and distributed throughout the microchannel. These pumps required cumbersome micropump devices and special tubing to regulate the pressure (fig 2). However, a more convenient device is the electroosmotic pump, which generates the movement of liquids by applying an electric field. If the walls of a microchannel have an electric charge, as most surfaces do, an electric double layer of counter ions will form at the walls (21, 40). When an electric field is applied across the channel, the ions in the double layer move towards the electrode of opposite polarity. This creates motion of the fluid near the walls and transfers via viscous forces into convective motion of the bulk fluid (fig 3). The electroosmotic pump allows the fluid flow to be controlled by adjusting the voltage, but typically high voltages are needed. Also by adding specific protein or molecules to the walls of the microchannel can alter the fluid flow due to their charges (40).

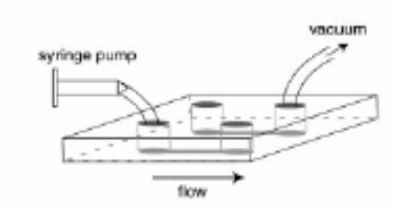

Fig. 2: A schematic representation of a pressure driven flow, here a syringe pump connected to a tube is incorporated to a PDMS microchannel with a vacuum outlet to direct the fluid flow (Sia, Whitesides 2003).

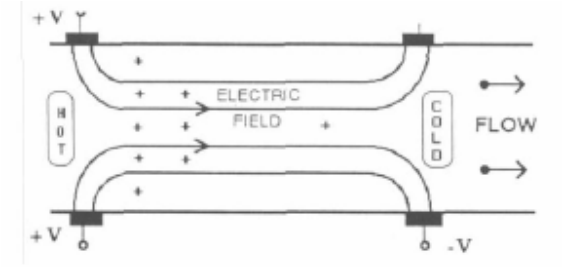

Fig. 3: A diagram of an electrokinetic flow, an applied electric field to the channel with a conducting fluid layer to control the fluid flow. The fluids are pump driven by coulomb forces top and the traveling wave of the potential (P Gravesen et al 1993).

This technique was further utilized for applications such as miniaturizing electrophoresis on planar chips. Electrophoresis enables the separation of amino acids or proteins according to its molecular weight by implementing electrosomotic pumping to regulate flow with interconnected channels in silicon substrates. This allowed the separation of amino acids to occur in less than 30 sec with a plate height of 0.3 µm (40), while conventional gel electrophoresis chamber with a height 100 mm and width of 75 mm took approximately 2 hours. This led to the evolution of the lab on a chip technology where a minituarized PCR chip was developed to amplify DNA. SAW was utilized for this application as a pump to move a droplet of DNA covered in mineral oil (to prevent dehydration) on a SAW chip with integrated heating devices. The SAW PCR lab chip was able to manipulate and mix the droplet of DNA from one heating device toward another with varying temperatures to regulate the denaturing of DNA, annealing with

primers and elongation steps which are necessary to amplify the gene of interest. A microarray with labeled oligonuleotides was used to detect the gene of interest by epi-flourescence microscopy (22).

Micromixers

In conjunction with micropumps are micromixers, these are essential for various applications especially in the field of biology and chemistry. The basic concept of mixing involves diffusion, which is the distribution of particles or molecules to minimize a concentration gradient in an aqueous solution. The laws of Brownian motion states that there is a random movement of particles in a solution (37). In another words spherical beads in a water solution are subjected to forces which pushes it to the left and right creating an imbalance causing a random motion. In order to determine the distance a bead diffuses (x) depends upon the diffusion time t and the diffusion constant D of the bead.

$$<X^2> = 6Dt \qquad (1.1)$$

The diffusion constant of a Brownian sphere is a function of its radius R, and the Boltzmann constant and the temperature T, and the viscosity η of the surrounding medium.

$$D=\frac{K_b T}{6\pi\eta R} \qquad (1.2)$$

diffusion length (μm)	potassium ion (0.2nm)	Oligonucleotide (6nm)	PCR product (100nm)
1	0.2 ms	6 ms	100 ms
10	20 ms	600 ms	10 s
100	2 s	60 s	20 min
1000	200 s	100 min	30 h

A table summarizing the time a particle diffuses of different sizes, the diffusion length of the molecules such as a potassium ion (0.2 nm), oligonucleotide (6 nm) and a PCR product (100 nm) is measured (courtsesy A Wixforth).

In macroscopic scales, mixing of particles flowing along its path can occur by turbulence. Turbulence is a random variation in fluid flow causing a dispersion of the molecules. In microscopic scales to create turbulence can be a daunting task, therefore micromixers specifically designed to cause disturbances or alterations to fluid flow are incorporated into these microchips. There are two categories of micromixing methods employed to induce a more rapid mixing in microfluidic systems either by passive or active mixing. Passive mixing relies on diffusion by creating obstacles to multiple fluid streams to fold the liquid layers to enhance diffusion in a defined area of the channel. Some designs have included parallel lamination micromixers, where a basic design of a microchannel with a geometry consisting of a T shaped mixer (4a) and a Y shaped mixer (fig 4b) were introduced. The T-mixer depended on molecular diffusion, where a long mixing channel is needed. Typically two fluids of similar viscosities would be inserted into two seperate inlets and would merge into a central channel where they run in a parallel laminar flow and eventually diffuse into one stream at the end of the channel (37). A simpler method was to narrow the mixing channel realizing that parallel laminar flows are a result of

multiple streams which narrows the diffusive path of the particles (fig 4c), another method used a parallel laminar mixer with 32 multiple streams.

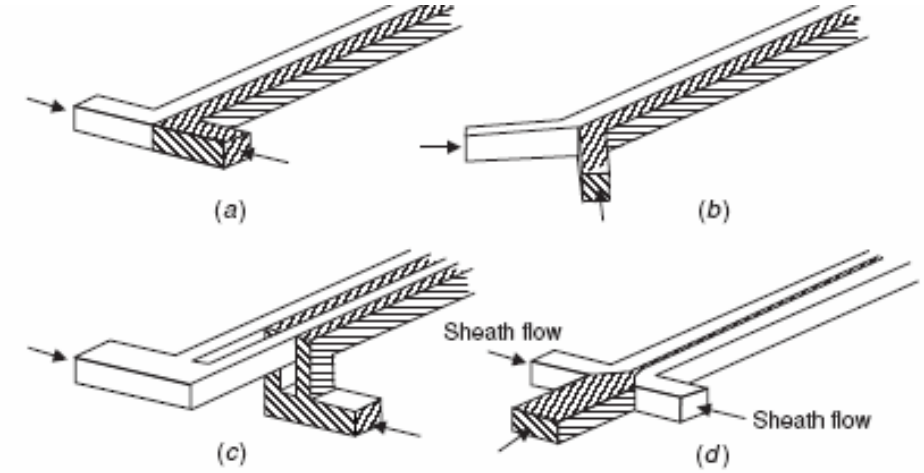

Fig 4: A cartoon of the different models of the parallel lamination micromixer: (*a*) the basic T-mixer and (*b*) Y-mixer, (*c*) the concept of parallel lamination and (*d*) the concept of hydraulic focusing (N. Nuygen, Z Wu 2005).

Hydrodynamic focusing was also introduced to reduce the mixing path (fig 4d). This technique employed 3 inlets, the middle inlet is for the sample flow and the outer two inlets were for the solvent flow which acts as a sheath flow. The hydrodynamic focusing reduces the stream width and eventually the mixing path. The sample fluid is focused onto a narrow width by adjusting the pressure ratio of the sample flow and the sheath flow which reduces the mixing time (30, 37).

Active micromixers utilize externally driven pumps to achieve dynamic mixing. Some examples of active micromixers such as SAW, electoosmotic and electrokinetic generated flow have already been mentioned, other mixers such as electrohydrodynamic mixing, magneto hydrodynamic mixing and thermal disturbances has also been successfully employed. Electrohydrodynamic mixing implemented two platinum wires which were placed perpendicular to the mixing channel and by changing the voltage and frequency mixing was induced. The magneto hydrodynamic disturbance requires an external magnetic field applied DC voltages on the electrodes to induce a mixing

movement in the chamber (37, 49) and thermal disturbances uses heating devices to regulate temperature causing thermal energy to enhance mixing of the fluid layers.

1.3 Physics of Microfluidics

When analyzing fluid flow whether it be turbulent or laminar is indicated by the Reynolds number. The Reynolds number typically range at most several hundred in microfluidic systems in which fluid flow is generated in smaller scales (*diameter of channel ~10^{-4} m* and smaller). However Reynolds numbers exceeding 2300 will result in turbulent flow. It (Re) is defined by the equation,

$$\mathrm{Re} = \frac{\rho \bullet \upsilon \bullet d}{\eta} \qquad (1.3)$$

where the flow speed υ as a function of density ρ and fluid viscosity η, the Reynolds number Re is defined as the ratio, d is the characteristic length of the system. For instance when there is a flow of water over a sphere, at low speeds the flow is laminar but when the speed increases it results in an unsteady flow resulting in turbulence (5, 21, 49). Typically in microfluidic systems the fluid flow is usually laminar due to the low surface to volume ratio where the frictional forces supercedes the inertial forces There are two governing concepts in microfluidics used for the analysis of fluid flow; which are the mass conservation (continuity equation) and the momentum equation (Navier-Stokes equation). The mass conservation law states for any control volumes or fixed volumes the mass entering per unit time=mass leaving per unit time + increase of mass in the control volume, for steady or laminar flow is mass entering per unit time=mass leaving per unit time. Fluids are considered continuum materials, properties of a fluid such as pressure, density and velocity are continuous from one point to another rather than discrete molecules. There are also internal forces acting on the fluids creating fluid stresses σ (forces/per unit area) in addition to the externally applied body forces which are factored into an equation. This is described by the complete Navier-Stokes equation,

which is derived by the principles of mass, energy and momentum. The velocity field for a Newtonian fluid obeys the Navier-Stokes equation which represents the continuum version of F=ma on a per unit volume basis:

$$\rho(\partial u/\partial t + u \bullet \nabla u) = -\nabla p + \eta \nabla^2 u + f \qquad (1.4)$$

The inertial acceleration terms appear on the left and the terms for viscous forces on the right. When the inertial forces are small compared to the viscous forces, which usually occurs in microfluidic scales, the nonlinear term can be neglected leaving the Stokes formula (49).

$$-\nabla p + \eta \nabla^2 u + f \qquad (1.5)$$

1.4 The Surface Acoustic Waves

The application of surface acoustic wave technology in microfluidics has been an important tool. It was originally discovered by Lord Rayleigh in 1880, who observed when there is an earthquake there is a surface wave and the ground begins to roll. As a consequence, wave forms consisting of transverse and longitudinal waves are found in solids. A particle in a solid under Rayleigh waves can move in an elliptical path along the surface without much of the energy being dissipated into the air due to the boundary conditions of the earth's surface. These principles have been applied to the development of surface acoustic waves using a piezoelectric substrate coupled to interdigital transducers and rapid changes in the electric field can generate ultrasonic waves similar to Rayleigh waves.

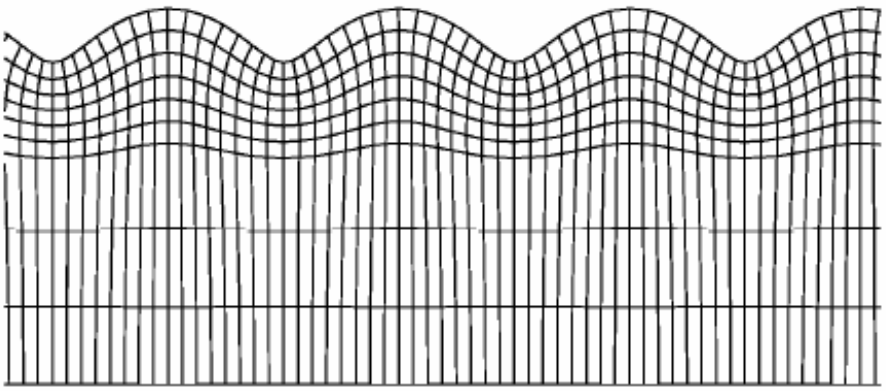

Fig. 5: A sketch of a Rayleigh wave propagating on a piezoelectric substrate. The Rayleigh waves move particles in an elliptical motion along the surface. The typical wavelengths are in the micrometer range and the amplitude is less than a nanometer (C Wurtsel 2006).

1.5 Background on the Stress of Solids

To understand the properties of the piezoelectric substrate and how it can generate waves, the background on the elasticity of solids will be discussed. When a solid is subjected to force there is a change in the properties of the solid, the atoms begin to change their orientation resulting in a deformation. This depends on the stiffness of the solid using the principles of Hookes law.

In a 3-D solid object, this concept in which force and deformation results in displacement of the object from its original equilibrium is extended. This analysis will be simplified by assuming that the material is homogenous and isotrophic. The body forces which act on all volume elements of the material (such as gravity and inertia) will be ignored. The type of forces to consider are called surface forces, these are units of forces per unit area and is viewed as acting on a surface element of the object. In order to describe the deformation of an object by forces, the gradient of the displacement is introduced (33).

$$\left(\nabla \vec{u}\right)_{ij} = \frac{\partial u_i}{\partial x_j} \qquad (1.6)$$

Where i is the component of the displacement, and j is the spatial coordinate. Therefore the rigid body of a solid undergoes a displacement which is the sum of the displacement gradient and its transpose called a strain tensor.

$$S_{ij} = \frac{1}{2}\left[(\nabla \vec{u})_{ij} + (\nabla \vec{u})_{ji}\right] = \frac{1}{2}\left(\frac{\partial u_i}{\partial x_j}\right) + \left(\frac{\partial u_j}{\partial x_i}\right) \qquad (1.7)$$

A strain is defined as the change in length per unit length in the solid equilibrium. The diagonal strain term S_{ij} represent the axial strain, while the off diagonal terms, S_{ij} with i=j are shear strains. An application of force results in a strain to a unit volume dV of a solid. The forces which give rise to the deformation and act on a unit volume element dV can be represented as

$$dF_i = f_i dV = \sum \frac{\partial T_{ij}}{\partial x_j} dV = \sum T_{ij} ds_j \qquad (1.8)$$

Where f_i is the force density of the i^{th} component, T_{ij} is the stress tensor, S_j is the surface of the solid normal to the ith component of the force per area acting on the jth face of an infinitesimal volume element. Stress on any direction on the plane interior can be determined by the stress tensor (33).

Both the strain tensor S_{kl} and the stress tensor T_{ij} are made up of 3x3 matrices corresponding to the nine combinations available, an equation to relate these two components is called a constitutive equation. The form of the constitutive equation depends on whether the material is a fluid, purely elastic or viscoelastic. In a purely elastic deformation, the stress is independent only on the strain $S_{kl}=C_{ijkl}T_{ij}$. This equation is generalized to the 1D spring, but it accounts for the forces and deformation in all three directions. The quantity is the modulus tensor of elastic coefficients and is the equivalent of the spring constant k, used to describe the deformation of a spring. The four subscripts indicate the four sets of a 3-D coordinate system that is required for a general description

of the relation between the strain and stress tensors, and the stiffness coefficient C_{ijkl} has (3^4) 81 components. In most materials, the stress and strain tensors are symmetric and therefore each contains at most six independent components. Therefore, the modulus tensor for infinitesimal elastic deformation is also symmetrical and contains at most 36 independent components. By assuming a material to be completely isotrophic, it can be shown that the number of elastic coefficients can be reduced to two (33).

1.6 Piezoelectric Material

Usually in most solids there are no net dipole moments because the structural arrangements of the atoms have no charge differential. In the case of a piezoelectric material it can develop a net dipole moment when compressed. Therefore when a mechanical stress is applied to the piezoelectric material it will produce an electric field and the application of an electric field to the material will generate a change in the dimensions to the structure of the material known as the "piezoelectric effect". Both of these applications will result in a change in the distribution of the atoms and bonds. In order to generate surface acoustic waves a spatially periodic electric field was applied leading to a spatially periodic deformation in the material. This produces a mechanical wave at the sound velocity which depends on the property of the piezoelectric material. The sound velocity traveling through a material ($v=c/\rho^{1/2}$) has to be further extended to account for the electric field of the piezoelectric material and the boundary condition of the surface. The piezoelectric tensor (p_{ijkl}) is used to solve the equation for the wave propagation of such a material which results in a revised elastic tensor $c'_{ijkl}=c_{ijkl}\ (1+K^2_{ijkl})$ and K^2_{ijkl} is the measure of the piezoelectricity in the material. Since K^2_{ijkl} is always positive c'_{ijkl} is larger than c_{ijkl} therefore the material is stiffer and the sound velocity increases (52).

For our studies, lithium niobate ($LiNbO_3$) was selected with a (YZ-cut) with a wave propagating in the Z direction. The crystal is rotated 128° so that an electric field is aligned with the Y axis, the resulting deformation is a along the Z axis. The interdigital transducers (fig 6) which are deposited onto the piezoelectric crystal are aligned at a

certain distance to one another to excite and amplify the surface acoustic waves (fig 7)(59). The $LiNbO_3$ crystal is used as a resonator where the applied electric field across the YZ cut causes the free surface to move in a longitudinal and transverse wavelike motion. The frequency is calculated as follows:

$$f = v/\lambda \qquad (1.9)$$

Here v denotes the sound velocity of the $LibNO_3$ substrate, and the wavelength λ is identical to periodicity of the IDT. Typically SAW amplitudes are less than a nanometer in the direction normal to the surface.

Fig. 6:A schematic diagram illustrates the structure of the interdigital transducers. The two contact points are connected to a meshwork of alternating figers to excite the piezoelectric substrate (courtesy C Wurtsel 2006).

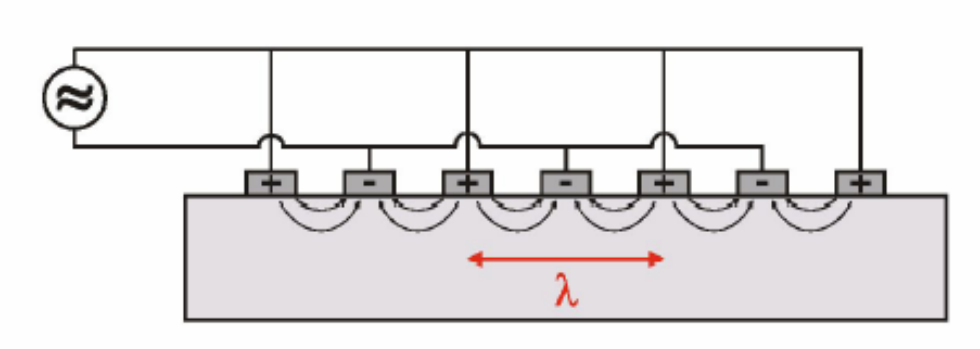

Fig. 7: The contact of the tranducers to an electric field results the elecltrodes to one electrode to another until an amplification of the waves causing SAW. The distance between the finger pairs of the transducers determines the excitation frequency to deform the piezoelectric crystal to generate SAW (C Wurtsel 2006).

1.7 Microfluidics for Biological Applications

The emergence of microfluidics has become a useful tool for biological applications and analysis, since most biological assays and biological procedures involve the motion of fluids. The pumps, micromixers and valves mentioned previously have been utilized for techniques such as immunoassays, PCR, electrophoresis, cell counting and cell sorting. The fabrication of microchannels can be molded using polymers such as PDMS (polydimethyl sulfoxide), other molecules such as self assembled monolayers (SAM) are typically used to functionalize substrates with certain chemical compounds to immobilize proteins, DNA or cells and nanostructuring of channels using PMMA (polymethyl methacrylate), a transparent thermoplastic, for photolithographic techniques (29, 36).

The main advantage in miniaturizing these biological assays is the capability to analyze single molecules such as proteins, DNA and eventually to single cells. In earlier studies, DNA has been an ideal molecule to be explored in a microscale level. Microfluidic techniques has been utilized to look at linear DNA specifically using restriction endonucleases, which are enzymes that cuts double stranded DNA (54). The fragments of DNA within the microfluidic channels can be functionalized with fluorescent proteins which bind to transcriptional factors or fluorescent hybridization probes to look at methylation sites. The analysis of the DNA stretched on a surface is determined by the size of the base pairs (bp) such as single base pairs (0.34nm) to binding sites for control

factors (20bp=6.8nm), to individual genes (1Kbp=0.34μm). To visualize the DNA fragment nanometer scale channels were fabricated with metallic slits perpendicular to the length of the channel which is aligned close to the light source to capture the size of these linear DNA. This technique uses lower amounts of DNA (50 femtograms) compared to the more traditional method of gel electrophoresis which uses higher amounts (5 or more nanograms). The natural advantage of this technique is useful for restriction mapping of plasmids (54). These techniques have enabled us to analyze how proteins can control DNA modifications, the genetic contents of DNA and the sizes of DNA fragments by using small volumes of analyte.

Another important technique which has been optimized using microfluidics is immunoassays. Immunoassays are used to detect the activity of enzymes, where in a microtiter plate an antibody or antigen is immobilized within the plate and a secondary antibody which is tagged with a fluorescent or chromogenic dye emits a signal which can be detected. However it can be a time consuming process, typically when an antibody or antigen is added to a well and hours are needed for the analyte to diffuse to the bottom of the plate and to bind. Recently, however micofluidic methods have been developed to optimize these conditions by shortening the reaction times and washing steps. One method employed is to construct microchannels made of PDMS which would minimize the diffusion distances and by replenishing the diffusion layer with molecules (47). A signal of the analyte to be detected could take a time interval of about 1 min to 6 min. Multivalent ligand binding studies have been performed by using a PDMS glass/microfluidic chip where channels have been constructed. Within these channels supported lipid vesicles with the incoporated ligand to be analyzed, the lipid compound 2,4 dinitrophenyl (DNP) were fused onto the glass surface to form a continuous lipid bilayer. A fluorescently labeled anti-DNP with pre-determined concentrations were injected into these microchannels and the surface bound antibodies were imaged using total internal reflection fluorescence microscopy (TIRFM) (28, 47).

Cell based assays has also been implemented using PDMS microchannels. One example was to use laminar flow to send gradients of molecules through the solution onto surface bound cells. In one set of studies, PDMS was constructed with 2 inlets and various staggered channels which were used as chaotic mixers to serially dilute the molecules which are connected to a main channel. A PDMS gradient generator was employed to study the effects of chemotaxis, therefore concentration gradients of interleukins ranging from 0 to 80ng was administered onto a neutrophil substrate at the main channel to monitor cell migration. The migratory characteristics of the neutrophil shifted to the region of the highest gradient of interleukins (47). The use of PDMS to control fluid flow was also used to deposit cells and proteins onto the microfabricated channels. The biocompatibility of the PDMS microchannels enables cells such as endothelial cells to be cultivated within these channels where dyes binding subcellular compartments can be tracked fluorescently (47). These are tools that have been previously used and in my thesis some of the applications of the SAW based microfluidic systems will be discussed

We introduce a SAW based microfluidic chip as a novel method for microfluidic and micromixing applications. The following chapters will discuss the successful employment of SAW in a variety of applications. In chapter 2, I will discuss how the SAW device was effectively coupled to a microfluidic channel to disrupt the flow paths of the liquid layers to induce a more rapid mixing. This followed by implementing pluronics, a thermoresponsive polymer, to the SAW driven flow in microfluidic channels to form valves which alters fluid flow leading indirectly to a passive mixing phenomenon is investigated in chapter 3. In Chapter 4 the application of SAW as a pump to analyze how circulating melanoma cells can bind to a shear induced stretched conformation of von-Willebrand factor a blood glycoprotein involved in coagulation within our blood vessel, a new in-vitro model to analyze cancer metastasis. In Chapter 5 we simulate a blood vessel by culturing an endothelial cell layer onto a microfluidic channel and witnessing the release of VWF from the endothelial cell layer to bind circulating melanoma cells. Chapter 6 introduces a new way to detect and analyze velocities and sizing of particles. By depositing metallic slits onto the microfluidic channel along with a

fluorescent detection system we can analyze velocities and sizing of particles freely flowing by Fourier analysis. In Chapter 7 micropipette aspiration is applied to quantify the adhesion energies of VWF conformations from an applied shear can regulate melanoma cell adhesion.

Chapter 2

Acoustic Mixing in Low Reynolds Numbers

2.1 Introduction

In these set of studies, we wanted to test the applicability of SAW for micromixing purposes in a 3-D microchannel. Therefore a Y shaped channel was selected to optimize large Peclet number regimes so parallel streaming of liquids could be undertaken for longer distances without mixing. The Peclet number (Pe) which represents the ratio between mass transport due to convection and that of diffusion, determines how far particles or molecules can diffuse across the entire channel until a uniform homogeneity is achieved (37). Fluids can be injected into the arms of the Y shaped microfluidic channel and circulate side by side in the principle channel. Along this channel solutes can be transported by the hydrodynamic flux, and at some region in the channel a diffusive zone in the shape of an angular sector opens up gradually along the flow (37). If streams of fluids move with a velocity (v), this process requires a distance $V\frac{h^2}{D}$ ~Pe with h as the height of channel and D as the diffusion coefficient. For a biomolecule such as hemoglobin ($D=7 \times 10^{-7}$ cm^2sec^{-1}) to completely mix as it travels at a constant velocity of 1cm/sec in a channel with a height of 200 um would require a channel length of approximately 5.7 meters to completely mix. In smaller scales mixing is mainly based on diffusion. According to the diffusion laws the distance a particle travels varies with time to the square power so diffusion becomes very important in the microscale level (Chp 1). For example for a 1 micron particle to diffuse 1 mm would take 300 hours or 2 weeks, but to diffuse 1 μm would take milliseconds. Larger dye molecules or biomolecules would take even longer. Therefore in a 1mm wide tube diffusion can be neglected but in a microchannel 100 μm wide the distance traveled becomes important.

It can be time consuming to effectively mix small volumes of liquids in microfluidic channels due to the low Reynolds numbers which affects the hydrodynamic behavior of

the fluid. By employing SAW as a unique micromixer can help to alleviate some of the mixing constraints typical for most microfluidic systems. This can be a useful tool for microarray technology, ELISA's or other minitiuarized biological assays which require agitation of small volumes of biological or chemical fluids. The interaction of SAW and the fluid layer results in a streaming of the fluid layer which can agitate the path of the streamlines creating an internal stirring motion. For our studies, the SAW chip was coupled to the Y shaped microfluidic channel and the mixing of the two liquid streams were analyzed.

2.2 Materials and Methods

2.2.1 Construction of Microchannel

To construct the PDMS microchannel, we first mixed the chemical contents of the liquid PDMS pre-polymer containing 1 part curing agent and 10 parts elastomer (Sylgard, Michigan, USA). When mixed together a polymerization occurs resulting in a hydrosilylation reaction between the vinyl ($SiCH=CH_2$) groups and (SiH) groups. The pre-polymer is then poured onto a metal mold which has a Y shaped relief structure milled onto the surface. The PDMS is cured at 70 celsius overnight to produce the final replica of the microstructure which is then peeled off the master. The PDMS structure is then plasma oxidized to render the surface hydrophilic to a silonol compound (Si-OH) which can then irreversibly bind to the glass surface to form a tight seal so that the leaking of fluids could be eliminated. The Y structure was designed with the two inlets to inject two sets of fluids simultaneously until they merge onto a main channel. Therefore 1 micron size fluorescent beads mixed in water were administered in one inlet and water on the other. The size of the beads were ideal for our studies to monitor its path along the channel (53).

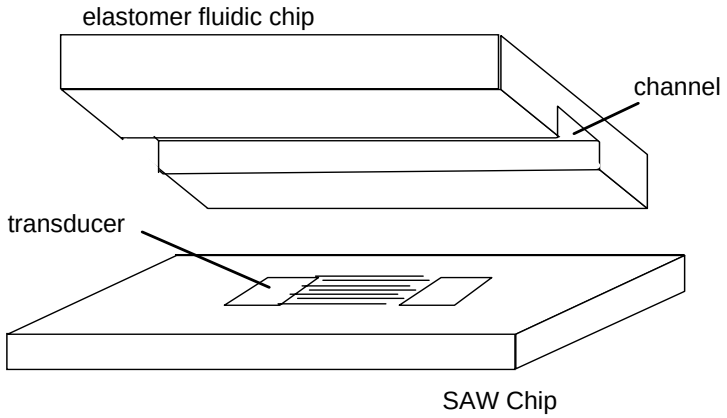

Fig. 1: Elastomer (PDMS) / piezoelectric ($LiNbO_3$) hybrid before assembly. The elastomer contains a microfluidic channel network. The fluid in this channel is effectlively coupled to and agitated by the SAW being generated by the transducer on the piezoelectric.

2.2.2 Surface Acoustic waves induced Acoustic Streaming

The surface acoustic wave chip was designed to effectively interact with small volumes of liquids located at the surface of the piezoelectric substrate. As mentioned previously the transducers are responsible for generating surface acoustic waves. The number of fingers and their distance to each other can amplify the surface acoustic waves to move small droplets or thin fluid layers called acoustic streaming. This depends on the amplitude of the wave which is generated, for small SAW amplitudes can lead to an internal streaming of fluids which is ideally suited for nano and micro mixing. At larger SAW amplitudes, droplets and fluid layers can be actuated leading to droplet transport and streaming of closed fluid layers at the surface of the substrate (23, 38, 56, 57).

The basic mechanism for acoustic streaming is depicted in fig 2. As a droplet is placed along the SAW chip ($LiBNO_3$) near to the transducers, the SAW as it travels along the surface enters the droplet which is diffracted under a Rayleigh angle θ_R generating a longitudinal pressure wave (56). The Rayleigh angle θ_R which represents the diffraction

angle is given by the ratio of the sound velocities in the substrate and fluid. In our studies the same concept can be applied however for a three dimensional Y shaped microfluidic channel which is coupled by a layer of water to the SAW chip (fig1). The interdigital transducers are placed perpendicular to the region of the channel where the two fluid streams merge to the main channel shown in fig 3. Fluorescent video microscopy was used to record the mixing efficiency of the fluid streams. The intensity distribution of the fluorescent beads is a marker for mixing along the microfluidic channels, which were analyzed using open-box imaging software.

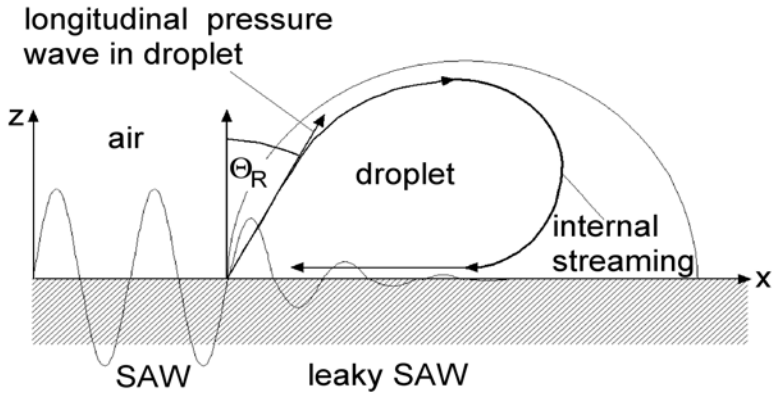

Fig. 2: Sketch of the acoustic streaming acting on a small droplet on the surface of a piezoelectric substrate. The acoustic energy is radiated into the fluid under an angle Θ_R, leading to internal streaming in the small fluid volume.

2.3 Results/Discussion

2.3.1 Acoustic Mixing

First, we wanted to test the coupling efficiency of SAW to our microfluidic channel. In previous studies, acoustic agitation was applied to semiclosed liquid volumes. A capillary gap where a liquid volume is placed between the SAW substrate and coverslip has been studied. A detailed understanding of vortex formations and internal streaming patterns

with analytical solutions has been tested to accurately measure velocity and pressure fields (15, 52).

The diffraction angle is an indication as to how the sound wave propagates through our microfluidic device and how it finally enters the fluid channel. As a result, the diffraction angles between the PDMS glass channel and the SAW chip which has a layer of liquid which is sandwiched in between is examined. To achieve this, beads were placed in the channel to measure the diffraction angle. As the SAW is excited on the piezoelectric substrate, the sound velocity gets diffracted onto the water and then again onto the microfluidic device (fig 3a). As the SAW waves gets diffracted through the different mediums there is a transfer of SAW into so-called bulk acoustic waves (BAW) as visualized in fig 3a and 3b. To test the coupling efficiency of other materials to the SAW chip, a plastic cuvette can be also coupled effectively showing similar diffraction angles to glass observed by pumping an ink dye (fig 3a). Other microfluidic chips consisting of silicon or similar materials can also be utilized for these applications. The diffraction angle can vary depending on the sound velocity, coupling liquid and the material of the microfluidic device (50).

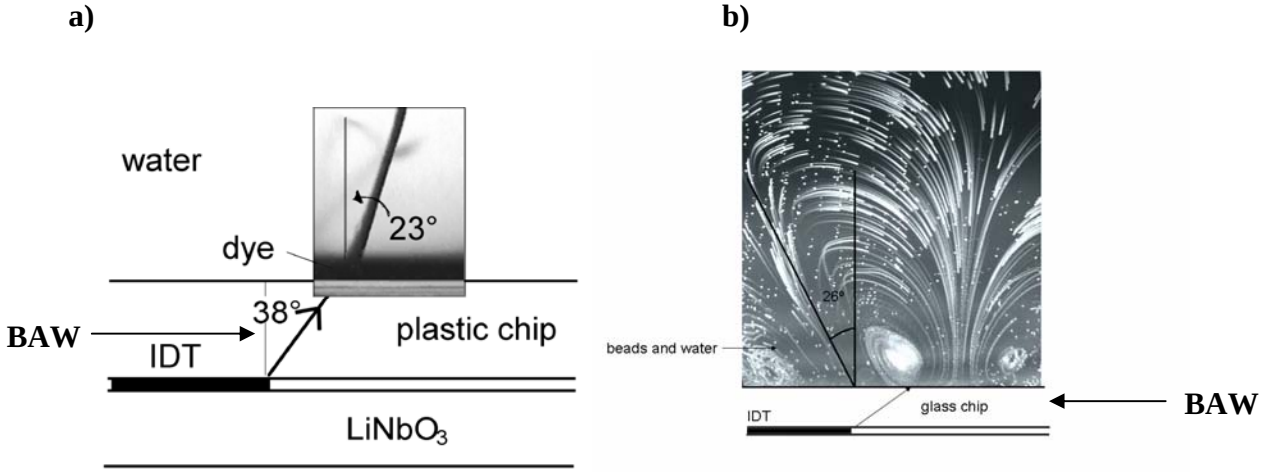

Fig. 3: SAW coupling through the bottom of the microfluidic plastic (a) and glass (b) chip into the fluid in the microfluidic channel. In water, the angle of diffraction has been visualized by acoustically pumping a small amount of dye (a) and fluorescent beads (b). Note that there is no significant change in the angle of diffraction for both substrates.

To demonstrate this hybrid technique, our newly designed Y shaped microfluidic channel with a steady velocity of 250μm/sec was generated by applying a constant back pressure to the inlets (fig. 4). A moderate flow rate was chosen to visualize the parallel streams of fluorescent beads and water for our mixing studies. However at higher velocities, up to 1mm/sec, similar mixing results was obtained (50).

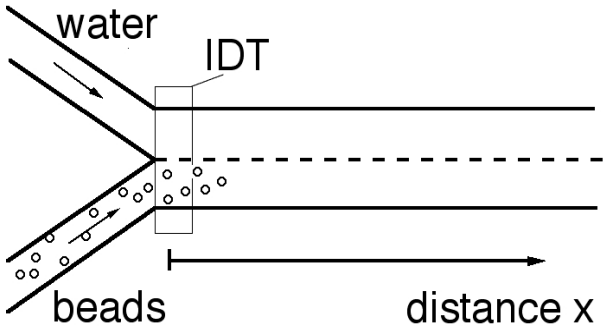

Fig. 4: Sketch of the Y-shaped microfluidic device which was used to investigate the acoustic mixing. The two inlets were flushed with pure water, to one of them we added fluorescent beads. Close to the junction, a SAW chip was acoustically coupled to the bottom of the channel

In fig 5 to capture the applicability of the parallel flow channel system, we can directly visualize the laminar flow of liquids and beads as they merge from the inlets to the main channel where there is a parallel flow between the fluorescent beads and water. In these snapshots SAW is turned off, so as to monitor the natural laminar flow within the channel. In the channel no distribution of the beads over the virtual center line is observed. This is in accordance with the Peclet number of 12.5 for this system which signifies that flow dominates over molecular diffusion.

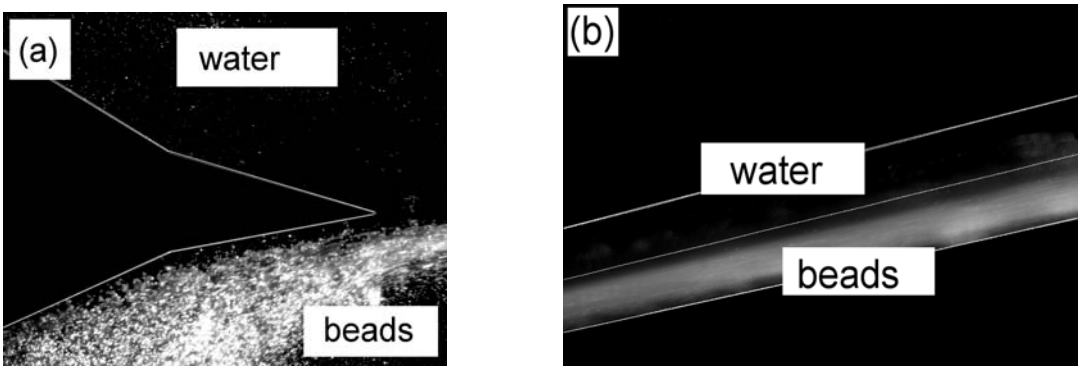

Fig. **5**. (a) Bead distribution at the junction of the two inlets, (b) laminar flow downstream of the channel, when no SAW is present. The white lines indicating the boundaries and the virtual center of the channel are superimposed to the camera images as a guide to the eye.

As a high frequency (f=146 MHz) signal was applied to the transducer of the $LiNbO_3$ substrate the SAW is diffracted onto the region of the channel where the two liquid streams merge. The SAW propagation is directed perpendicular to the flow direction in the channel. A simple channel design without any special obstacles or structures was used to simply evaluate the effects of SAW, to avoid any additional parameters which can influence mixing from such geometries. Here we show the successful employment of the SAW pump as an active micromixer. As an applied RF power is turned on, mixing of the fluids in the channel is observed (fig 6). Note that vortices are generated resulting in a distribution of the fluorescent beads throughout the channel (50).

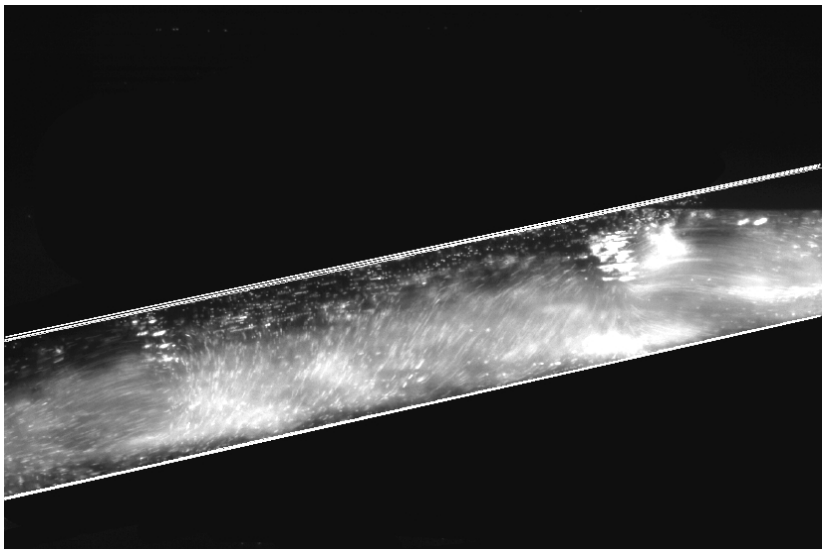

Fig. 6.Snapshot of the acoustically induced mixing in the microfluidic channel with the fluid flowing from left to righjt as in Fig 5. The white lines are superimposed on the camera to visualize the boundaries of the channel. The picture shows a distributed fluorescence signal across the whole channel width shortly after switching on the SAW at high power. The images show the same channel region as the one in Fig. 5 (b), approximately 2.5 mm downstream from the mixer chip. Note the occurrence of vortices along the channel.

To evaluate the mixing efficiency, time averaged fluorescence images were taken at different positions of the microfluidic channel from where the SAW transducers are placed. The pixel fluorescence intensity was measured in the upper part I_u and the lower part of the channel I_l from the virtual center line. A ratio was taken between the upper and lower half of the channel to calculate the mixing fraction $E=I_u/ I_l$, which we assign as the quantitative measure for the mixing efficiency. Prior to the onset of SAW when beads reside in the lower part of the channel and no beads are visible in the upper channel then the mixing fraction is $E=I_u/I_l=0$. Once complete mixing and distribution of the fluorescent beads across the entire channel is achieved, this results in $I_u= I_l$ and hence E=1 (50).

A line graph plotting the efficiency of SAW induced mixing within the channel is shown in fig 7. The graph is plotted for the mixing efficiency E as a function of distance X from the transducer downstream towards the outlet of the channel. For control purposes, no SAW was applied to track the natural laminar flow of the fluid layers until there is diffusion between the two streams. The fluorescent beads and water flow along the channel to approximately x=25 mm downstream before a mixing fraction of only E=0.5 is reached. Once SAW is generated underneath the channel the mixing process is expedited. As the SAW amplitude is gradually increased the mixing process takes place at shorter distances from the transducer. At the highest SAW amplitude a complete mixing (E=1) was achieved at a distance of X=2mm, which is a factor 10 less than without mixing. The mixing graph shows steps on the lines which could be a result of the vortices leading to a dynamic accumulation of fluorescent beads along the channel. Further investigations were not undertaken to explain this effect. In this study the SAW agitates the fluid layers producing complex folding lines so that complete mixing can be achieved in seconds.

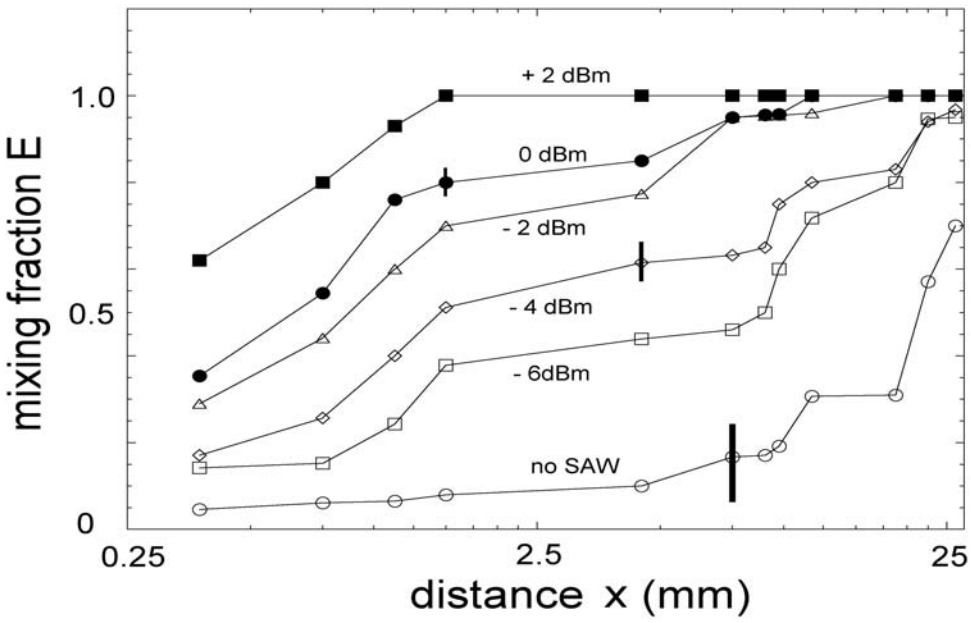

Fig. 7: Experimentally obtained mixing fraction E as a function of the distance x from the IDT generating the SAW. The different symbols correspond to different SAW amplitudes. Note the logarithmic scale of the x-axis.

2.4 Summary

We have show a very efficient method to induce mixing in a microfluidic channel by employing surface acoustic waves coupled with a liquid layer through the channel material which then goes into the fluid. Since diffusion alone for mixing can be a time consuming and risky process, the use of SAW to agitate the fluid layers in a controlled manner introduces a new and convenient method to achieve mixing in seconds. The construction of the SAW hybrid system is relatively simple way to produce without the need to manufacture cumbersome channel geometries or pumps, rather a single SAW chip can be used to mix complex fluids in micro or nanoscale regimes. In our studies acoustic streaming can generate complex folding lines, which enhances the mixing efficiency between the fluorescent bead and the water layers within the microfluidic channel. The acoustic coupling of the piezoelectric substrate to the microfluidic device provides the versatility of the SAW chip for pumping and mixing of fluids.

Chapter 3

The Effects of Pluronics in Acoustically Driven Flow

3.1 Introduction

To control fluid flow and to achieve mixing in microfluidic systems by far is a challenging topic. Previously we introduced SAW as a new way to enhance mixing in microfluidic channels under low Reynolds numbers. However in these studies, SAW is used as a pumping device on a PDMS fabricated microchannel and to the control fluid flow an electrically switchable valve called pluronics was incorporated. Pluronics is a versatile compound used for drug delivery especially as a stealthing tool to coat liposomes from being attacked by the immune system (9). For our purposes, pluronics is used as a valve to regulate fluid flow and as a micromixer. Due to the complex problems of mixing small volumes of liquids, various passive and active micromixers mentioned previously have been designed to solve this problem. Active micromixers require pumps or electro-osmotic/kinetic methods to disturb fluid flow, but for passive micromixers special obstacles have to be designed into the microchannel to narrow the distance of the pathlines or to create flow distortion (51).

Pluronics are classified as surfactants which are organic compounds that are ampihilic so they can spontaneously aggregate as a function of temperature. It consists of a hydrophobic tail group and a hydrophilic head group. Pluronics also have the unique property that when in aqueous solutions and when the temperature is increased, i.e above room temperature, it can reversibly convert from a liquid state to a gel state. This heat sensitive co-triblockpolymer has a chemical composition of PEOx-PPOy-PEOx, the PEO (polyoxyethelene) and PPO (polyoxypropylene) with two 96 unit hydrophilic PEO chains surrounding the one 69 unit hydrophobic PPO chain (60). In an aqueous solution at relatively low concentrations the hydrophilic-hydrophobic block copolymers form micelles upon passing a critical micelles concentration (cmc) or temperature. Micelles

form when unimers such as single polymer fragments aggregate with the hydrophilic "head "regions in contact with surrounding media, while the hydrophobic tail groups from the center form a liquid colloid which are often globular or spherical in shape. However, at higher concentrations these micelles tend to overlap and form into a liquid gel (13).

In our studies, we wanted to utilize the chemical nature of pluronics, to reversibly form liquid gels so that localized valves can be formed within our microfluidic channel. This is accomplished by integrating heating units to clot regions of the bifurcated channel to redirect the laminar flow and to induce a quasi-chaotic motion at the branched regions of the channel. By applying SAW as a pump, along with pluronics as a clotting agent to alter the channel dimensions to control fluid flow, we have created a much easier and more convenient way to pump and to indirectly mix fluids. With this new method, complex pumping systems or channel geometries are not required. In order to avoid complex structures and geometries a rectangular continuous flow microfluidic channel was designed with a branch leading to two parallel flow channels to directly visualize the effects of pluronics.

3.2 Materials and Methods

First we fabricated a parallel flow channel using PDMS on molded metal structure. A continous flow rectangular channel (1mm wide) with a branch leading to two parallel flow channels (500μm wide) with a height of 1mm was designed to test the effects of pluronics as a micromixer. Second a heat sensitive polymer used for valving is pluronics p127 which is available from BASF. The p127 concentrations of 10%, 15%, 16% and 17% wt/vol were prepared by mixing in distilled water, sonicated and dissolved at 4°C. These concentrations were used to quantify viscosity changes as a function of temperature and then were tested using our microfluidic flow chamber to monitor fluid flow. Viscosity (η) is the measure of the internal friction of a fluid. As the friction increases, the greater the amount of force is needed to move the liquid called shear.

Two parallel planes of fluid of equal area "A" are separated by "dx" and are moving in the same direction at different velocities V1 and V2. The force required to maintain this difference in speed was proportional to the difference in speed through the liquid.

$$\frac{F}{A} = \eta \frac{dv}{dx} \qquad 2.1$$

3.2.1 The Falling Ball Viscosimeter

The gelling of pluronics is the result of viscosity and temperature shifts. To measure changes in viscosity of the pluronic solutions in relation to temperature the falling ball viscosimeter was employed (Haake, Munich, Germany). This technique can measure the kinematic viscosity of solutions which are translucent. By measuring the falling speed of a spherical ball in a vertical tube filled with the concentrations of the pluronics (10%, 15%, 16%, 17% wt/vol) the kinematic viscosity is deduced.

$$\eta = \frac{d^2}{18 U_\infty} (\rho_b - \rho) g \qquad 2.2$$

wherein η is the dynamic viscosity of the fluid (Pa s), d the diameter of the ball (m), U_∞ the speed limit of the ball (m s^{-1}), ρ_b the density of the ball (kgm^{-3}), ρ the density of the fluid (kgm^{-3}) and g is the gravitational acceleration (m s^{-2}) where $\Delta\rho$ is difference between the density of the sphere and the liquid, g is the acceleration due to gravity and a is the radius of sphere (8).

3.2.2 Cone and Plate Viscometer

The application of pluronics as a valve to control fluid flow, the rheological properties of pluronics is examined. A controlled shear rate was applied using the Haake rheometer (Munich, Germany) with a cone and plate geometry for rheological measurements. The pluronics (15% wt/vol) is sheared between a stationary plate of 40mm diameter and a revolving cone which has an angle of 0.0397 radians. The temperature is provided by a peltier plate. The temperature was increased from 30°C to 70°C under varying shear rates (10, 100, 1000 Hz).

3.2.3 Parallel Flow Microchannel and Resistive Heating Structure

The ohmic resistive heaters utilized for our studies are made from chromium, 100nm thick layers of chromium was sputter deposited onto a silicon dioxide glass slide (fig 1a). These resistive heaters convert electricity to heat, as an electric field is applied the current running through the element encounters a resistance resulting in heating of the element. A resistance of 8000 Ω was measured for the chromium heating device. One half of the PDMS parallel flow microchannel was plasma etched to the resistive heating device (fig 1b). The SAW is utilized as a pump by placing the IDT's at the corner of the rectangular parallel flow channel to drive the liquid along the channel. In order to monitor laminar flow, 4.5 micron size fluorescent beads were mixed in pluronics. The fluorescent bead distribution in the microfluidic channels is visualized using a CCD camera mounted on a fluorescence microscope with the illumination provided by a mercury lamp (Zeiss, Germany).

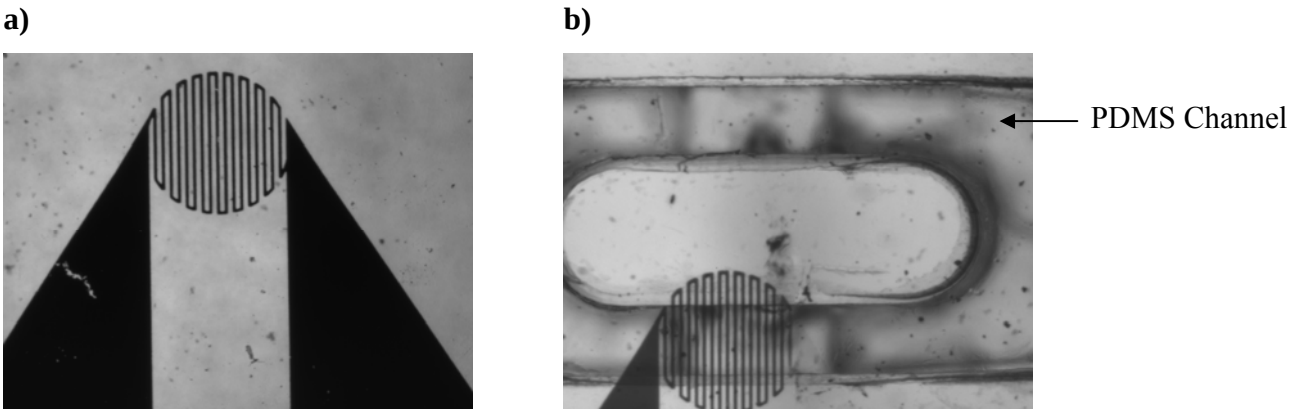

Fig. 1: a) A snapshot of the chromium heating element imprinted on a glass slide by photolithography and b) a PDMS parallel flow channel attached to the chromium heating element.

3.3 Results/Discussion

3.3.1 Viscosity Measurements of Pluronics

Viscosity measurements were taken from the falling ball viscometer to detect changes from the liquid to the gel state of the pluronic concentrations (p127). The graph shows the viscosity changes of the pluronics of the concentrations (10%, 15%, 16%, 17% wt/vol) as a function of temperature (fig 2). Note that during the gel point of the pluronics (15%, 16% and 17%) there is an increase in viscosity in orders of magnitudes over temp increase of 1°C. At higher concentrations the gel point occurs at lower temperatures. The pluronics with a concentration of 10% wt/vol showed no polymerization, this is due to the low concentration which is well below the gel point.

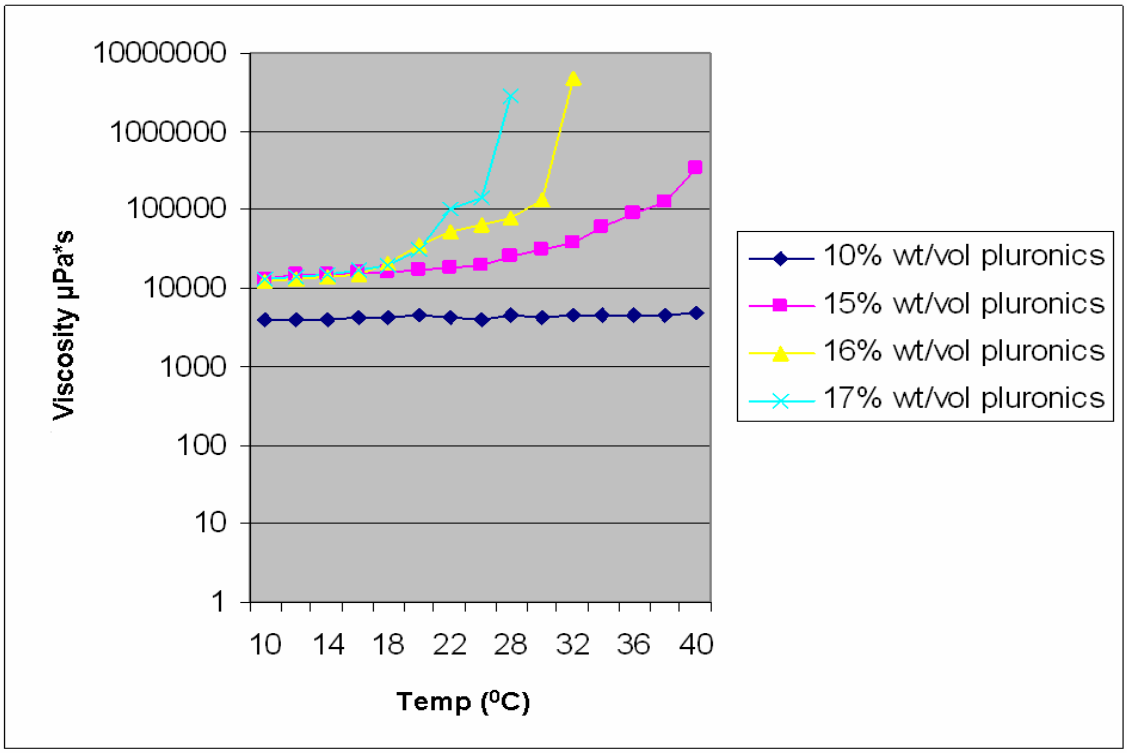

Fig. 2: A graph showing viscosity changes of pluronic concentrations in relation to temperature measured by falling ball viscometer.

3.3.2 Determination of the Rheological Profile and Viscosity of Pluronics (15%wt/vol).

From the previous experiments we were able to control the liquid-gel transition of the pluronics at a concentration of 15% wt/vol over a wider range of temperatures. The rheological properties of the 15% wt/vol pluronics was analyzed using the cone and plate viscometer. The data values show a dramatic reduction in viscosity as the shear rates are increased from 10-1000 Hz (fig 3). Under different shear rates an increase in viscosity from 30°c to 40°c is measured and a gelling point above 40°C is observed. However temperatures ranging between 50° to 70°C show an apparent inhomogeneity of the sample which creates a reduction in the shear viscosity for the varying shear rates.

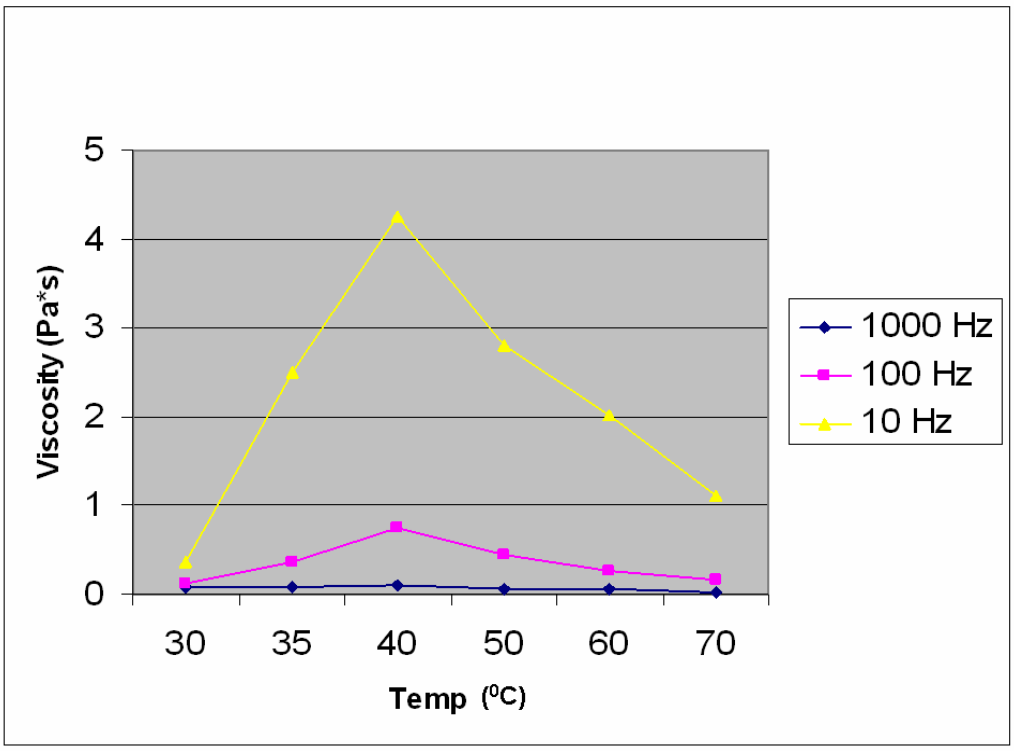

Fig. 3: A line graph plotting the shear viscosity of the pluronics (15%wt/vol) using the cone and plate viscometer in relation to temperature and the varying shear rates**.**

3.3.3 Multiphysics Modeling: Interaction of Hydrodynamics and Heat Conduction in Pluronic Mixtures

Model simulations are implemented to take a closer look at the dynamic events of pluronics as a microvalve in SAW induced microfluidic systems. We took the original CAD layout of the channel floor of the milled structure and imported it into a computer program (Comsol Multiphysics). This channel floor was extruded to the appropriate height (1mm) used in the experiments. In the third model of the bifurcated channel, side and bottom walls are modeled no slip (velocity is zero). At the top of the channel there is no ceiling coverage but a free surface, boundary condition is assumed to be slip there. For our flow simulations the parameters for pressure driven flow is not implemented but rather for the effects of acoustic streaming. At the inlet or corner of the channel there is a

limited region where a volume force drives the fluid. This domain represents the acoustic streaming effect generated by an IDT far away from the branch. This is important for our experiments since we don't want to observe SAW induced acoustic streaming but the laminar flow at the bifurcation without the secondary effects generated by the pumping system, e.g. SAW induced vortices like depicted on the corner of Fig 7d in Chp 4. The implemented force field was adjusted to drive the flow at a velocity ~1mm/s (15).

The parameters were set so the heat flux (q) is modeled according to the environment of the system for FEM lab simulations. The heater is designed as a circular region which is at the channel floor and they are at a constant user-defined temperature. The PDMS subdomain splitting the channel is meshed and hence heat transfer is simulated by FEM there. All boundaries exterior to the channel geometries (the surrounding), are set at a defined heat flux which has been estimated using the following expressions (Stöcker).

Heat flux through a layered system (here the side walls)

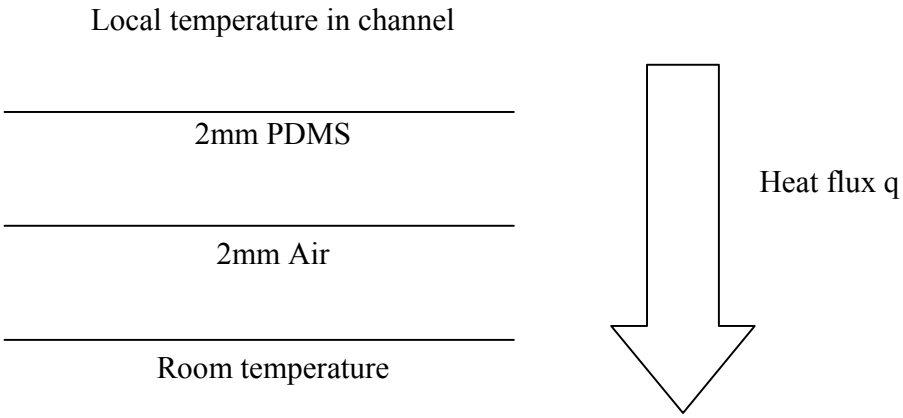

q=(T[outside=environment]-T[inside=heater])/(s1/l1+s2/l2)

s1=thickness of layer 1 (here pdms)

s2=thickness of air

l1=thermal conductivity of layer 1 (here pdms)

l2=thermal conductivity for layer 2 (air) accordingly

At the floor the layer consists of the glass slide (150µm glass) and the SAW chip underneath (500µm) before environmental conditions are reached. At the channel surface you have direct contact to air so there is only one layer:

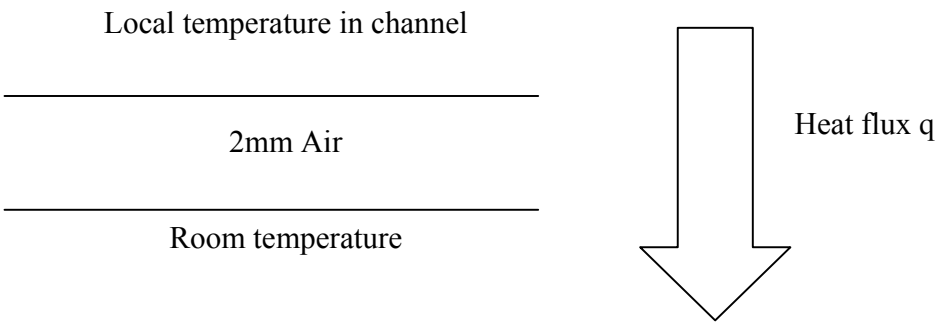

q=(T[outside=environment]-T[inside=heater])*l/s
s=thickness of the layer (here air)
l=thermal conductivity of the layer (here air)

Inlet and outlet temperatures are defined to be room temperature.
Now the interaction: At first there is the temperature dependent viscosity (η) of the pluronics mixture which was implemented by a steep function

η [T]=(min(10^(exp(0.12*1/K*(T-273)-4.45) – 1.9),1000)

which models the transition measured in the experiments and limits the maximum viscosity to 1000 Pa*s. This is important because much larger viscosities created by the exponential function would cause dramatic numerical errors and prevent the convergence of the solution progress. In fact, the viscosity ranges over 5 orders of magnitude (from 0.017 Pa*s at RT up to the limit of 1000 Pa*s) in our simulation. The second interaction is the convection (the heat transport by advection of the fluid) which distorts the temperature distribution around the heater in direction of flow. This happens only at low temperatures (fig 7a) but as soon as the channel is clotted (fig 7b) only diffusion occurs and the distribution is not skewed (15).

An outline of the fabricated parallel flow region of the rectangular channel to analyze pluronics as a microvalve with the integrated heating unit is discussed. The circular region of the bifurcated channel denotes the region where the integrated chromium heating unit is placed. At 20°C the pluronics at 15% wt/vol is in the liquid state so laminar flow and uniform streamline of the 4.5 micron size beads are visualized at a flow rate of 1mm/sec (fig 4a, 4b). A velocity of 1mm/sec was applied to test the effectiveness of the pluronics as a microvalve for high throughput applications. The dynamic viscosity of the pluronics from a cross-sectional view shows the flow entering the bifurcated channel with a homogeneous viscous layer in relation to the height of the channel (fig 4c).

However, as the heating unit is turned to 40°C a transition to the viscous layer occurs at the base of the microchannel where there are no-slip boundary conditions. The heat then gradually rises but is dissipated near to the top of the fluid layer (fig 5c). This results in a partial blockage of the branched channel where the flow rate is reduced and redirected to the other branch. As the flow is re-directed, there is a complex flow and streamline distribution of the particles (fig 5a, b). Once there is a complete blockage of the channels at 51°C, a complete redirection of the flow to other branch is observed (fig 6a). The cross sectional view of the clotted branch shows the distribution of the heat has completely solidified the pluronics.

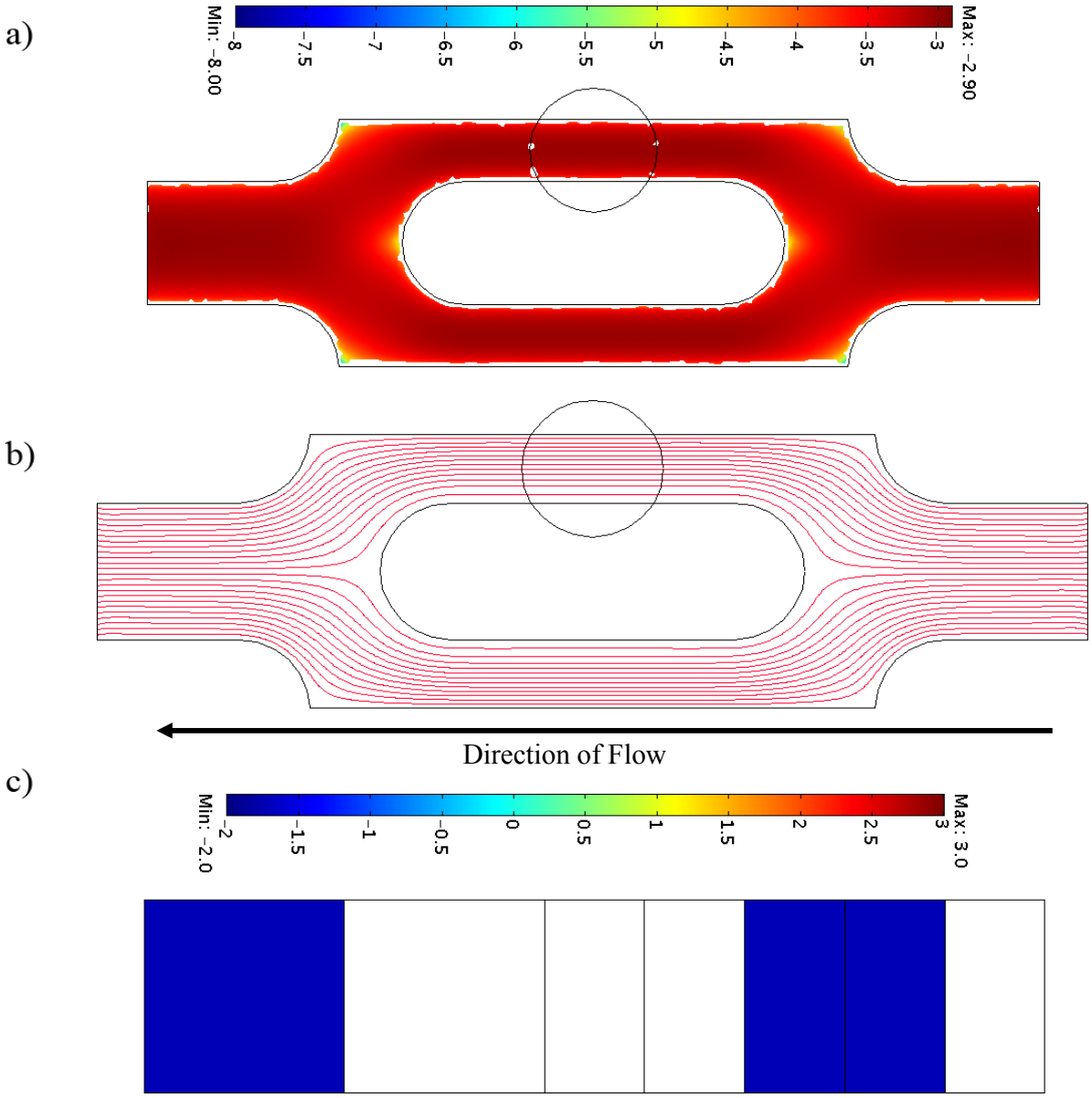

Fig. 4: a) A simulation showing laminar flow of the pluronics (15% wt/vol) mixture at the branched region of the channels when no heat (circle) is applied (20°C). The scaling is logarithmic where the maximum flow 10^{-3} m/sec (red) and minimum flow rate is 10^{-8} m/sec (blue), (b) along with the streamline of the fluid layers. A cross sectional view of the branched channel of the incoming flow shows at a temp of 20°C, which is well below the gelling temperature, on both sides of the branched channel a low viscosity of 10^{-2}Pa●s of the pluronics is visualized. The scaling for the viscosity measurements is logarithmic ranging from maximum 10^{3} Pa●s to a minimum value of 10^{-2} Pa●s (courtesy T Frommelt).

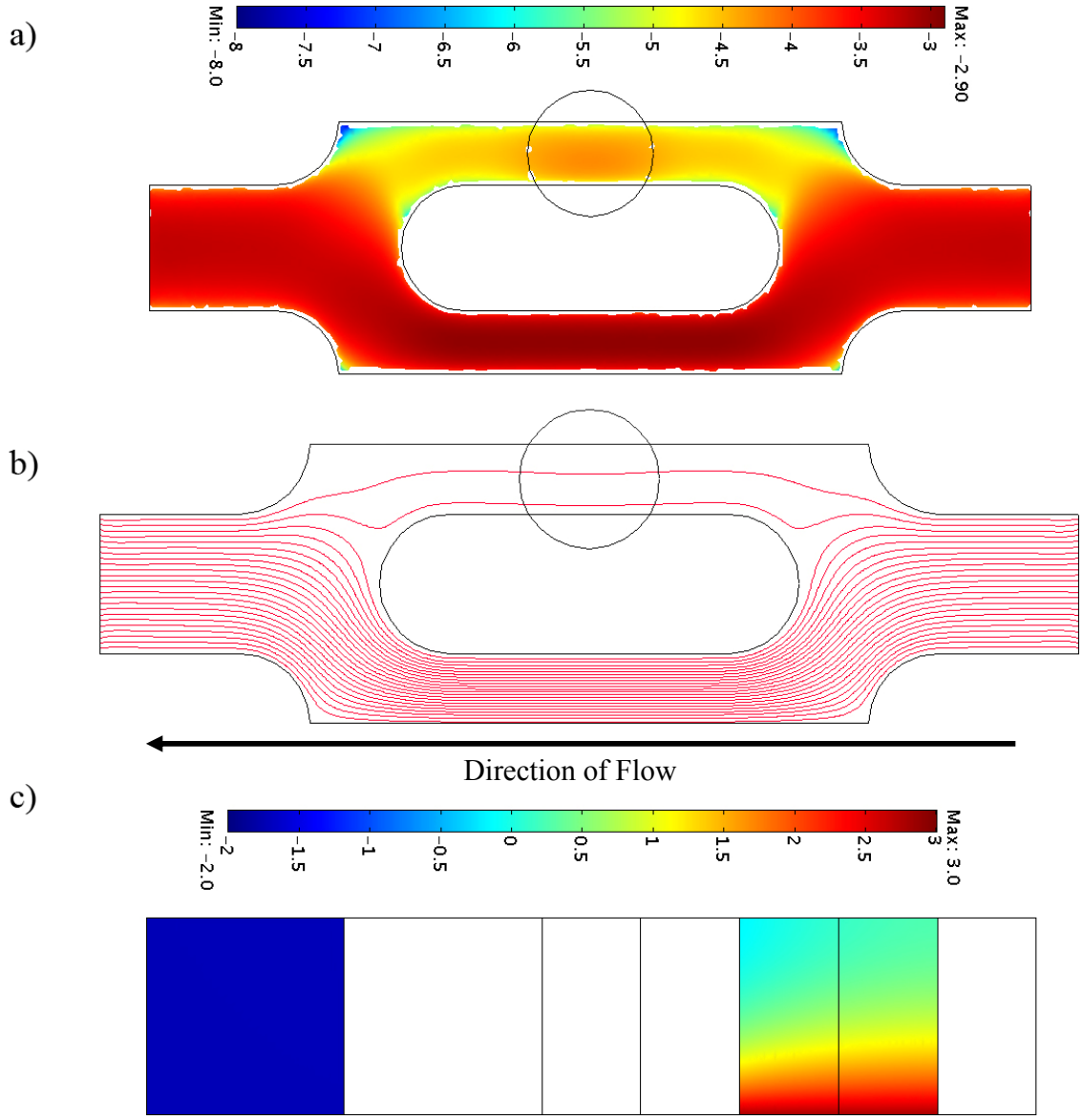

Fig. 5: a) A simulation showing the transition point of the pluronics 15% wt/vol. The flow rate is disrupted at the upper branch of the channel once the heating unit (circle) reaches 40°C as noted by the color change, (b) along with the streamlines c) A change in viscosity is evident at the surface of the right branched channel of the incoming flow where heat directly gels the pluronics (red) while the rest of the heat is transferred resulting in a partial gelling (yellow) at the mid-region of the channel height and a partial liquid state (light blue) near the top of channel (courtesy T Frommelt).

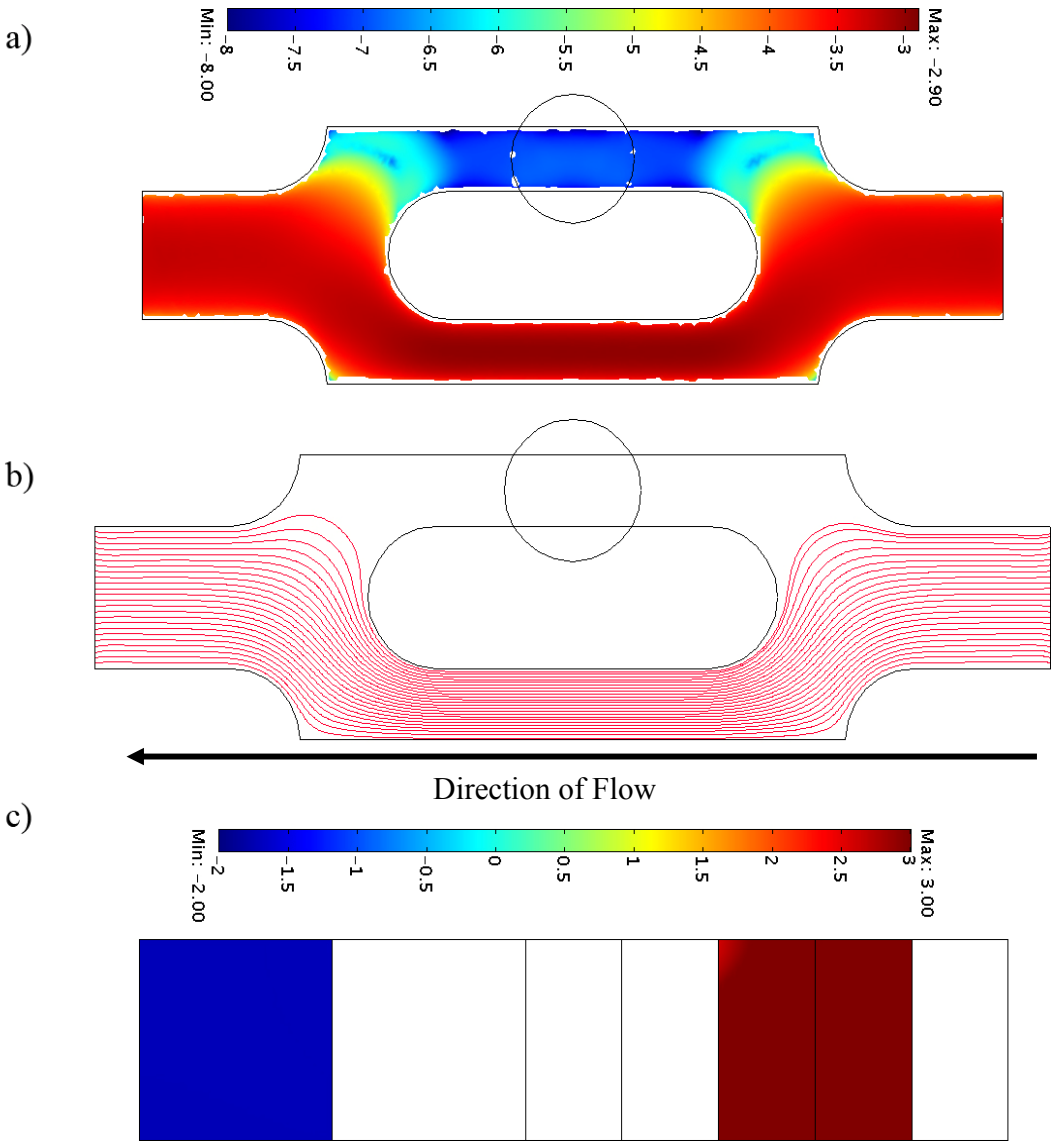

Fig. 6: a) A simulation showing how flow is completely blocked when the heating unit is turned to 51°C and b) redirection of flow is to the lower branch of the channel c) as the whole top branch of the channel is solidified (courtesy T Frommelt).

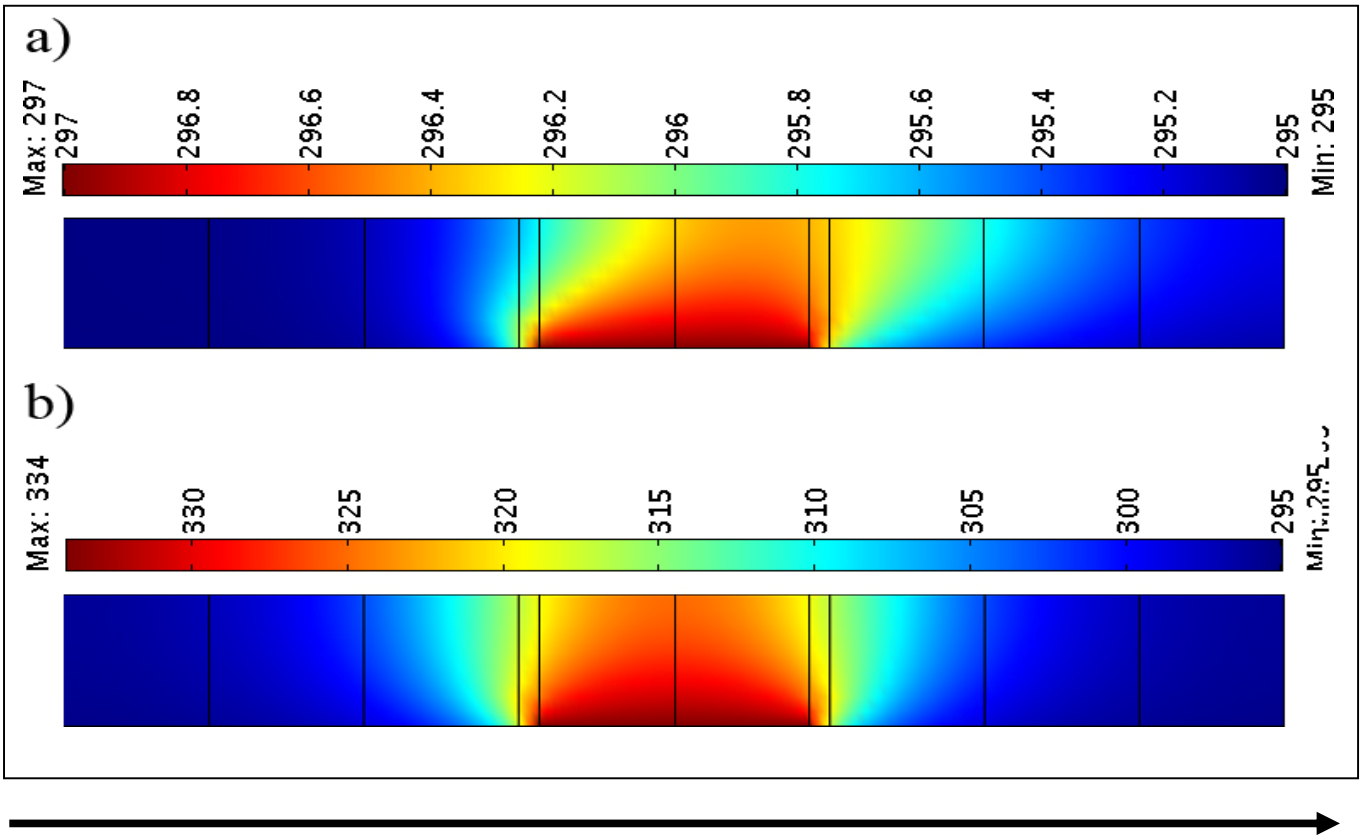

Fig. 7: a) A side view of the region of the branched channel where the heating unit is placed. This shows at slightly above room temperature with a channel filled with pluronics (15% wt/vol), there is still fluid flow and heat is transferred by convection. b) As the heat is raised the channels begins to clot resulting in an isotropic distribution of the heat which is not affected by the flow (courtesy T Frommelt).

3.3.4 Valve Formation of the Pluronics

In the next set of studies, we wanted to test experimentally the dynamic effects of pluronics (15% wt/vol) as an adjustable microvalve. To keep the parameters similar to our FEM simulations, a constant velocity of 1 mm/sec were maintained by the pluronics (15% wt/vol) mixed with 4.5 micron beads. Once the heating unit at the lower branch of the channel is turned on to approximately 40°C, the channel gets clotted and a redirection of the flow to the upper branch of the channel is visualized, causing a quasi-chaotic motion at the channel region where the fluid layers merge (circle) (fig 8b). Once the heating unit is turned off the natural fluid flow is resumed at the lower branch within seconds (fig. 8c). These experiments demonstrate the applicability of pluronics to valve regions of the channel which can control fluid flow and may indirectly enhance the process of passive mixing. Presumably as flow is redirected, the fluid layers stretch leading to mixing. However above 51°C a complete blockage of the channel is visualized and the reversibility of the pluronics back to the liquid state is inhibited (fig 8d). With higher concentrations of pluronics (>15% wt/vol) there are spontaneous gel formations occurring in regions of the channels that affect the flow without the aid of a heating element. Under acoustic streaming a gelling phenomenon begins to form within seconds resulting in a solid wall where fluorescent beads are trapped while there is flow visualized further away from this region near to the SAW pump.

This suggests that perhaps the thermal fluctuations on the microfluidic channels by the environment result in a rapid gel-like formation of the pluronics. The quasi-chaotic flow near to the SAW transducers is due to the solidification of the channel away from the transducers, as a result liquid bounces off the solid wall formed by the pluronics (data not shown). However a concentration of 15% wt/vol of the pluronics was ideal for our studies because it could be easily pumped and controlled by adjusting the heat to reversibly convert from a liquid state to a gel state.

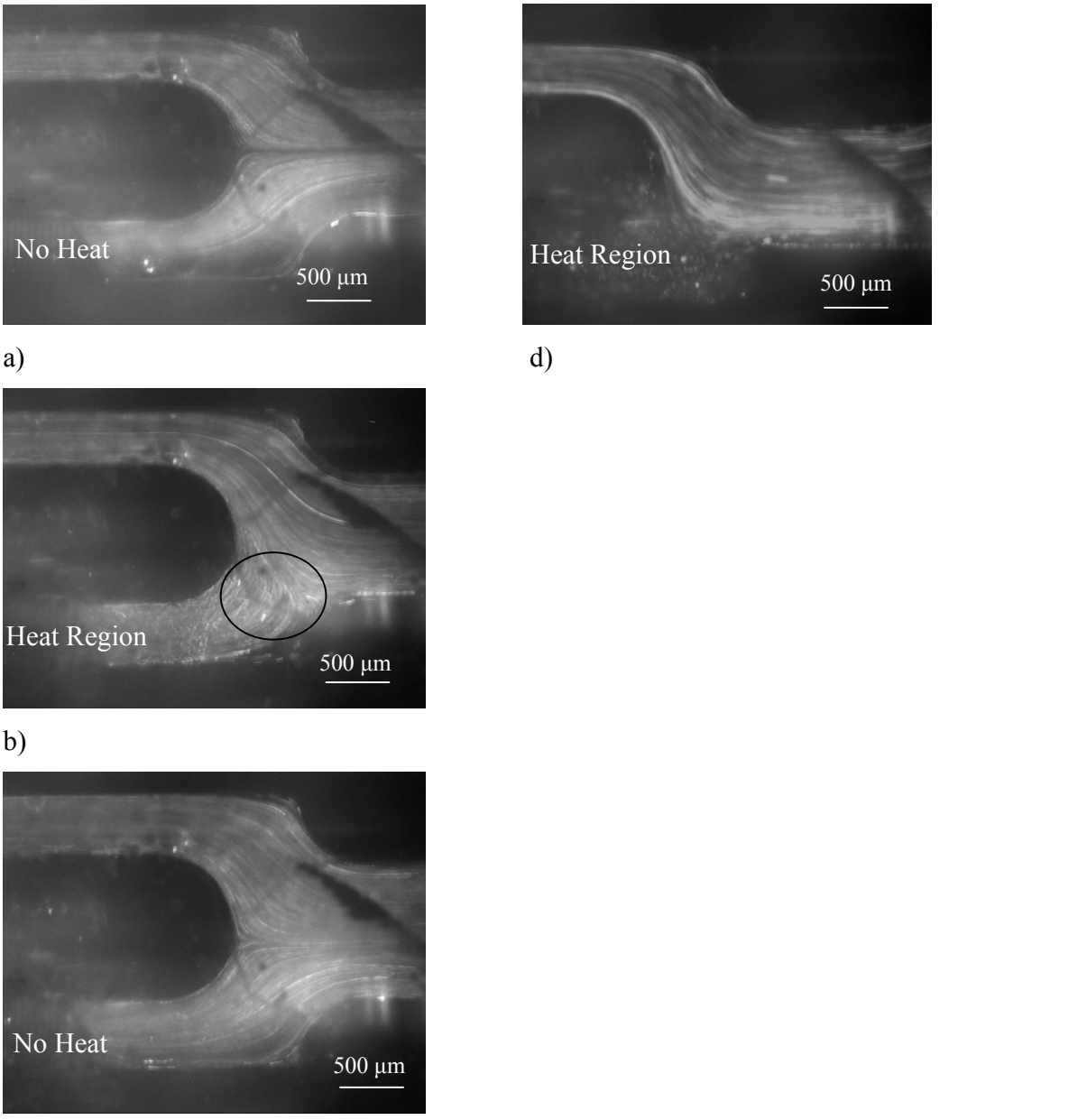

Fig. 8: a) the onset of SAW drives the 4.5 micron beads in pluronics under a laminar flow across the branched channel. b) Once the heating unit is turned a transition point of the pluronics shifts to a gel state redirecting flow to the upper branch resulting in a quasi-chaotic motion. c) As the heating unit is turned off uniform flow in both branchs is visualized. d) A complete blockage of the lower branch of the channel.

a)

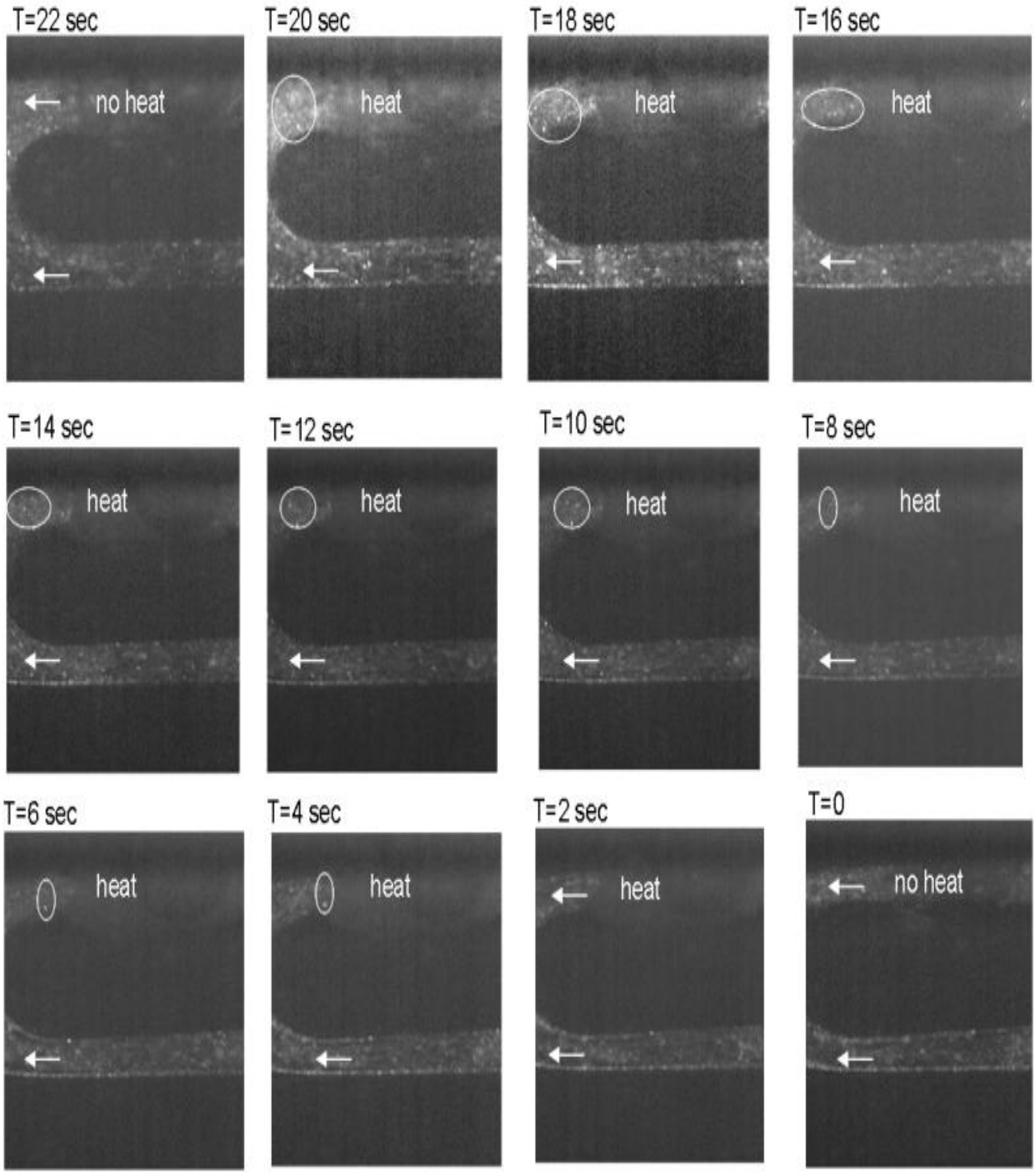
T=22 sec
no heat
T=20 sec
heat
T=18 sec
heat
T=16 sec
heat
T=14 sec
heat
T=12 sec
heat
T=10 sec
heat
T=8 sec
heat
T=6 sec
heat
T=4 sec
heat
T=2 sec
heat
T=0
no heat

b)

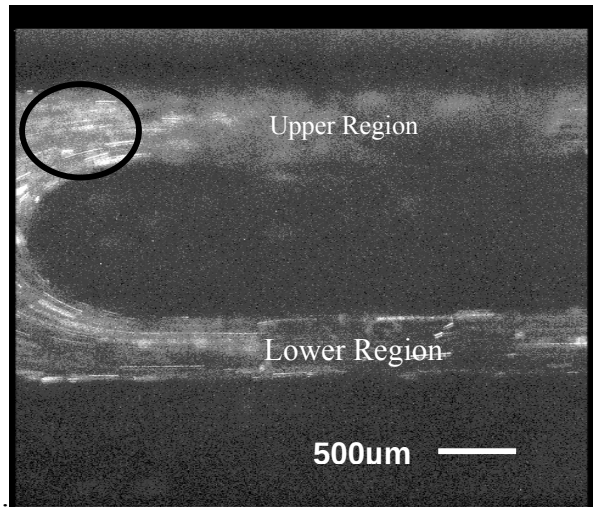

Fig. 9: a) A time course to monitor the flourecent beads in pluronics (arrow shows direction of flow) as the heating device is gradually turned on. An accumulation of beads is observed over time in the top branch of the channels. A velocity of 1000µm/sec is achieved by acoustic streaming. b) An overlay of all the pictures taken from the time course showing an accumulation of beads over 22 sec time period (circle).

Fig 8 shows sequential snapshots that were taken to visualize the effects of the pluronics in local gel formation and blockage during an incremental increase (approx 5°C) in heat in the upper branch of the channel (fig 3a). Initially, the heating device was turned off to monitor proper laminar flow (t=0) and then as the heating unit is gradually turned on starting at t=2 sec until maximum heating is achieved at t=22 sec, we see an accumulation of beads (circle) corresponding to the pixel brightness. Once the heating unit is turned off flow is resumed. The pluronics can form a valve which can close and open leading to an entrapment and release of beads. During the gel point beads accumulate locally in the channel and once the pluronics reverts back to the liquid state the beads then chaotically disperse. An overall time accumulation of the pictures taken from the time course shows a higher distribution of beads within the upper branch of the channel.

3.4 Summary

We here show the combination of SAW and pluronics as a novel method to investigate micromixing in microfluidic systems. Heating elements such as chromium were utilized to reversibly form a gel point of the pluronics in our parallel flow microfluidic chamber to distort the flow and to induce a quasi-chaotic motion at the branched region of the channel to enhance the effects of passive mixing. Both the experimental and simulated data correspond to the clotting characteristics of the pluronics (15%wt/vol) under fluid flow. However higher concentrations (>16% wt/vol) resulted in uncontrolled clotting conditions due to the thermal fluctuations of the system without the effects of the heating element. Our study show that periodic valve like actuation can be formed within the microchannel and can indirectly lead to mixing.

Chapter 4

Acoustic Streaming as a Model System for biological applications

"Melanoma Cell Adhesion Depends on VWF Conformation studied using an Acoustically Driven Microliter Flow Chamber Chip"

4.1 Introduction

The SAW microfluidic flow chamber is utilized as a new in-vitro model system to study tumor cell adhesion in our microcirculatory system. Although there are many underlying factors which can promote tumor cell adhesion within our blood vessel, we wanted to specifically investigate tumor cell adhesion dynamics of melanoma cells to von-Willebrand Factor under blood flow conditions.

Blood Fluidics

One important biological topic covered in microfluidics is the study of the human microvascular system. The mechanism of blood flow is an important component in our circulatory system. Our heart is made of four chambers where the right side pumps deoxygenated blood into the lungs where it then picks up oxygen and the left side pumps oxygen soaked blood through the blood vessels out to the body. Within the heart there are valves or actuators which prevent the backflux of blood so smooth blood flow is maintained. To maintain smooth or steady blood flow, the reaction that induces blood clotting (initiation) is balanced by factors which prevent blood clotting (inhibition). When a blood vessel is damaged the initiation reaction dominates.

Our vessel geometries are important parameters during the initiation reaction which affects the physiological function of blood. The failure to localize blood clotting to the site of the vessel injury can lead to thrombus formation beyond this site. This can lead to a disruption in the laminar flow of blood which can result in heart murmurs. Typically a blood vessel of various geometries (15μm-25mm) can be visualized as an elastic tubular channel consisting of an inner lining called endothelium and is surrounded by

subendothelial connective tissue (10, 48). Our blood is a non-Newtonian fluid where the viscosity changes during an applied shear, so a shear thinning (viscosity decreases) process is taking place as the shear rate increases. The components of our blood are made of plasma (water, protein, platelets) and particles called red blood cells. The viscosity of blood is determined by the viscosity of the plasma and the amount of hematocrit (packed cells). Under blood flow conditions, the viscosity of blood is calculated by the ratio of the shear rate and the shear stress. The shear rate is the radial derivative of the velocity in the blood vessel v from the distance of the cylinder r, $\gamma(r) = \left| dv / dr \right|$ and the shear stress $\sigma = \gamma \eta$ is an indicator of the actual force needed to obtain a certain velocity between the fluid and surface of the blood vessel. It can also initiate the forces denaturing proteins or the causes for the deformation of cells in our micro-circulatory system (7). However for our applications, blood flow is analyzed for smaller blood vessels where the flow is laminar (fig 1) as opposed to large arteries where a turbulent flow can occur.

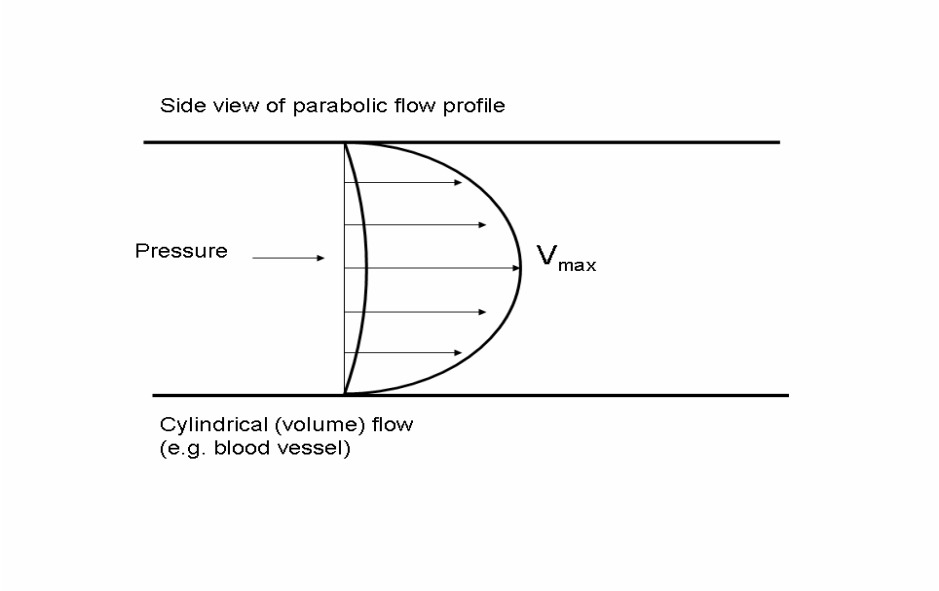

Fig 1: A schematic view of parabolic flow within a blood vessel. As a pressure is applied the fluid flow is maximal at the central region of the channel followed by velocity approaching zero near the vessel wall.

In medicine, blood flow can be measured by the ability of our blood vessel to conduct flow similar to that of electrical conduction where there is a current flow through a medium, in response to an electric field. Simplified, our blood vessel can be considered cylindrical in shape of radius r with no slip conditions at the walls and a fixed pressure gradient between the ports so a volume flow rate in the blood vessel is calculated using the formula known as Pousille's law:

$$Q=\frac{\pi\Delta \mathrm{P} r^4}{8\eta l} \qquad 3.1$$

Where Q is the rate of the blood flow, P is the pressure, r is the radius of the vessel, η is the fluid viscosity, l is the length of the vessel. This shows that the diameter of our blood vessel can cause dramatic changes to the flow rate of our blood. The SAW induced microfluidic systems, with the use of photolithography to construct channel geometries similar to our microvascular system, can be an ideal technique to generate blood flow velocities comparable to our blood vessel. This enables us to analyze protein folding dynamics, cell-protein and eventually cell-cell interactions within our blood vessel. One of the main advantages of SAW microfluidic flow chamber is that small volumes are required for our analysis. This becomes especially useful when working with expensive substrates such as purified protein or antibodies. The transparency of the SAW chip enables us to visualize and capture the dynamic events of cell-protein and cell-cell interactions during blood flow by video microscopy.

4.1.1 Shear-induced unfolding triggers adhesion of VWF fibers

We first wanted to investigate how SAW induced acoustic streaming could influence the hydrodynamic stress of proteins which are involved in the blood clotting process. The major protein identified for the blood clotting cascade is the protein von Willebrand factor (VWF). The purified VWF is a multimeric protein complex from the blood reveals

a molecular weight 250 kDA (44). It has a multimeric structure made up of 50-100 dimers (similar subunits of the protein linked together) which makes it the largest human plasma protein. As a response to blood vessel injury, this ultra large protein has the unique ability to unroll under shear from its multimeric complex into abrupt long fibers of a length up to 100 micron in solution (45). This mediates platelets adhesion to the subenothlium and to collagen at high shear rates (42). The monomer units of VWF contain domains which have specific functions (fig 2): The D1/D2 domain bind to factor VIII, the A1 domain binds to a glycoprotein complex on platelets, heparin and possibly collagen. The A3 domain binds to collagen and the C1 domain, in which the RGD domain binds to platelet integrin $\alpha_{IIb}\beta_3$ when this is activated. The hydrodynamic response of VWF has not been clearly elucidated, specifically how varying shear rates affects the conformational changes to the structure of the protein (41).

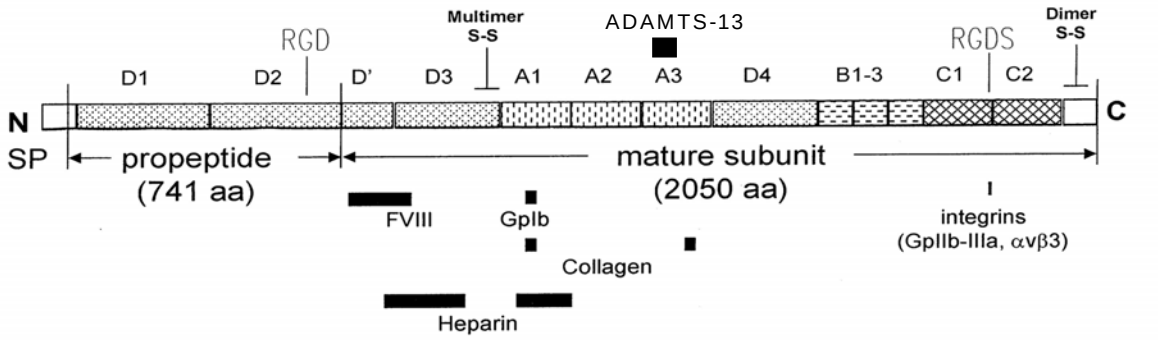

Fig. 2: Structure and functional sites of the VWF and the VWF propeptide. The right part represents the propetide-vWF which is about 741 amino acids long. The right part shows the monomer with the length of 2050 amino acids. The different scale bars designate the six different groups of domain structures .

Previous studies on DNA which have a size comparable to VWF, have shown an elongation when a shear rate of 30 s-1 was applied at a viscosity of 1cp. Recently, the hydrodynamic response of VWF was analyzed using our SAW microfluidic flow chamber with channel geometries similar to our microcirculatory system (small arteries and veins). The studies have shown an abrupt elongation to the VWF conformation resulting in fiber like extensions when a high shear (γ=5000s^{-1}) is applied. When no shear

is applied an immediate relaxation of the protein to the coiled state is observed (fig 3). These observations led to the understanding of the dynamic physical properties of VWF which gives insight to the functional role of this protein to vascular diseases (2, 45). This unique work has redefined protein folding from a mechanical viewpoint utilizing microfluidics(45). The stretching transition of VWF don't necessarily unfold biochemically but rather elongates and cross-links with other VWF fibers to increase the adhesive activity of this protein. This led to the motivation of my next topic which is to take a closer look if this mechanically activated protein plays a role in tumor cell adhesion in the blood vessel.

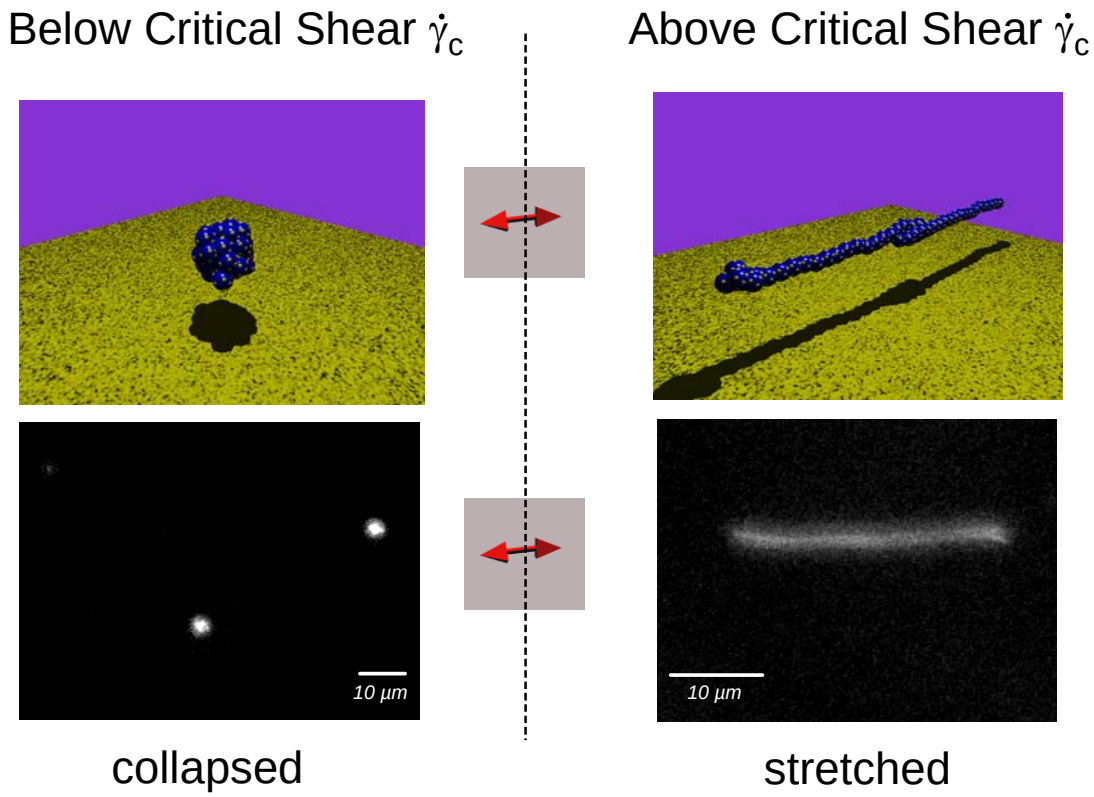

Fig. 3: Cartoon (upper panel) and selected fluorescence images of a video sequence (Movie S1, acquired at 25 frames a second) of VWF below and above the critical shear rate of a few thousands s^{-1}. Above $\dot{\gamma}_{crit}$, the protein is in an elongated conformation. The little yellow spots on the protein are meant to represent a variety of known binding sites. To assure that only unbound VWF was detected, the focus of the microscope was set approximately 10μm above the surface of the chip in the middle of the channel (courtesy Schneider et al PNAS 2007).

4.1.2 Tumor cell adhesion in blood

As mentioned, we wanted to determine whether shear dependent conformational changes to VWF can promote tumor cell adhesion. The onset of cancer begins when a normal cell transforms itself into a cancerous cell it then starts to replicate uncontrolled forming a tumor in the tissue. The tumor can be benign if these clump of cancerous cells lack the ability to spread. However malignant cancer cells can spread in two ways, either by invading the neighboring tissue or by implantation into distant sites by metastasis. During the process of metastasis, cancer cells can leave the primary tumor (intravasation) and be transported through the blood stream or through the lymphatic system until implantation (adhesion) onto the blood vessel or lymph vessel (1).

4.1.3 Background Cancer

The formation of cancer is caused by genetic abnormalities such as mutations to the DNA which codes for the proteins that regulate the cell cycle process. These mutations can transform a normal cell into a malignant one. The damage done to the DNA results in mutations to the genes that encode for proteins which regulate the cell cycle. The cell cycle pathway is controlled by genes that regulate cell growth called proto-oncogenes and discourages cell growth for DNA repair called tumor suppressor genes, when there are alterations to these genes it results in cancer. These are important for intracellular functions to control both the cell cycle and cell death (apoptosis). During cell proliferation, cells are stimulated to replicate and the process of apoptosis is blocked. However in cancerous cells the tumor suppressor gene becomes defective which results in uncontrolled cell division (1).

One of the serious forms of skin cancer is melanoma, it has a high metastatic ability at the early stages of this disease. Melanoma is developed in melanocytes (pigment producing cells) by long term exposure to ultraviolet radiation. The main UV radiation linked with the melanoma development has been the B spectrum (290-300 nm wavelength).

Typically the UV radiation affects the DNA stability causing genetic alterations to the oncogenes (n-ras, c-myc) and tumor suppressor genes (p53, p16) have been implicated in melanoma growth (24). The melanoma cells also have a high expression of antigens which are associated with invasion and metastasis. The most prominent antigen the integrin αvβ3 plays an important role in invasion and metastasis (24).

4.1.4 The Hydrodynamics of Cell Flow

The adhesion of melanoma cells to the blood vessels is determined by many factors, such as the key elements of the role VWF plays in the blood clotting process. The knowledge of the types of adhesion molecules expressed by the melanoma cells and the extracellular matrix proteins of the blood vessel are important for the physiological conditions of melanoma cell adhesion (26). Previous studies have shown that circulating melanoma cells must be able to arrest onto the extracellular matrix and stabilize their interactions which are initiated by integrins (34, 55). The shear rate close to the blood vessel is an important parameter which describes the interaction of melanoma cell to the vessel wall. For example, the adhesion of platelets to the subendothelial structures is determined by the shear rates close to the blood vessel wall because the transport of the platelets toward the vessel wall and the chemical reactions involved in the binding depend on these conditions (46).

The SAW induced microlfuidic flow chamber was employed incorporating these blood flow conditions to analyze tumor cell-VWF interaction. Our analytical system was simplified by choosing a buffer perfusion system and biofunctionalized microfluidic channels coated with collagen 1 and subsequently with VWF. Collagen which is well known to immobilize VWF (4, 19) are bundles of fibers made up of 3 polypeptide strands which acts as a strong adhesive binding protein to bind the connective tissue to strengthen our blood vessel. In our experimental setup, we wanted to investigate whether the ultra-large VWF fibers which are formed when a critical shear is applied can promote melanoma cell adhesion. An antibody directed against VWF was used to analyze whether melanoma-VWF interaction is specific. This is followed by taking blood serum from

healthy patients expressing ADAMTS13, it is a VWF cleaving protein found in blood which cleaves VWF rendering it inactive, to test if these ultra-large VWF fibers are necessary for melanoma cell adhesion under laminar flow (11).

4.2 Materials and Methods

4.2.1 Cells and culture

Human melanoma cell line, subclone A7 were grown using modified Eagles Medium cell culture medium (PAA, Germany). In preparation for the functional tests, cells were starved in serum-free medium overnight to reduce any residual effects of the serum in our adhesion studies, harvested in trypsin/EDTA buffer (Biochrom, Germany), and resuspended in Hepes/Tyrodes buffer, pH 7.4 (10mM Hepes, 140mM NaCL, 2.7 mM KCl, 0.4 mM NaH_2PO_4 x H_2O, 10 mM $NaHCO_3$, 5 mM dextrose). Hepes/Tyrodes buffer is an organic chemical buffering agent was chosen to resisit changes to the pH to maintain proper cell integrity. Also physiological bood has a pH of 7.4 which is important to regulate the chemical reaction between the blood and the endothelial cell layer and any major variations in the pH levels can lead to cell death. For each experiment, $MgCl_2$ (1mM) and $CaCl_2$ (1mM) are added directly before the superfusion assays.

4.2.2 Measurement of Cell Adhesion under Flow

Melanoma cell arrest was measured by real-time video microscopy. The SAW chip with a hydrophobic/ hydrophilic channel border was pretreated with collagen and then von-Willebrand factor (100µg/ml) (was unrolled or stretched under SAW. In figure 4 a model illustrating how a pre-coated collagen substrate anchors the stretched VWF under hydrodynamic flow. For the blocking of VWF in the channel, we used monoclonal anti-VWF antibody with a concentration of 127µg/ml (Acris). For the VWF cleavage study, plasma serum obtained from healthy patient was diluted 50% in Hepes/Tyrodes buffer. The channels are pretreated with the plasma serum under a constant shear flow (1000 s^{-1})

and then melanoma cell suspension is added to the channel. The cell suspensions were superfused at a shear rate starting at 1000 s^{-1} for 2 minutes. During the experiments the automated stage of the microscope (Zeiss, Germany) was directed to a predefined area of the channel to monitor cell flow, cell rolling and cell adhesion by capturing images at the same position. To quantify cell adhesion and cell rolling, images were analyzed by open box software. The given data represent a ratio between total cells adhering/total cells moving and total cells rolling/total cells moving ±standard error of the mean (SEM).

4.2.3 Antibodies and Fluorescence Microscopy Study

Fluorescence microscopy was used to analyze the unrolling or stretching phenomena of VWF under SAW, and to look at localization or adhesion of melanoma cells to a immobilized VWF on the channel during flow. Two important components for immunostaining for the analysis of VWF conformation are methanol to cross-link the intramolecular bonds to preserve the structure of the protein and antibodies to detect the protein fluorescently. Antibodies are Y shaped proteins produced by B-cells when there is foreign object (e.g bacteria) in our system. This leads to an inflammatory response where the antibody binds to the appropriate foreign object (antigen) to block the activity while the rest of defense mechanism destroys it. For biological applications specific antibodies (IgG) are produced in animals to elicit a response to the antigen (protein) being analyzed. The antibodies are purified from the animal and secondary antibody with a fluorescent tag designed to bind to the original antibody is used to identify a specific protein localized either in a substrate or tissue.

The protocol goes as follows: The hydrophilic channel of the SAW chip were then gently rinsed , cells and VWF protein were fixed with 100% methanol (20 min), blocked with 1%BSA in PBS (20 min), and then stained with monoclonal anti-VWF antibody with concentration of 2.54µg/ml (Acris) followed by a alexifluor 2° antibody. The SAW chips were then mounted onto a coverslip in anti-fade medium and stored at 4°C. The fluorescence images of the channels were analyzed using open-box software. Images are taken using a Zeiss Axiovert 100 microscope and a digital camera system.

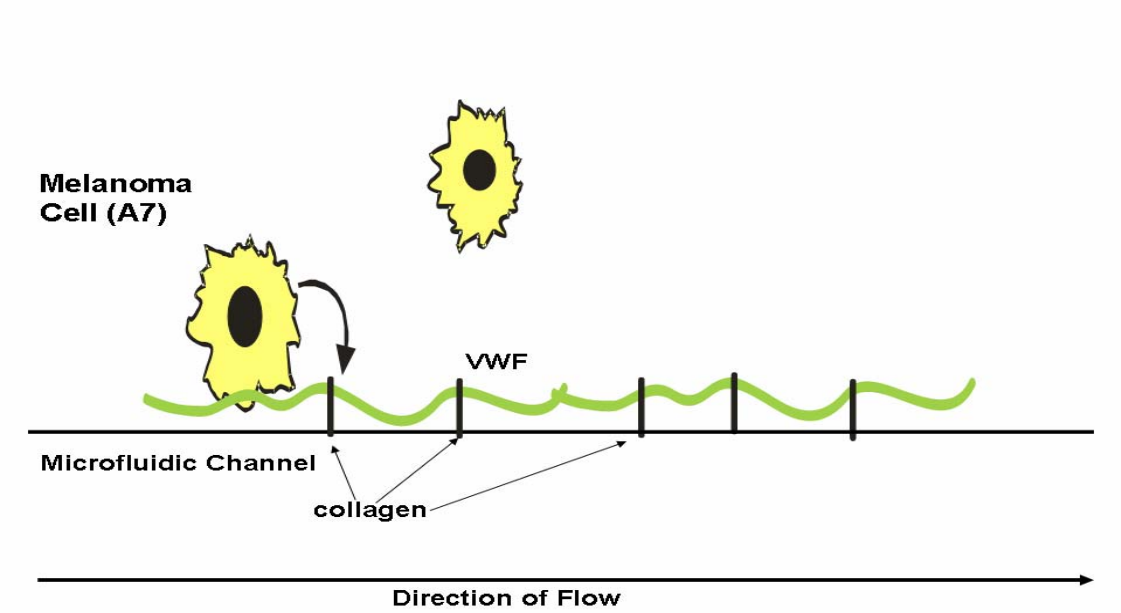

Fig. 4: A cartoon of melanoma cell superfused under a defined shear rate to a stretched VWF (green) adhered to a collagen coated surface.

4.2.4 Surface Acoustic Wave Chip

We use surface acoustic waves to effectively radiate acoustic energy into the two dimensional open channel. SAW can interact with the fluid layer confined to the hydrophilic channel inducing continuous laminar flow of the liquid. The typical channel length is a 40mm and a decay length of ~ 100µm, the pump basically acts as a point-like pressure source, driving the liquid to flow according to conservation of mass. Also low volumes are needed for our channel dimension the circular geometry shown in figure 5 requires a total volume of 8 µl.

4.2.5 Photolithography (hydrophobic/hydrophilic channels) on SAW chip

The SAW chips are layerd with SiO_2. The chips are silanized to create a hydrophobic monomolecular layer of Octadecyltrichlorsilan (OTS) which is mixed in hexane. The actual channel structure is then transferred onto a chip using standard lithography methods involving UV-Illumination and development of a photoresistant coating. The exposed silane is removed using oxygen plasma and the leftover photoresist is washed away by acetone. This forms a hydrophilic track on a hydrophobic substrate without any physical walls. By combining channel with the SAW nanopump described above provides a simple in vitro modem which allows us to observe cell protein interaction.

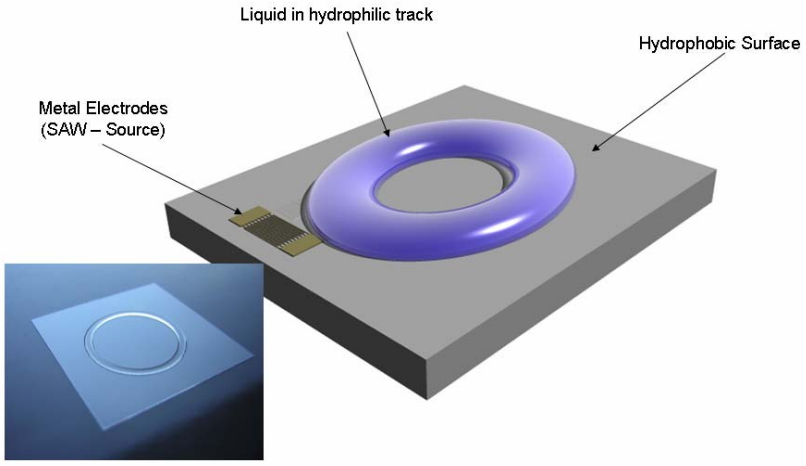

Fig. 5: The silianized hydrophobic layer on the SAW chip is only ~1 nm thick. After spincoating, UV illumination and oxygen plasma treatment, a planar hydrophilic channel (black) is left in a hydrophobic environment. If employing planar technology, there are basically no restrictions for the shape of the lane. (b) Water placed on the lane is confined to the hydrophilic region of the chip, forming a 'virtual' channel.

4.3 Results/Discussion

4.3.1 Model simulation of the SAW driven planar channels

To visualize the pattern of flow in our planar SAW driven flow chamber, we used a open channel simulation according to the raytracing approach described in [Frommelt07].

The modeling of the channel geometries, velocity and shear rates was performed by FEM lab simulations. Similar to previous SAW driven systems the interdigital transducers used to excite the surface acoustic waves are normal split IDT which are 26.5 um wide with 42 finger pairings. The floor geometry of the microfluidic track was extracted from the photolithography layout and then the shape of the water volume was determined by a computer program called a Surface Evolver. There the surface area of the channel is kept constant where the fluid rests. The free surface of the liquid volume is adjusted to minimize the surface energy which is created by nature. This shape of the liquid layer in the microfluidic track is imported into the raytracing program and the hydrodynamic solver Comsol Multiphysics. Parameters such as the fixed channel floor is modeled no slip and the free surface as slip boundary. Then the flow pattern induced by the acoustic streaming force is simulated and scaled to a maximum value of 1mm/s far away from the IDT. As usual, vortices are observed in the region where the SAW couples to the fluid but this doesn't disturb our investigations far away from the IDT (fig 7c)(15).

In order to measure the velocity profiles of melanoma cells from the point when their adhered or rolling to the channel floor to freely floating at regions in the 2D planar channel (total height 300 μm), a line graph plotting the velocities of the melanoma cells in relation to the height of the channel shows a linear increase in velocity until a plateau at the top of the water layer is reached (fig 7a). We then took a closer look at our rectangular microfluidic track from a cross-sectional viewpoint of a semi-circular shape of the water layer which is confined to the hydrophobic/hydrophilic channel border (fig 7b). In fig 7c a flow profile of the liquid layer in the region of the channel (fig 7c) away

from the IDTs to prevent the secondary effects of SAW. The colors show the velocities of the liquid layers and the shear rates to the dimensions of the 2D channel geometry (fig 7e).

a)

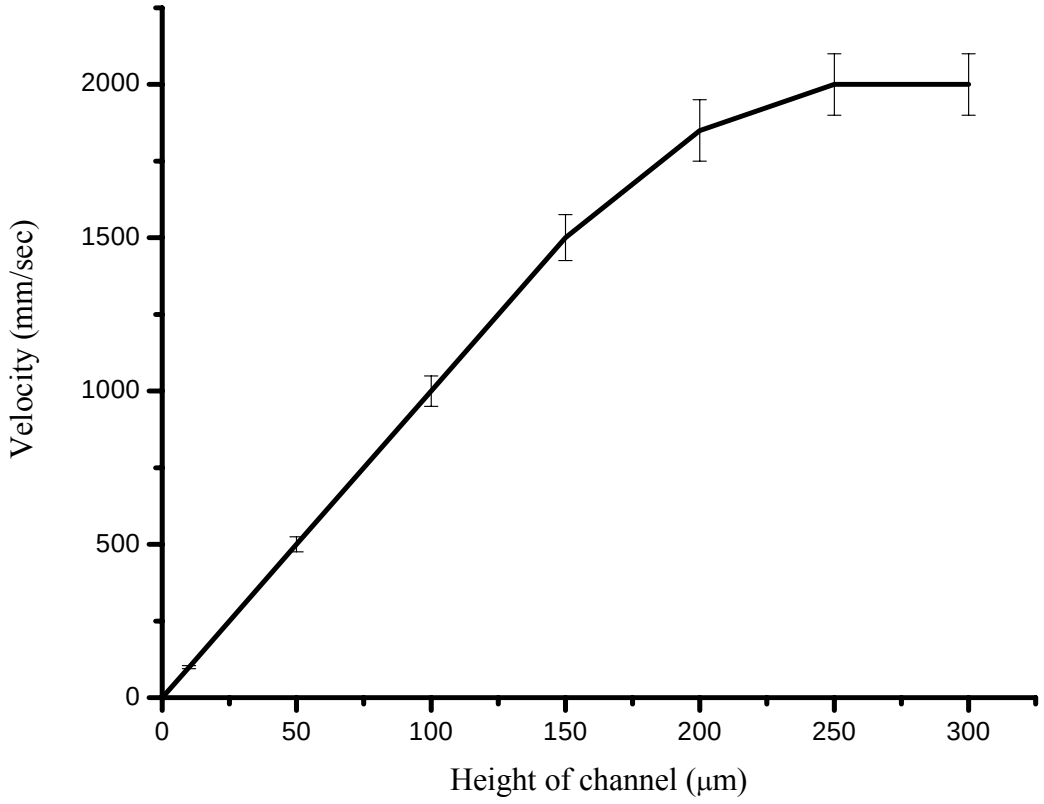

Fig. 7a: A line graph plotting the velocity distribution in relation to the height of the fluid layer from the floor to the top in the 2D planar channel. The total height of the water layer is 300 μl so there is a linear increase in velocity until it levels off near to the top.

b)

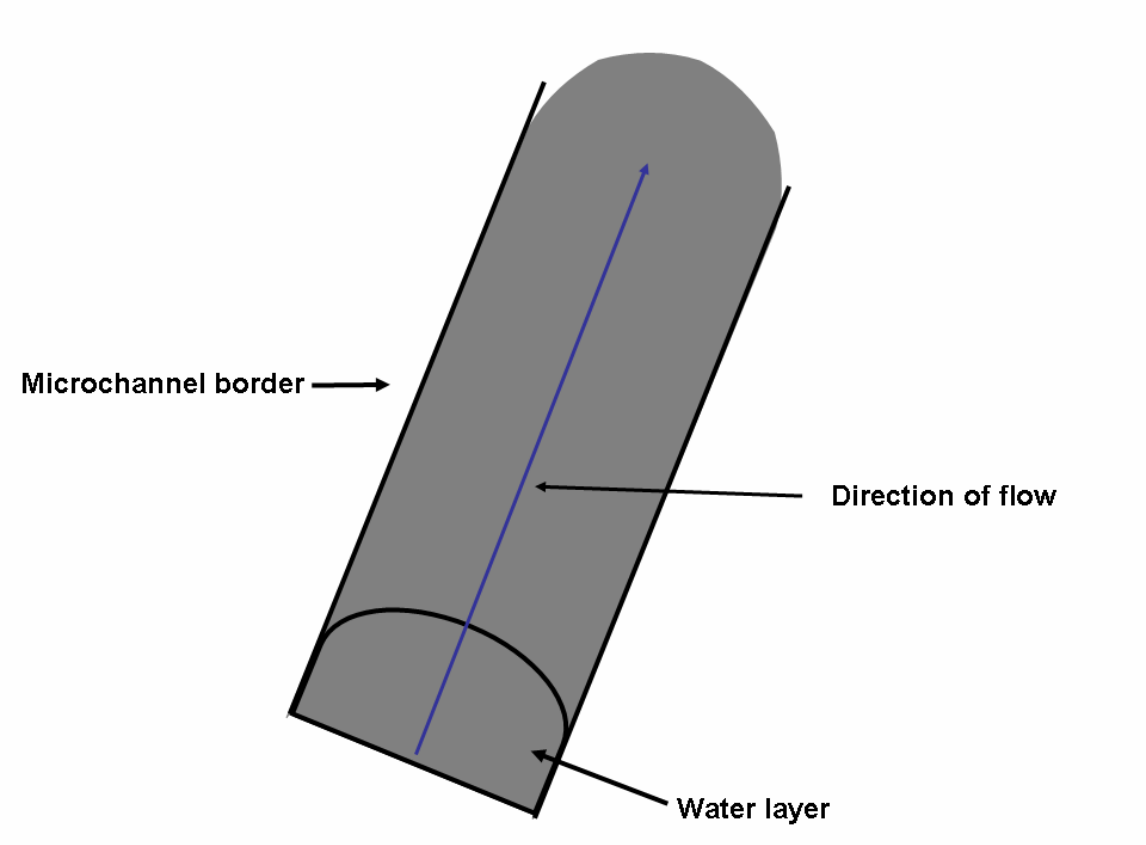

Fig 7b: A schematic model showing the shape of the water layer confined to the hydrophilic/hydrophobic channel border. An external pumping system such as SAW can drive the fluid layer.

c)

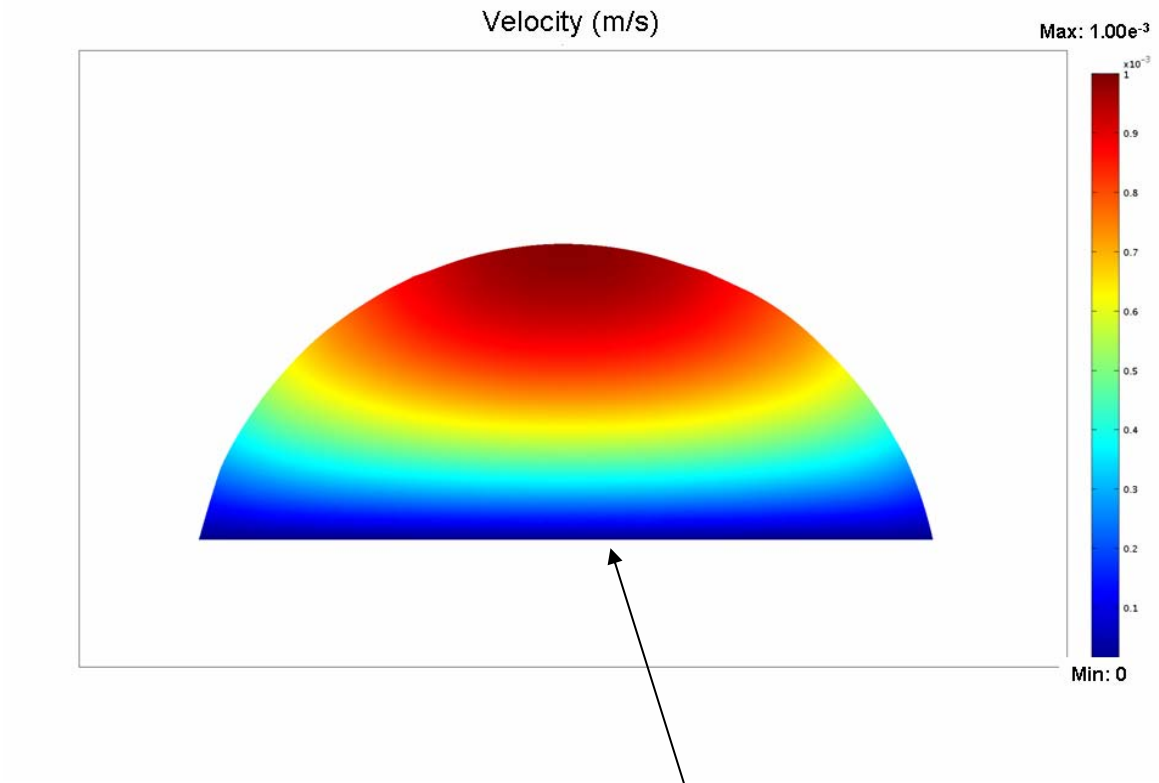

d)

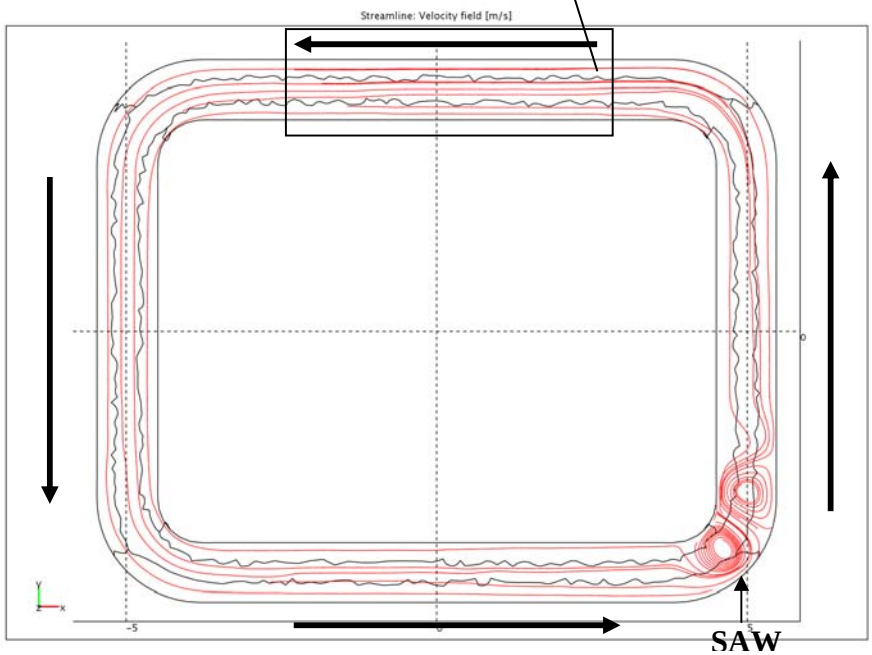

Direction of Flow

e)

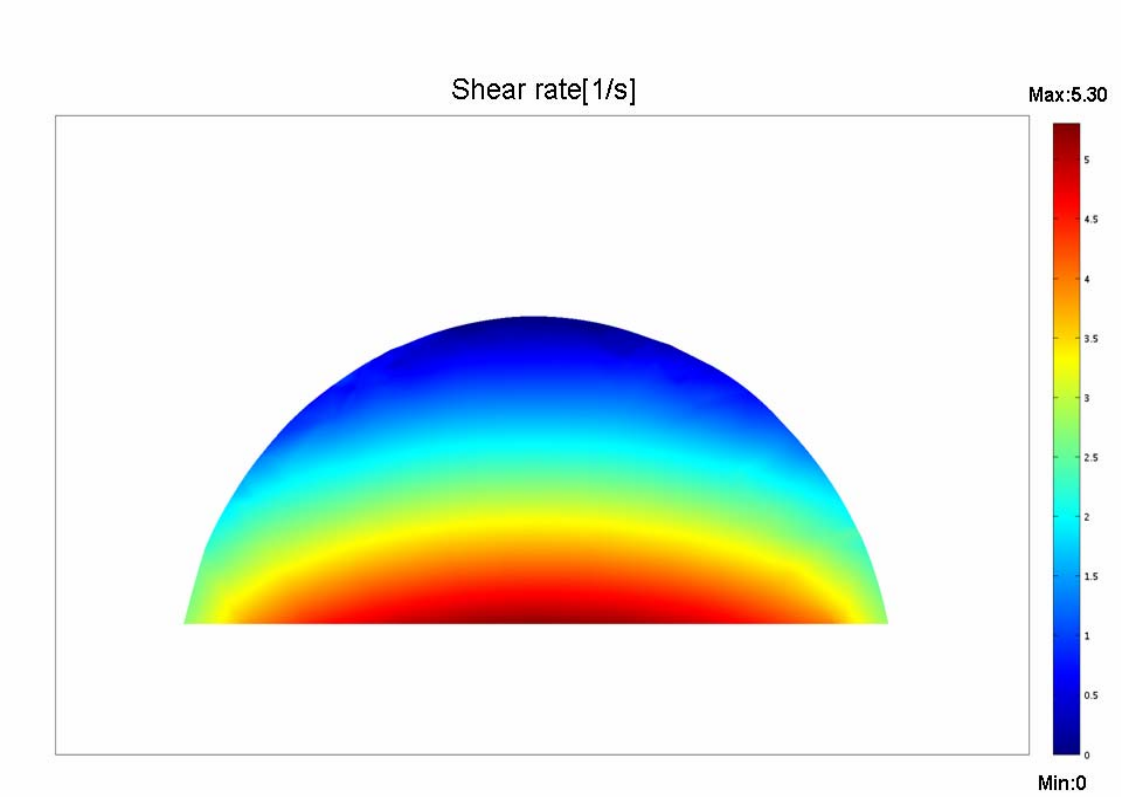

Fig 7: c) A flow profile at the mid-region of the channel (red) shows a maximal velocity of 1mm/sec. Due to the planar nature of our hydrophobic/hydrophilic channels a curved cross-sectional profile is shown of the fluid layer as shown from fig 7b which is captured from the (d) region of the channel where there is laminar flow and no secondary effects of SAW. The transducers are placed in the corner of the channel to optimize the continuous flow racetrack. Note that slip conditions exist at the sides of the fluid layer and the surface and no slip at the bottom of the channel. e) A shear rate in relation to the height of the fluid layer from the surface of the channel is visualized (courtesy T Frommelt).

4.3.2 Stretching of VWF using Acoustic Induced Shear Flow

Immunofluorescent images were taken to capture the conformational changes VWF undergoes during an applied shear. On a collagen coated surfaces without exposure to shear stress (fig 6c) and after exposure to shear stress >1000s^{-1} for 5 minutes (fig 6a). Clearly, VWF undergoes a collapsed - stretched conformation including the formation of a protein network. As a result an increase in melanoma cell adhesion is visualized once the VWF has formed a network. A representative immunofluorescent picture shows that the adhesive ability of VWF increases during the network formation promoting melanoma cell adhesion as evidenced by fig 6b. The melanoma cells seem to attach to the threadlike or unrolled regions of the VWF rather than the globular regions of the protein.

a)

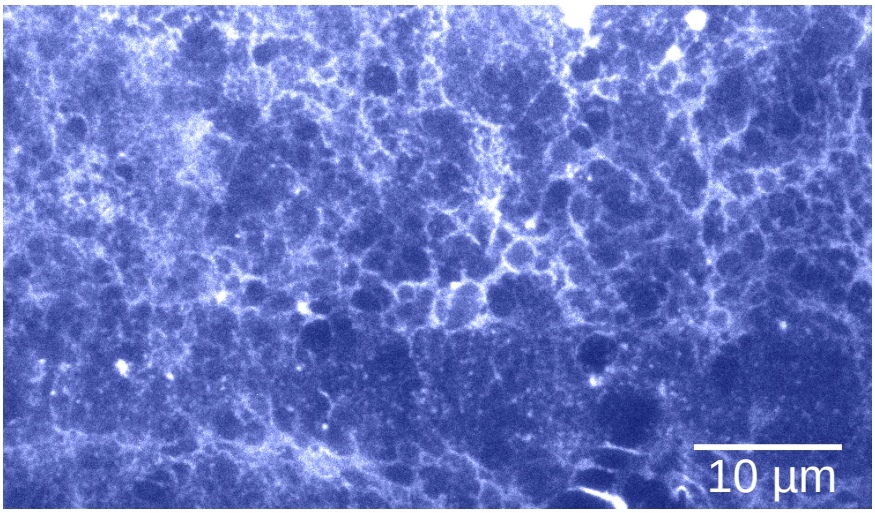

Fig. 6a: An immunoflurescent picture showing SAW induced unfolding of VWF to form network fibers.

b)

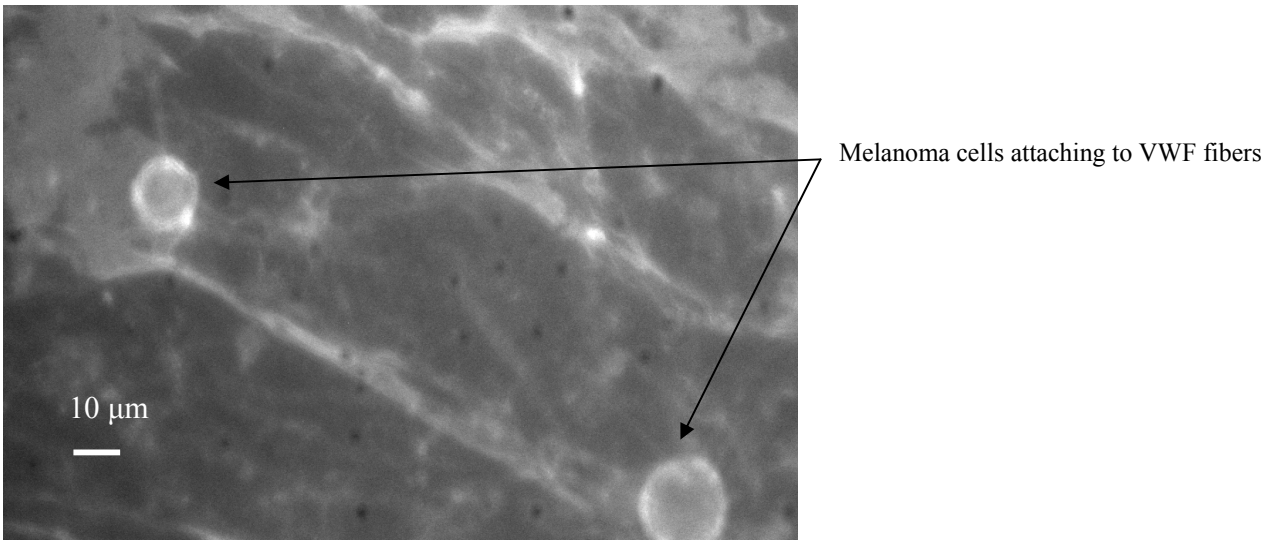

Fig. 6b: An immunofluorescent picture showing melanoma cell adhesion to an unfolded VWF

c)

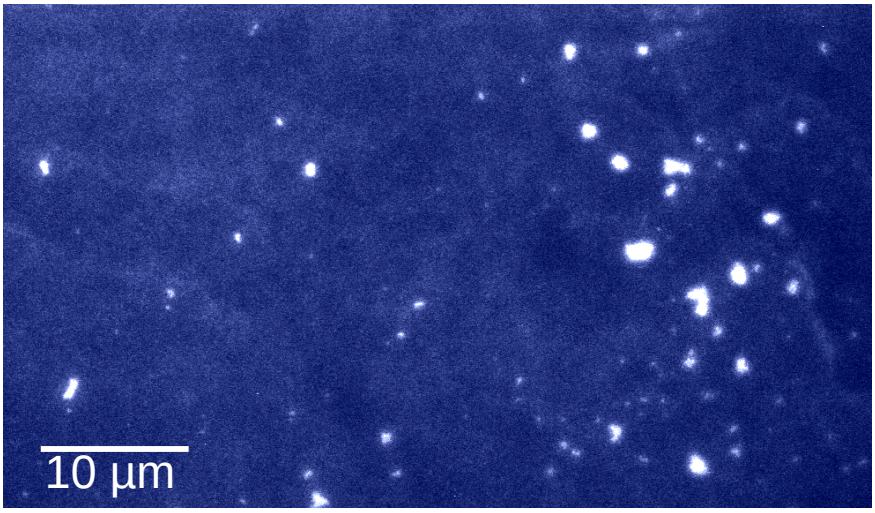

Fig. 6c: A globular clusters of VWF under static conditions (no shear applied) visualized by fluorescence

4.3.3 Melanoma Cell Adhesion and Rolling to VWF under Acoustically Induced Shear Flow

To analyze the adhesion and rolling mechanism of melanoma cells on VWF plus collagen and collagen alone (control), we applied different shear rates and monitored the cell activity under laminar flow generated by acoustic streaming. The melanoma cells were suspended in Hepes/Tyrodes buffer and superfused under a shear rate of $\geq$1000 s^{-1} for 2 min. The shear rate was quantified by measuring the flow velocities of cells in relation to the distance of the channel. The graphs were analyzed according to the ratio of cells moving to cells adhering and cells moving to cells rolling. The cells moving were construed as cells which were freely floating within the channel with velocities ranging between 10,000-600 μm/sec. To measure cells rolling, we monitored cells which were touching and rolling along the surface of the channel but not adhering. The velocity profile for rolling cells ranged from 100-10μm/sec. The cells which arrested completely to the channel had no velocity measured.

Both rolling and adhesion are important parameters when observing melanoma cell adhesion to the protein substrate (16). Depending on the type of protein analyzed, rolling is a prerequisite to adhesion so melanoma cells in motion are able to "put on the brakes" until firm binding at a selected region of the microchannel where the protein is localized has happened. For the VWF treated channels there are an increasing number of cells rolling and arresting to the surface matrix as the perfusion continues under different shear rates. We hypothesize that the abrupt rolling and adhesion of melanoma cells observed in our microfluidic track could be a result of the exposure of the secondary structure upon VWF stretching which is well known to attract platelets. Recent studies have shown that the binding of platelet GP Ibα to the VWF A1 enables a firm binding to the exposed thrombogenic surfaces on the vessel wall (42). The collagen (without VWF) treated channels showed less attachment and rolling. As mentioned previously, collagen is a natural binding agent for VWF. A possible assumption is that collagens role in melanoma

cell adhesion in blood flow conditions is minimal due its role as an adhesive protein in the extracellular matrix to maintain the structure of the blood vessel, while VWF increases its adhesive ability as it unrolls to bind melanoma cells as well as platelets under high shear flow conditions.

4.3.4 VWF mediates Melanoma Cell Arrest

We next examined to see if the VWF is primarily responsible for the arrest of melanoma cells. In our first set of experiments we added melanoma cells under a shear rate of 1000 s^{-1} to collagen and collagen + VWF treated channel. An increase in rolling and adhesion increased for the VWF treated channels. Rolling is increased from ~2% (SEM ± 1.07%, n=5) for the collagen-only coated surface to ~20% (SEM ± 3,52 %, n=5) for the VWF coating. Results for adhesion are less pronounced but a significant increase between ~1% (SEM ± 0.36 %, n=5) and ~8% (SEM ± 2.67 %, n=5) is still observed, demonstrating the role VWF may play in mediating melanoma cell adhesion under flow conditions. In the following studies, the unrolled VWF in collagen was then superfused with a monoclonal anti-VWF antibody for 5 min to completely block the activity of VWF. As the VWF gets stretched to form these ultra-large fibers an antibody directed against the full length sequence of the protein was chosen to assure complete blockage. As melanoma cells were superfused to the antibody treated channel showed less attachment and rolling compared to the groups which had a functional unrolled VWF under high shear rates ($\geq 1000s^{-1}$). The graphs show no significant difference in cell attachment or rolling compared to control levels (fig. 8a). This confirmed our expectations that VWF is the cause for specific binding events which can trigger melanoma cell adhesion. This study gives insight that specific binding between VWF and melanoma cells could be regulated by the conformational changes VWF undergoes as it form these fiber-like networks from an applied shear ($\geq 1000s^{-}$).

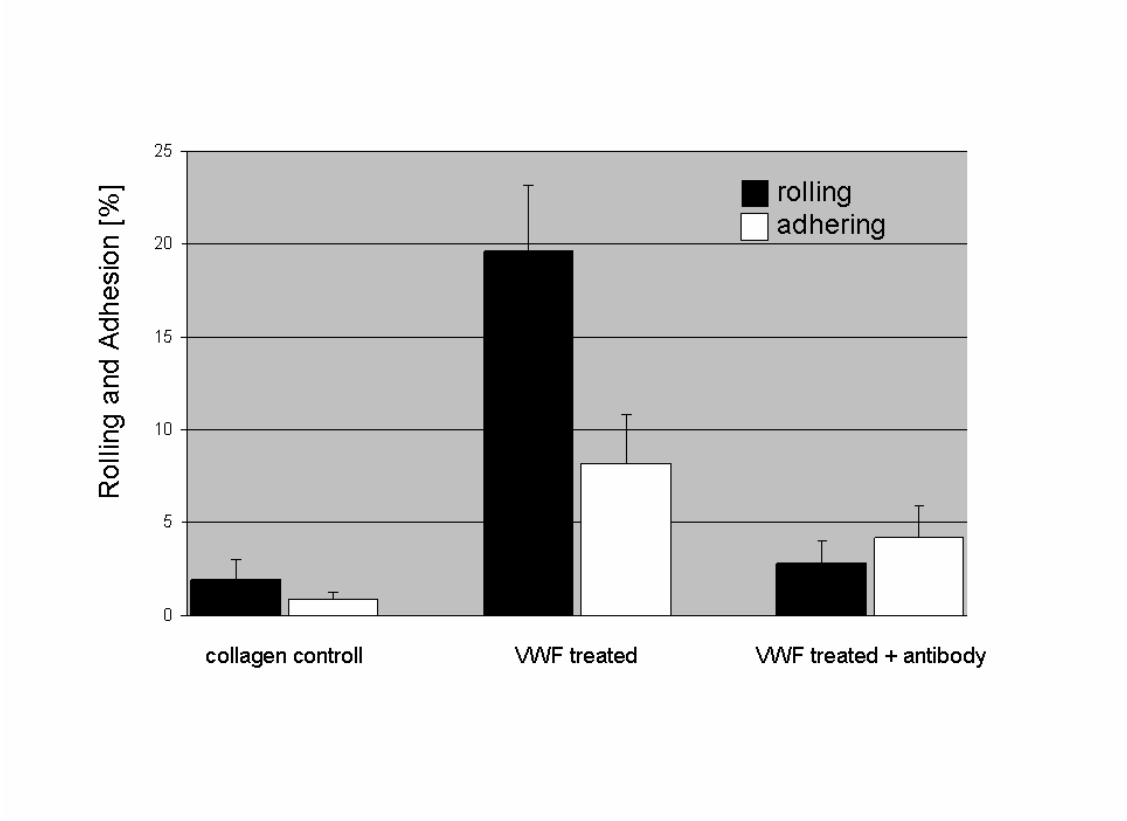

Fig. 8a: Percentual Melanoma cell rolling and adhesion to collagen (control), VWF and VWF+ antibody coated surfaces at shear rates around 100 s^{-1}.

4.3.5 Protease Cleavage of VWF affects Melanoma Cell Adhesion

To test to see if ADAMTS13 mediated cleavage of VWF from its ultra-large size into smaller fragments would affect melanoma cell adhesion, plasma serum was obtained from the blood of a healthy patient. The concentration of ADAMTS13 in the blood is 0.5-1 µg/ml. Previous studies have shaown that ADAMTS13 as it circulates through the blood stream docks onto the A3 domain of the large multimeric complex of VWF to initiate the cleaving step of VWF (11)(fig 8c). Typically our blood regulates the activity of VWF once the injury to the blood vessel is mended the ADAMTS13 is signaled to deactivate VWF (11). Deficiency to the expression of ADAMTS13 can result in abnormal blood clotting diseases.

To mimic the role ADAMTS13 plays in our blood we unrolled VWF on a collagen coated channel for two minutes. The unrolled VWF on collagen was superfused with a 50% diluted serum in Hepes/Tyrodes buffer for 2 minutes. A constant shear rate of 1000 s^{-1} was applied to monitor VWF cleavage under flow. In fig 8c we see complete cleavage of the ultra-large VWF fibers into smaller fragments after a two minute incubation period. The plasma serum was diluted in Hepes/Tyrodes buffer to maintain the activity of the protease. In a similar trend, we see less attachment and rolling of melanoma cells (fig 8b) to the collagen control studies. Therefore, a large multimeric complex of the VWF is necessary for melanoma cell adhesion.

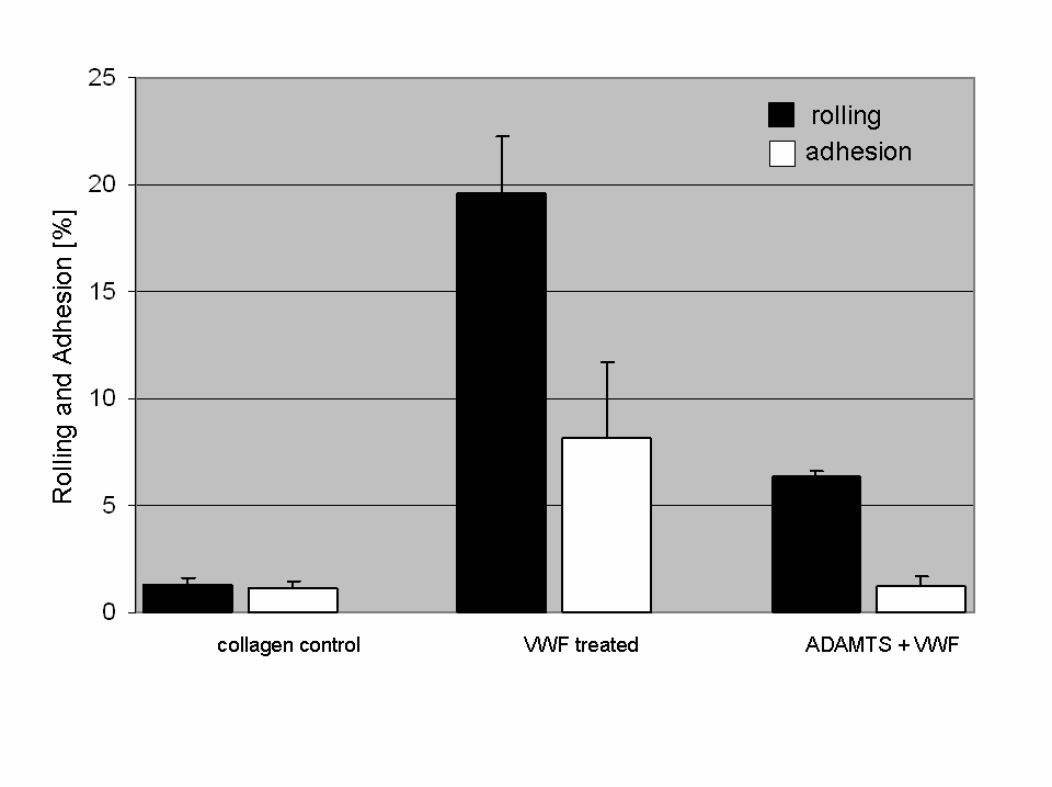

Fig. 8b: Percentual Melanoma cell rolling and adhesion to collagen (control), VWF treated (as in Fig. 4a) and VWF, which was treated with ADAMTS-13 at shear rates around 1000 s^{-1}.

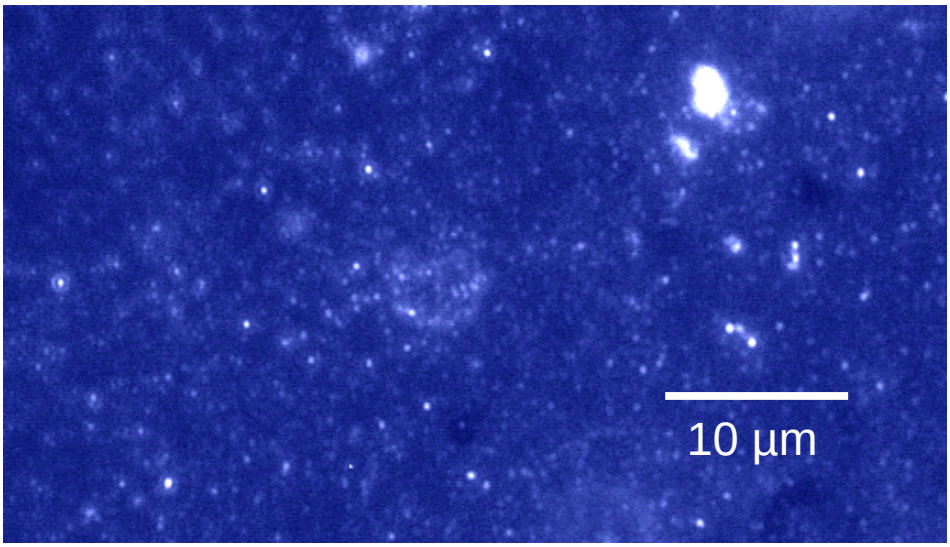

Fig. 8c: An immunofluorscent image of VWF cleaved by ADAMTS-13. Note that the ultra-large fibers have been cleaved into smaller fragments inactivating VWF.

4.3.6 Rolling and Adhesion under Oscillatory Flow – Role of the coiled – stretched transition of VWF

From the previous experiments we observe that the ultra-large VWF fibers are necessary for melanoma cell adhesion and when we block with an antibody directed against VWF it inhibits melanoma cell adhesion. Also the cleavage of the ultra-large fibers by ADAMTS13 also shows a similar inhibition of melanoma cell adhesion to VWF. The natural progression is to directly test whether VWF conformational changes as a result of oscillating (high and low) shear rates would promote melanoma cell adhesion.

An oscillatory flow experiments was performed to test this hypothesis. To perform the oscillatory flow experiments VWF was immobilized to the collagen coated microfluidic channel similar to the previous studies. This time, however, we start our measurements under static conditions where VWF is known to exist in its collapsed or coiled state shown in figure 9. We applied high (6000 s^{-1}) and low (100 s^{-1}) shear flow to measure the

average percentage adhesion after each cycle. As a result of the varying shear rates (high to low) the VWF fibers become gradually stretched and immobilized to the collagen substrate until complete saturation (fig 6a). The percentage of adhered cells for each cycle was always calculated with respect to the total number of cells “freely” floating right after the high shear flow was turned off. In other words, already adhered cells were not included in the calculation of the adhesion percentage. These experimental findings clearly demonstrate the role of VWFs conformation in mediating melanoma cell adhesion considering that the total adhesion increases roughly 7 times more when is exposed to oscillating hydrodynamic stress.

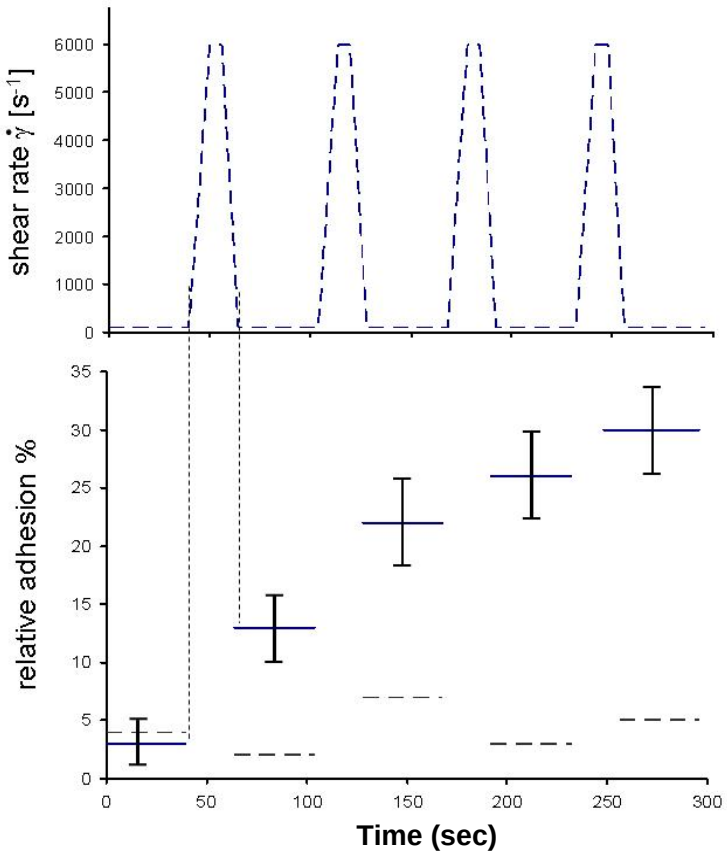

Fig. 9: Adhesion under oscillatory flow. The upper graph depicts the applied oscillating shear flow in the microfluidic channel. The shear rate was varied between $100s^{-1}$ (low) and $6000s^{-1}$ (high). During high shear flow, no rate of adhesion was calculated (see two vertical dashed lines). Lower graph: after each cycle of high shear, the percentage in adhesion was measured. Clearly, the adhesion increased with each cycle, indicating that the number of stretched and therefore exposed and active VWF fibers raises gradually. In the control experiments (dashed line) no VWF was present.

4.4 Summary

The work presented here is apt to reveal the interaction of melanoma cells with von Willebrand factor (VWF) under hydrodynamic flow using a novel planar surface acoustic wave (SAW) driven microfluidic flow chamber. The successful employment of this device allows to mimic our microcirculatory system by driving fluids along (bio) functionalized microchannels with velocities comparable to blood flow in smaller blood vessels. The benefit of the 2D planar design of the SAW chip is that any channel geometry can be designed to model the size of our blood vessels without the aid of cumbersome materials (tubing, valves etc) to control the fluid flow.

The new SAW microfluidic flow chamber has enabled us to study the mechanical properties of protein stretching under hydrodynamic flow and to show the impact of the shear dependent conformational state of VWF on melanoma cell binding. Under high shear flow, when VWF is in the stretched conformation, melanoma cell adhesion is significantly increased when compared to the coiled conformation present under low flow conditions. This is confirmed by antibody studies by blocking the stretched VWF conformation where less melanoma adhesion is measured. Under physiological conditions ADAMTS13 obtained from blood serum was added to cleave the stretched VWF into smaller fragments also showed less melanoma cell adhesion. The final confirmation as shown by the oscillating flow experiments shows that as VWF unrolls from its natural globular conformation to form into a network of fibers a gradual increase in melanoma cell adhesion is observed, showing for the first time that melanoma cell adhesion is promoted by the conformational changes of VWF under hydrodynamic flow from its coiled to the stretched configuration.

Chapter 5

Acoustic Streaming as a Model System for biological applications

"VWF initiates Melanoma Cell Binding to Endothelial Cells"

5.1 Introduction

We have successfully shown that the SAW planar flow chamber as a new in-vitro model can analyze melanoma cell adhesion to VWF, subsequently we wanted to look at a model which gives us a more realistic scenario of VWF release and stretching phenomena that occurs in our blood vessel. In order to tackle this problem we selected a cell line to layer the microchannel surface to mimic the blood vessel wall. The cell layer chosen for these studies are endothelial cells extracted from the luminal region of the endothelium. The endothelial cells regulate the materials taken in and out of the blood stream as well as secreting VWF to control the blood clotting mechanism. Since VWF acts as a mediator of melanoma cell adhesion as shown by our planar SAW device, we wanted to take a closer look at how melanoma cells under controlled shear flows interacts with the endothelial cell substrate.

The endothelium is a thin layer of cells that line the interior of our blood vessel. It is the interface between the blood and rest of the vessel wall. Once there is an injury or inflammatory response to the blood vessel, VWF which is packaged and stored in secretory vesicles (Weibel-Palade bodies) within the cytoplasm of endothelial cells is secreted to the blood vessel wall (6). A complex set of signaling events are undertaken prior to the release of VWF, one substance histamine (a biogenic amine) is an agonist which is released by mast cells due to an inflammatory response into the bloodstream. Once histamine is released into the blood stream it can bind to H1 and H2 receptor expressed on the endothelial cell layer which stimulates the release of intracellular Ca^{2+} from its calcium stores to induce Weibel-Palade activation and secretion of VWF (6) (fig

1). The objective of these experiments was to test whether our SAW microfluidic chip can efficiently simulate this physiological conditions of blood flow in smaller blood vessels (3, 26). An in-vitro cell-cell assay was designed to analyze whether a cultured endothelial cell layer once stimulated (with the aid of histamine) can release VWF to enhance melanoma cell adhesion under flow.

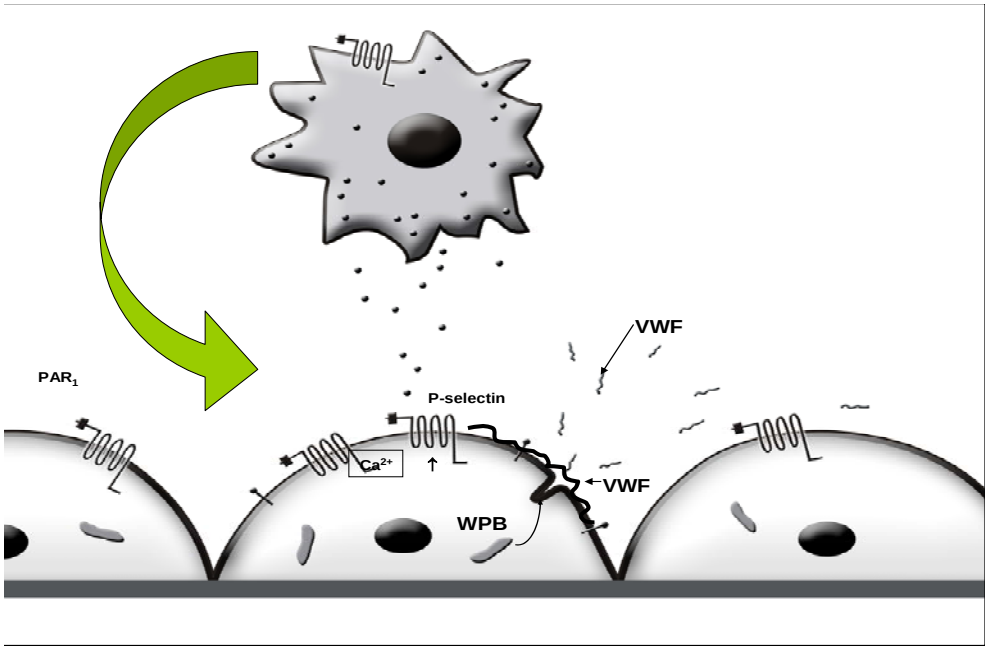

Fig 1: A cartoon illustrating an endothelial cell layer releases VWF upon stimulation of the Weibel-Palade bodies. Note that VWF fragments are released into the blood stream and these ultral-large fibers are attached onto the endothelial cell membrane (courtesy S Schneider).

5.2 Materials and Methods

5.2.1 Endothelial Cell culture

Endothelial cells were obtained from human umbilical veins (HUVEC). The endothelial cells were resuspended in medium 199 (invitrogen life sciences, Munich, Germany) containing 20% heat-inactivated fetal calf serum (Biochrom, Munich, Germany) and 0.2

mM L^{-1}) of l-glutamine (Biochrom, Munich, Germany), and plated on a culture dish coated with 1% gelatine.

5.2.2 PDMS Microfluidic Flow Chamber coupled to the SAW device

For the structuring of the PDMS microfluidic channel networks, PDMS is poured into a mold consisting of a metal master crafted as a rectangular racetrack similar to the planar channel. In fig 2a is a schematic model showing the PDMS channel structure with PDMS walls containing the fluid layer onto the channel with an open surface on top. The dimensions are w=500μm wide and L=40mm long channel in the shape of a rectangle with rounded corners. The PDMS is coupled to the SAW device to monitor the cell flow and to determine the functional integrity of fluidic channels under video microscopy.

5.2.3 Culturing Endothelial and Melanoma Cells on PDMS

In order to fabricate a blood vessel, endothelial cells were cultured in a PDMS microchannel bound to a glass surface which is directly coupled to our SAW chip. The cells were trypsinized and resuspended in fresh new media. In order to culture cells onto the PDMS channel structure, we first rinse the channel with 1% BSA to prevent cells attaching to the walls of the PDMS and then rinse with PBS++. We then add the cells onto the channel and let culture overnight in cell culture media as described above, until a confluent layer is formed.

The benefit of using PDMS for cell culturing is that the membrane passes gas easily and good chemical stability. The 2-D planar device was not employed for these studies due to the effects of the protein rich media on the hydrophobic/hydrophilic interface as it adsorbs onto the hydrophobic side affecting the channel dimensions. Endothelial cells along with melanoma cells are cultured directly onto a structured PDMS slab which has been sealed to a glass surface. Many cell types can be cultured in the PDMS channel without affecting its structural integrity. The PDMS channel is submerged in cell culture

media to prevent dehydration which can affect the pH and salt concentrations. Prior to the onset of our studies, the cell culture media was replaced by Hepes/Tyrodes buffer to prevent any influence of the protein affecting the adhesion studies.

5.3 Results/Discussion

5.3.1 Model simulations of PDMS Microchannel coupled to SAW Device

The PDMS channel was simulated in three dimensions similar to the Y-branch structure (chp 2)(50). We modeled a narrow region of acoustic streaming force driving the fluid at the inlet. Then we determined stable and unperturbed shear rates and velocity distributions far away from this region. The three fixed walls are modeled no-slip and the free surfaces (channel ceiling) as slip boundary. Again the flow pattern is scaled to a maximum velocity of 1mm/s to all for comparison with the free microfluidic track (15).

Simulations were made to visualize a cross-sectional fluid flow in the PDMS microchannel. In Fig 2b shows a velocity distribution (shown by color) of the fluid layers within the PDMS channel geometry where no-slip boundary conditions exist near the borders and the surface of the channel. The mid-region of the channel shows a flow profile similar to the planar SAW flow chamber. The shear rates are then calculated relation to the channel dimensions (fig 2c).

a)

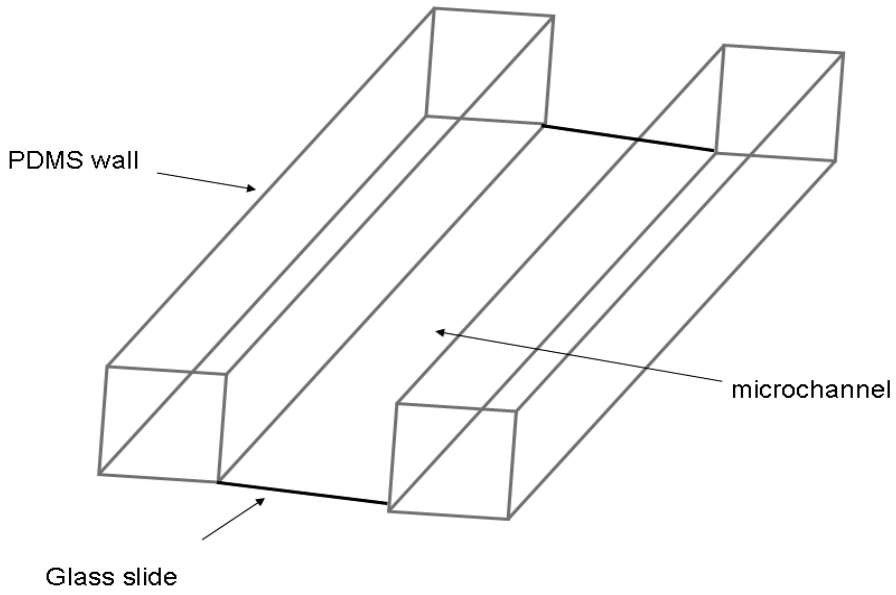

Fig 2a: A schematic diagram of the PDMS microfluidic flow chamber. PDMS walls provide the boundary to confine the liquid layer to the microfluidic track.

b)

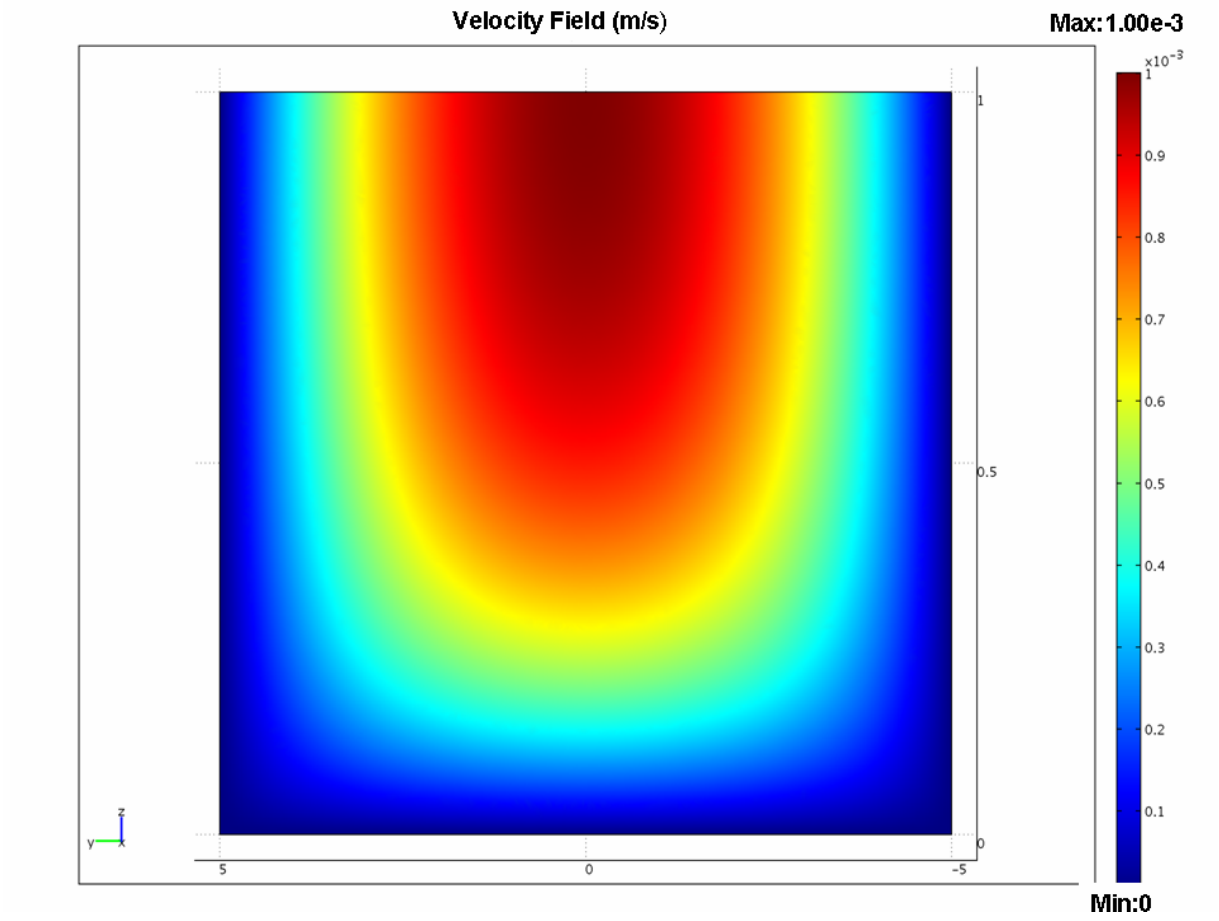

Fig. 2b: A cross-sectional flow profile (velocity 1mm/sec) in a PDMS microfabicated channel from the floor of the channel to the top. The maximal velocity shown in logarithmic scaling is 10^{-3} m/sec (red color) (Note that the no-slip boundary conditions near the walls and the bottom of the channel where the flow is zero (blue).

c)

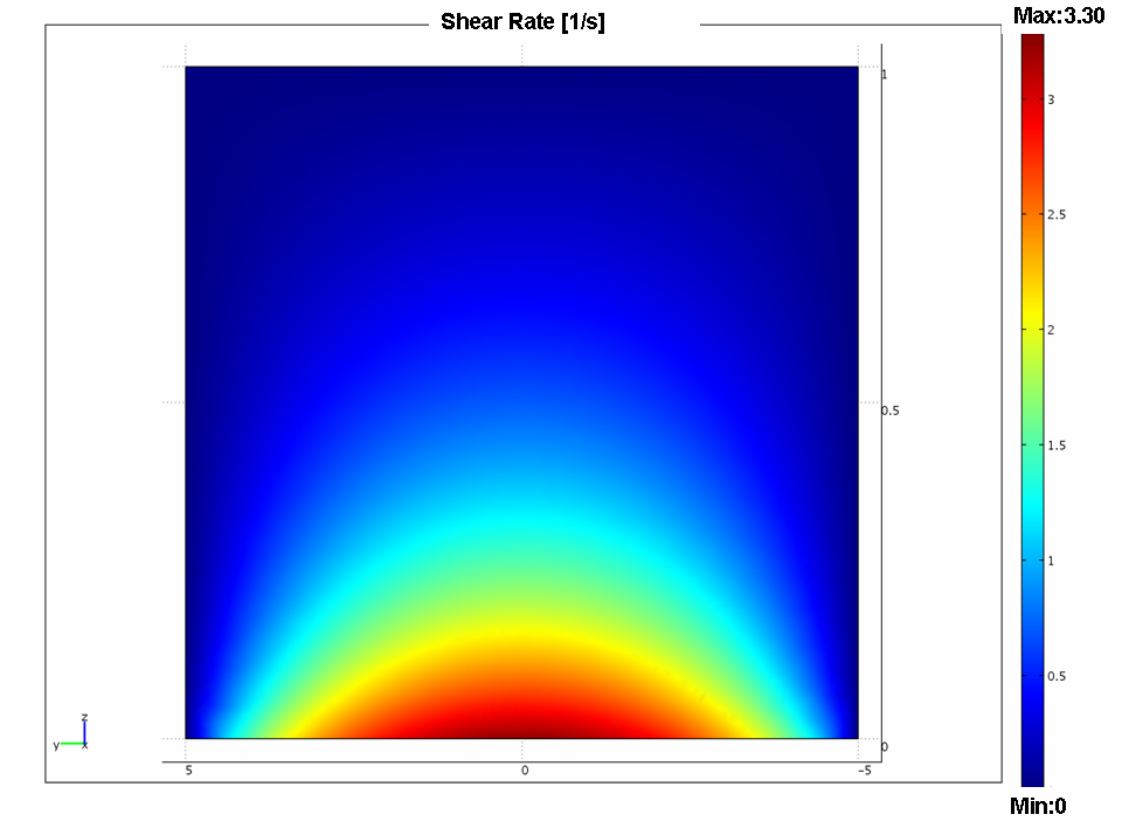

Fig 2c: The shear rates are measured in relation to the height of the channel.

5.3.2 Cultivation of Melanoma and Endothelial Cells to PDMS Channels

Once the PDMS microfluidic chip was completed, we successfully cultivated both melanoma and endothelial cells on the floor of the channel which consists of a glass surface. The cells were retained within the boundary of PDMS channel walls and did not grow on the walls or outside the channel, the cell culture media does not affect the tight seal formed between the PDMS and glass surface. This is evident by the sharp line marking the channel wall (fig 3). The confluent monolayer of melanoma and endothelial cells on the channel floor shows that the cells are healthy, divide readily and are securely attached.

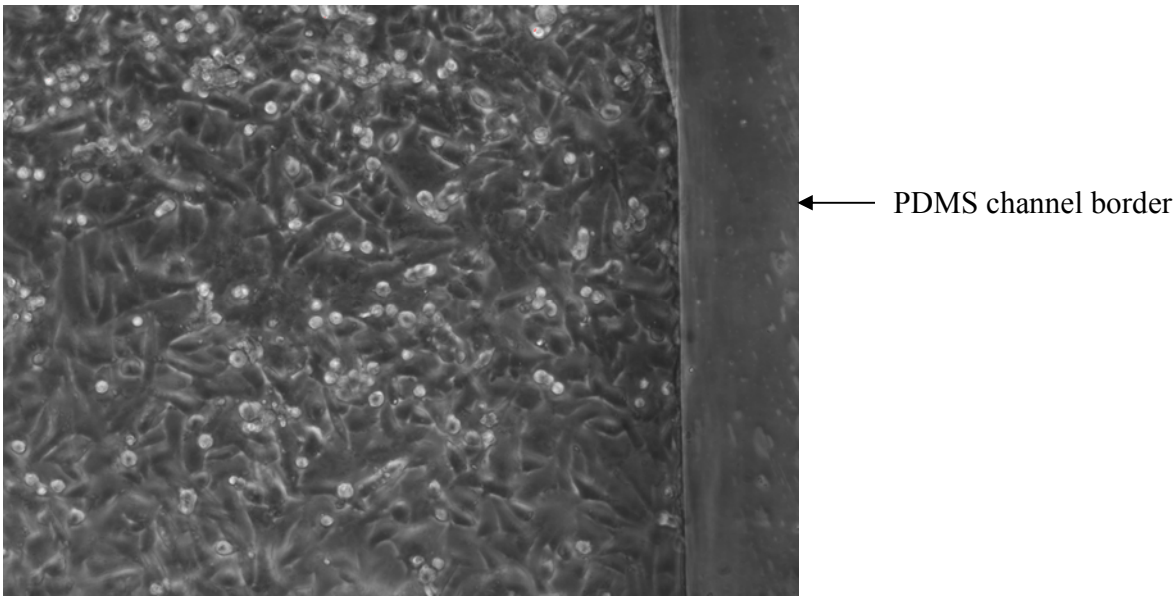

Fig. 3: Picture of a confluent layer of melanoma cells grown in a PDMS channel

5.3.3 Histamine stimulated Endothelial Cells release VWF to bind Melanoma Cell

To demonstrate the applicability of the SAW driven microfluidic system as an alternative to conventional flow chambers, melanoma cells superfused to a cultured endothelial cell layer was tested under a defined shear rate. A series of snapshots were taken during an experimental study to show two melanoma cells (circled) flowing over an endothelial cell layer at three different time points (0, 1 and 2 seconds) (fig 4). The transparency of the PDMS channel and the SAW chip enables us to track cells which are flowing, adhering, and rolling either qualitatively and quantitatively analyzed similar to our previous studies. Note that the underlying layer of cells are not detached from the surface from the applied shear rates and does not change the overall shape. To test if the viability of the endothelial monolayer was affected by SAW, tryphan blue vitality staining was applied. If the cells are healthy the blue dye does not permeate the membrane, for damaged cells an apparent infiltration of the blue into the cytosol is visualized. The cells seem unaffected by SAW ensuring monolayer integrity during the cell assays.

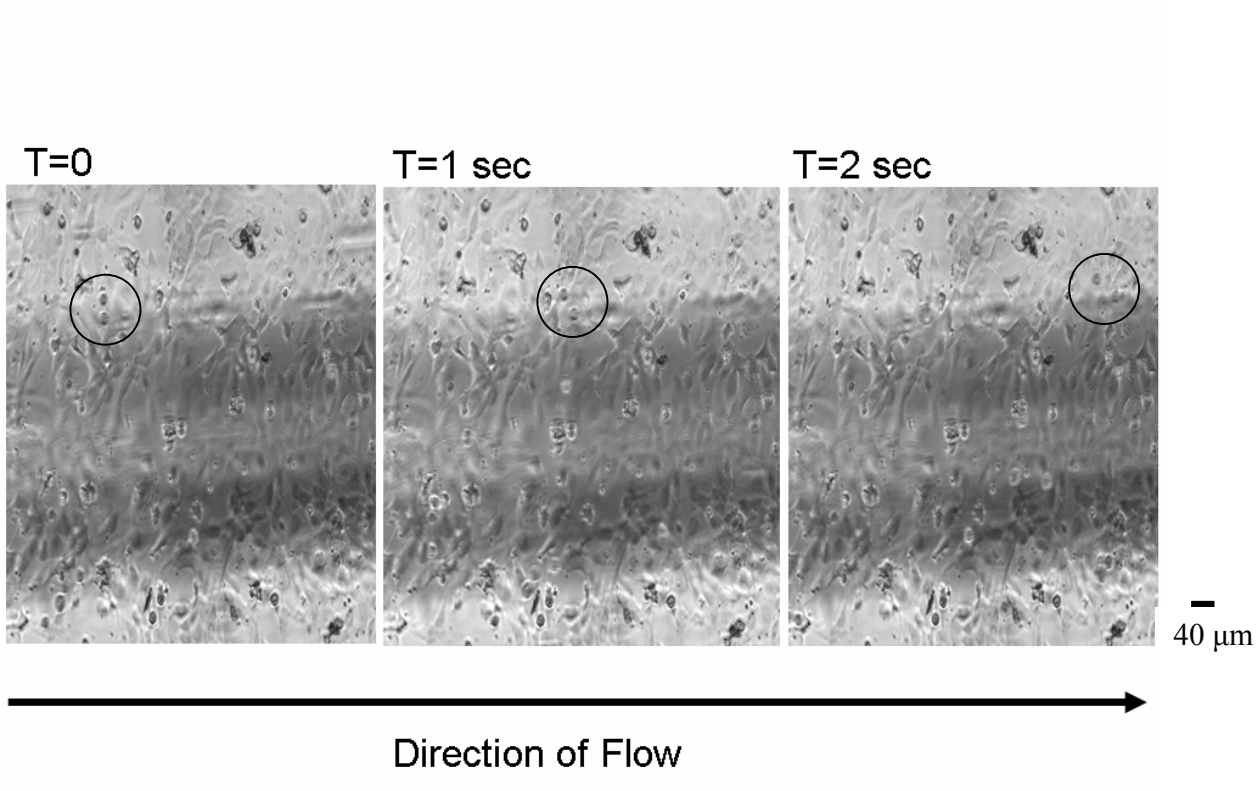

Fig. 4: A picture showing melanoma cells (circle) freely flowing over a cultured endothelial cell layer monitored from start time 0 (T) till 2 sec.

First to test our SAW microfluidic flow chamber a control study was performed on a cultured melanoma cell monolayer in the PDMS microchannel and then superfused with melanoma cells where minimal binding should occur. The lack of binding domains expressed by the cultured layer of melanoma cells result in a lower adhesion of melanoma cells under hydrodynamic flow (data not shown). Subsequently to test melanoma cell adhesion to VWF, a cultured monolayer of endothelial cells were stimulated with histamine under laminar flow and then superfused with melanoma cells In Fig 5 shows the pattern of melanoma cell adhering to the endothelial cell layer in a "string-like" manner which is confirmed by immunostaining (fig 6). Both the

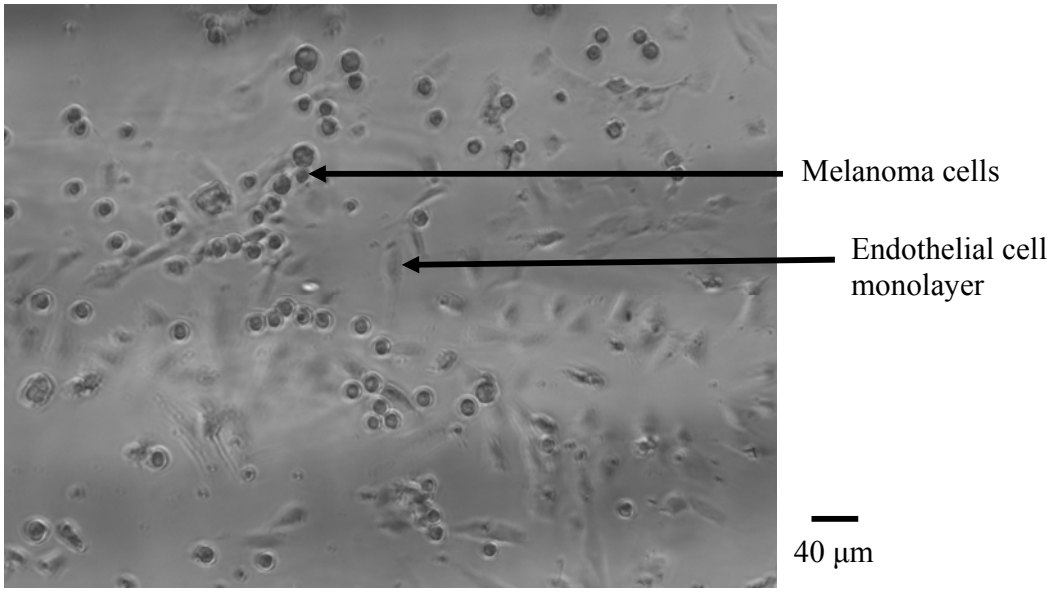

Fig. 5: A phase picture showing the attachment of melanoma cells to the endothelial cell layer in a string-like manner mediated by VWF.

immunofluorescent and phase contrast pictures were taken after 10 minutes of continuous laminar flow monitoring melanoma cell adhesion to VWF. A transient release of VWF from the endothelial cell layer under a constant shear rate of $1000s^{-1}$ during this time frame shows VWF stretching to the endothelial cell layer which gradually enhances melanoma cell adhesion (fig 7). In Previous studies have shown platelets adhering to VWF multimers released from endothelial cell layer forming platelet-strings similar to the pattern observed for melanoma cell adhesion(18). A line graph corresponds to our previous studies that under physiological conditions the endothelial cells secrete VWF which then unrolls due to the applied shear increasing the adhesive ability of this protein. In the presence of histamine endothelial cells release VWF over a 10 minute period enabling a high percent of melanoma cell adhesion (20% ±1.4) to the endothelial cell layer compared to the control levels (12%±2.2) (fig 5). When no histamine added there is also a gradual increase in adhesion of melanoma cells although at a much lower percent compared to the histamine stimulated studies. This could be due to a combination of the applied shear and possible involvement of melanoma cells to stimulate endothelial cell activation. One possible scenario is that an applied shear may stimulate certain receptors

on the endothelial cell layer to get activated to promote the release VWF. Another possibility could be the effects of metalloproteinases which influences the stimulation of the endothelial cells. Metalloproteinases are cell surface associated zinc proteases that cleave and disintegrate pericellular substrates and has been implicated in tumor cell invasion (32). S.W. Schneider and colleagues have shown that the invasive activity of melanoma cells to an intact cell layer is based on the extracellular activity of these metalloproteinases (MMP). They have also shown that melanoma cells release metealloproteinases MMP 2 and MMP 9 into the fluid layers which can stimulate the PAR1 receptor on the endothelial cell layer and may lead to the release of VWF (17, 32) . Further investigation of this study was not undertaken because it is beyond the scope of this chapter.

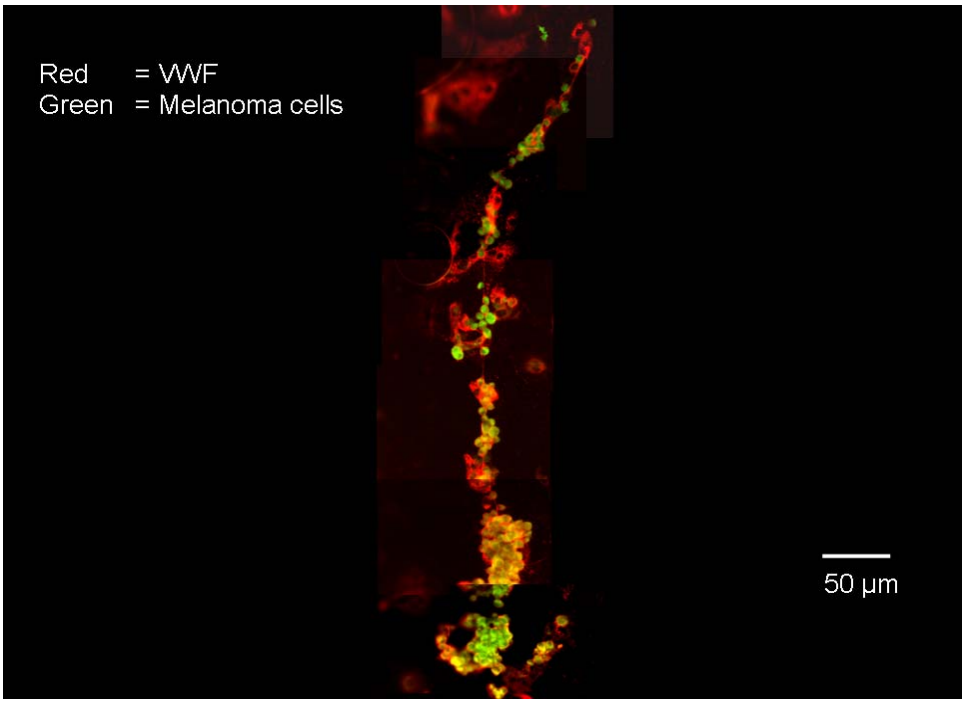

Fig. 6: An immunograph showing endothelial cell release of VWF which is labeled with a rhodamine(red) fluorescent dye binding melanoma cells labeled with fluorescien (green) fluorescent dye on a SAW driven PDMS microfluidic channel (Courtesy Stefan W Schneider).

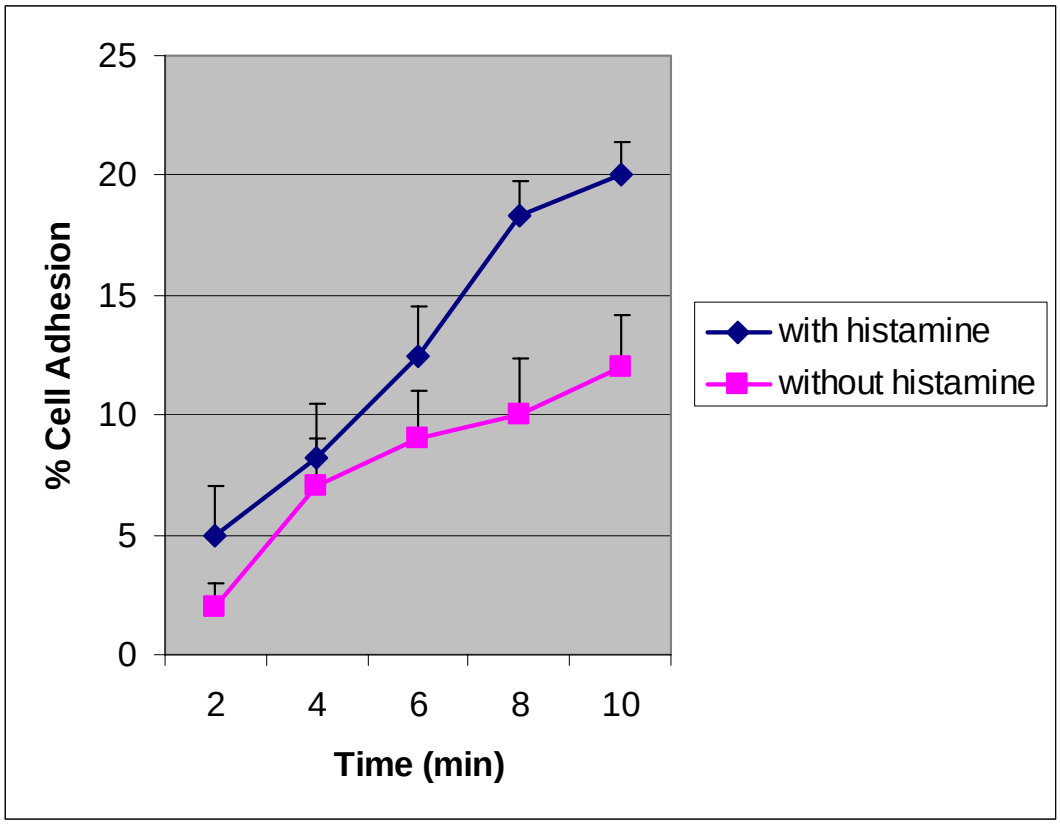

Fig. 7: A representative line graph plotting the percent melanoma cell adhesion to the endothelial cell layer under hydrodynamic flow. The values are recorded over a 10 min time period.

5.4 Summary

We have successfully implemented the SAW driven microfluidics into PDMS fabricated microfluidic devices for living cell assays. As evidenced by testing a cultured endothelial cell layer in the microfluidic channel and superfusing with melanoma cells under a constant shear flow. As endothelial cells release VWF, an increase in melanoma cell adhesion is visualized over time. This in-vitro model gives insight into the possible implications of cancer metastases and adhesion within our micro-vascular system. Also a large range of flow velocities can be achieved, while maintaining a homogeneous laminar flow with predictable shear rates ideally suited for many biological applications. These

studies provide a non-invasive method analyzing melanoma cell adhesion within our blood vessel. In our current study we observe under the influence of histamine an acute and sustained activation of endothelial cell by histamine.This activation leads to sufficient release of VWF fibers that can bind circulating melanoma cells at a localized site as visualized by video microscopy. Future studies using SAW microfluidic flow chamber can enable us to monitor melanoma cell adhesion and possible migration under flow. Since our bodies are assembled of millions of cells in a specific manner, cells can be considered natures “nanomachines”. The advantage of our system is that it is a non-invasive way to analyze the characteristics of specific cell types under hydrodynamic flow.

Chapter 6

Velocity and Size Measurements of Particles under Flow in a SAW Induced Microfluidic Flow Chamber using Fourier Transform Detection

6.1 Introduction

In the previous chapters we effectively studied melanoma cell adhesion dynamics by employing SAW as a nanopump. The velocity of melanoma cells were calculated by using video microscopy, this is done by measuring a fixed distance a cell travels over time. However maximum velocity measurement is limited by the frame rate of the software. A convenient method to overcome this obstacle is to implement detection systems to measure velocity of a particle in a microfluidic channel with integrated metal grids. A light source consisting of a mercury lamp is directed to the channel region where the metal slits are placed right below the device covering parts of the sample. As a particle moves through these metal slits a periodic signal will be obtained by a detector, the analysis of the Fourier spectra of the light intensity yields the velocity and size of the particle (fig 1a). The periodicity depends on the velocity (v) of the object and of course the grid width and the center to center distance (d). The following model was incorporated in our analysis, and the frequency (f) is proportional to velocity (12, 31).

$$d = v \cdot t \quad \text{and} \quad f = \frac{1}{t} \tag{6.1}$$

The frequency for our calculations is determined by Fourier analysis from a time (t) domain signal (fig 1b).

General Introduction to Fourier Formalism:

A complex periodic wave can be considered many simple sinusoidal waves with different amplitudes, wavelengths and frequencies according to the Fourier theorem. The periodic functions X(t)=X(t+nT), n =1,2,3… can be written as a sum of cos and sin functions. Often one combines both functions according to the Euler formula e^{ix} =cosx + isinx, so that the complex notation gives:

$$X(t)=\sum_{n=-\infty}^{\infty} X_n\, e^{i2\pi nt/T}\ ,\ X_n=\frac{1}{T}\int_0^T X(t)\ e^{-i2\pi nt/T}\,dt \qquad (6.2)$$

The sine converges if the function X(t) is "sufficiently smooth" ; e.g it is continuous and has finite number of extrema per period. The exact mathematical conditions are not relevant in our context here. Alternatively, if X(t) is real $X_n=X_{-n}^{*}$ (* complex conjugate) hold and equation (1) can be re-written:

$$X(t)=\frac{1}{2}\,a_0+\sum_{n=1}^{\infty} a_n\cos 2\pi nt/T + b_n \sin 2\pi nt/T \qquad (6.3)$$

$$a_n=\frac{2}{T}\int_0^T x(t)\cos 2\pi nt/T\,dt$$

$$b_n=\frac{2}{T}\int_0^T x(t)\sin 2\pi nt/T\,dt$$

a)

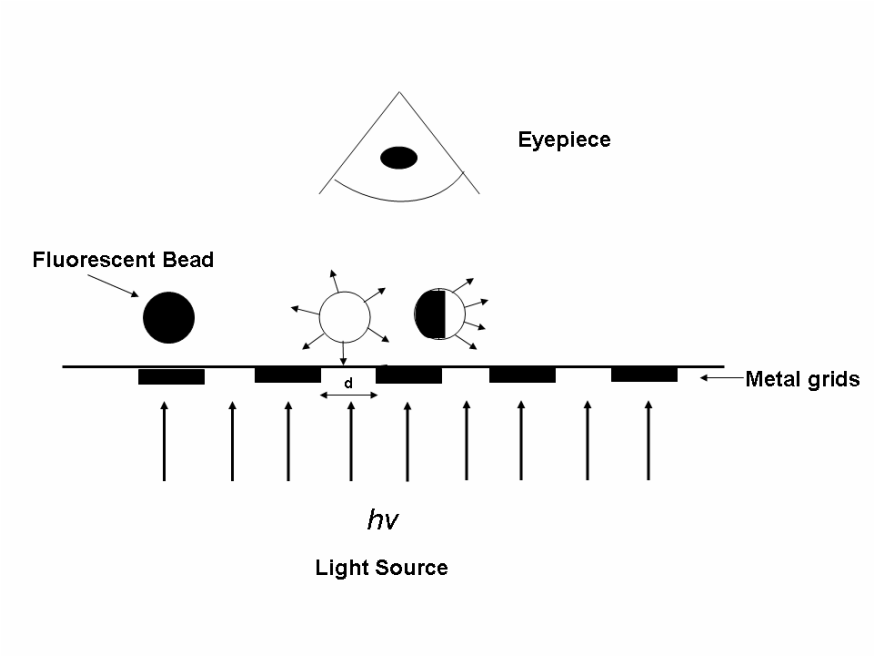

Fig 1a: A schematic outline for the fourier analysis from our light detection setip. The light source illuminates the fluorecent bead (white bead) when it passes the grid emitting a signal, however as the grid blocks the light source from illuminating the bead (black bead) results in a stable baseline a periodic signal is recorded.

b)

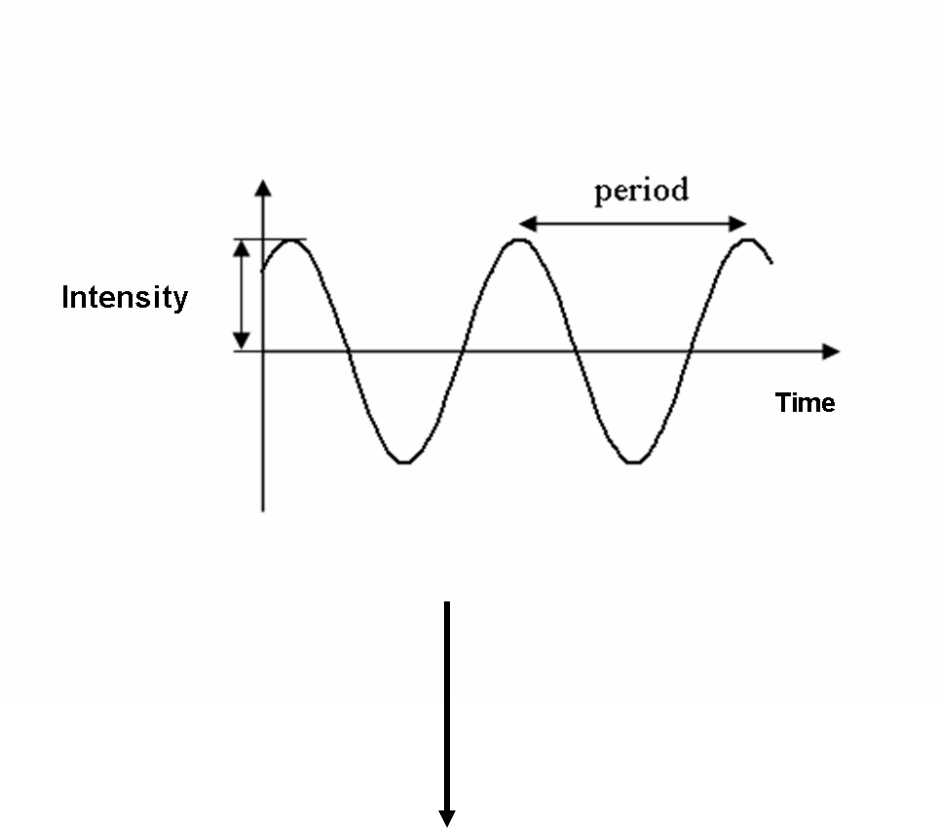

c)

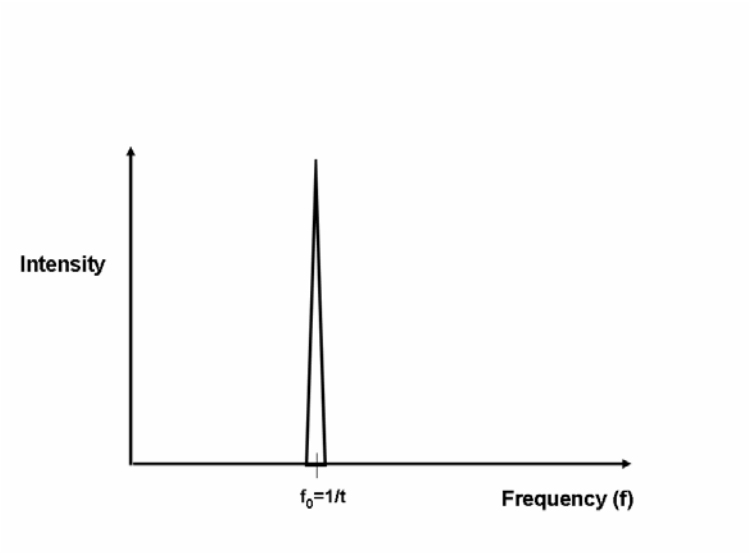

Fig 1: b) A representative diagram of a periodic signal wich gives an intensity signal as a function of time, c) which is then transformed to a frequency by Fourier analysis.

This becomes a useful technique for the measurements of solid-liquid systems especially analyzing blood flow. For example, the size and velocity of red blood cells as it flows through our blood vessels is critical for the proper maintenance of our blood circulation throughout the microvascular system. Our novel setup has the capability to detect flow, adhesion and rolling of red blood cells which gives insight into the docking mechanism to the blood vessel wall. This is an important parameter for the release of O_2 to our blood vessels. We introduce a simple non-invasive way to analyze such a phenomenon.

For our analysis microspheres coated with a fluorescent marker were tested using our SAW microfluidic flow chamber with metal detection slits. The use of photolithography can enable us to use to fabricate and align the PDMS channel to the metal slits. The accuracy and reproducibility of the results by Fourier analysis is highly dependent on these parameters.

6.2 Materials and Methods:

6.2.1 Microfluidic Chip with Metal Slits

A rectangular PDMS channel with dimensions of 1mm width and 500 μm height was coupled to our SAW device as mentioned in chapter 2. Metallic grids were integrated into the glass slide by standard photolithography (See appendix 2). The glass slides were spin coated with a photoresist (1813) and the grid structure was illuminated onto the glass slide by UV illumination. Gold metal layer were deposited on the top side of the slide with layer thickness of 100 nm to provide the detection slits. The 8 slits were each 20 μm wide and were spaced 50 μm center to center (fig 2). Fig 3 is a schematic layout of the PDMS channel where SAW induced acoustic streaming moves the fluid layer shown by the streamlines (red lines) and the grids are placed along the region of the channel.

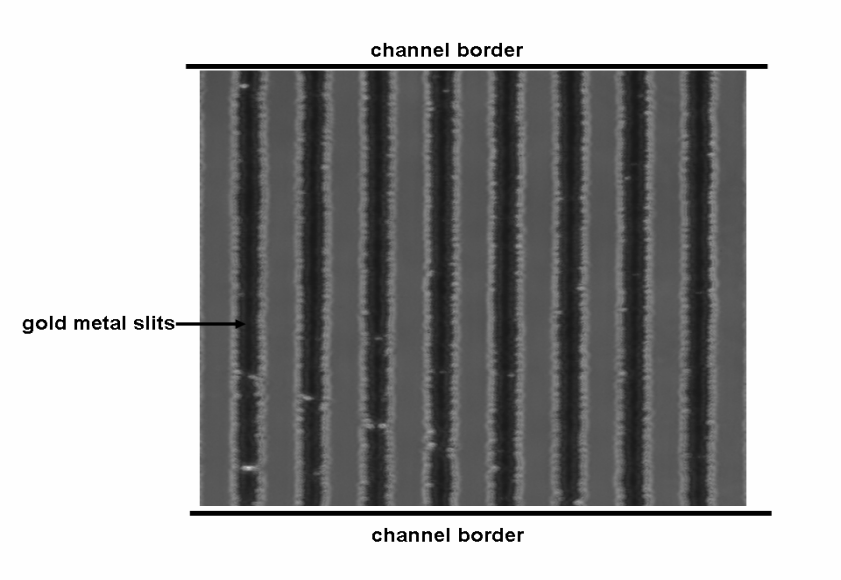

Fig 2: A snapshot of the deposited metal grid layers on the microfluidic channel.

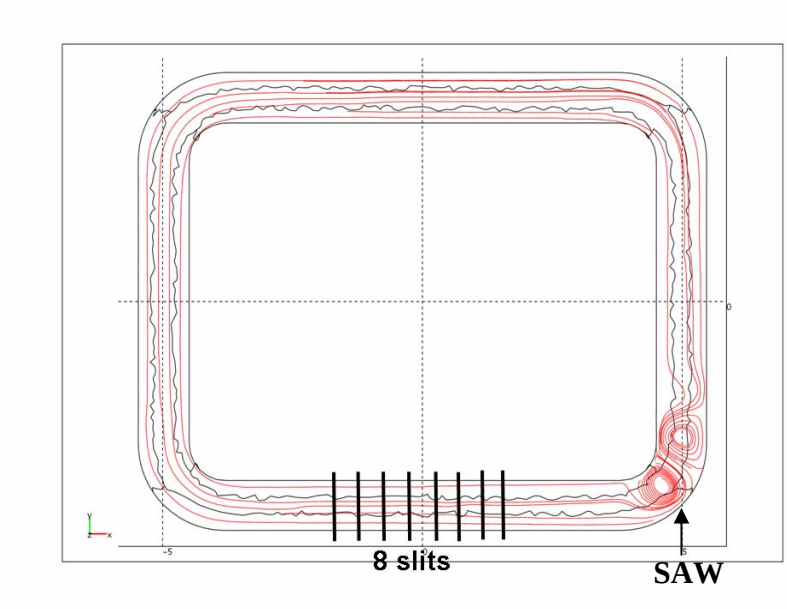

Fig 3: A schematic layout of the microfluidic channel where SAW transducers are placed at the corner of the channel to drive the fluid layers (red lines) in a continuous flow field with integrated grids at a region in the channel.

6.2.2 Preparation and Experimental Procedure

10 micron size latex beads labeled with fluorescein (excitation 505 nm and emission 515 nm) were diluted in deionized water (1:20) and sonicated to detach aggregates of beads prior to the experiments. The microfluidic chip coupled to the SAW device was placed on our inverted fluorescence microscope equipped with a fluorescence filter cube and mercury vapor lamp to illuminate the region of the microchannel where the metal slits are aligned (fig 4). A CCD camera is used to detect changes in the fluorescent intensity of the free flowing beads and recorded on hard drive. Prior to the start of the experiments, to test the accuracy of our CCD camera detection system a single fluorescent bead was placed on a glass slide and the intensity of the fluorescent bead to the background noise was measured. The shape of the fluorescent bead is assumed to be a circular object, the distance of the peak intensity shown by the line plot correlates to the diameter of the bead (fig 5). During the experiments under acoustic streaming a constant velocity of the beads is achieved for our analysis. The data manipulation and fast Fourier transforms (FFTs) were performed using Origin Pro 7.5.

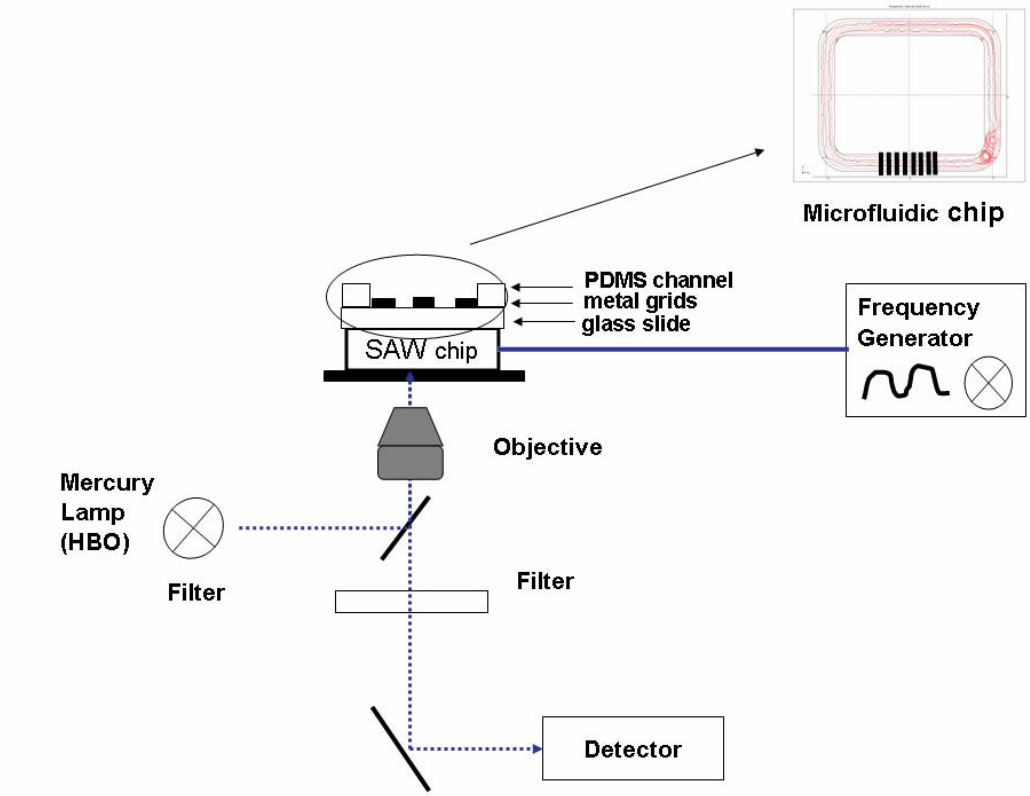

Fig 4: A schematic layout of the setup where the SAW chip is coupled to the microfluidic chip on an inverted fluorescence microscope. The grid is below the sample and the objective is directed towards the region of the channel where the metal grids are deposited.

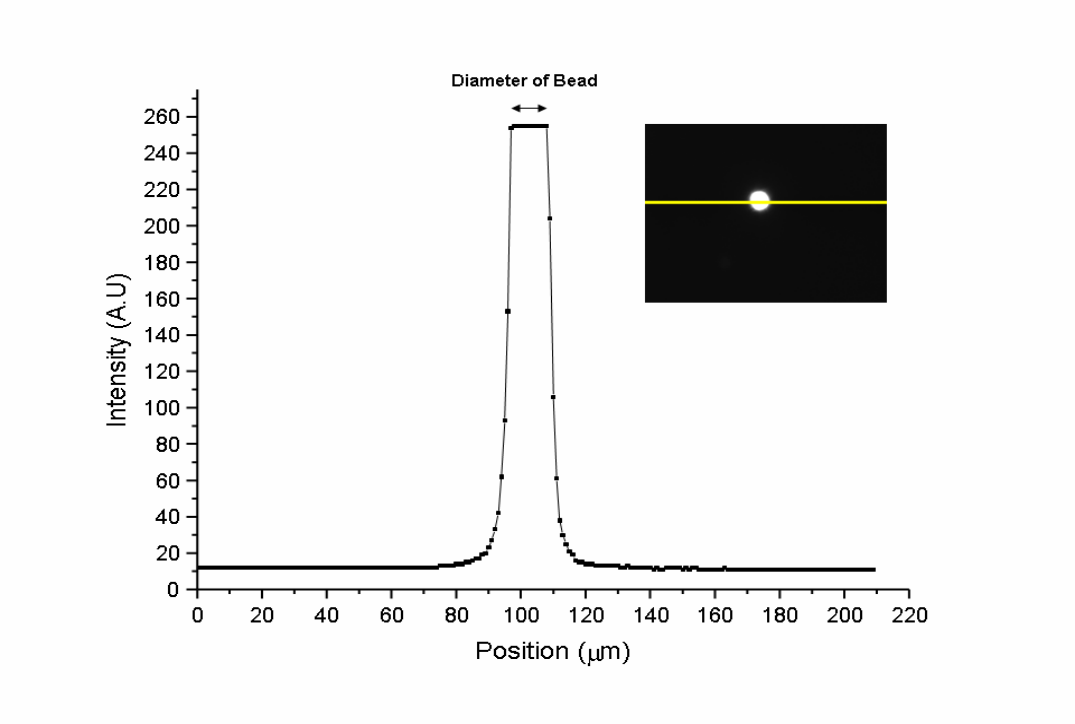

Fig 5: a) A graph plotting the intensity distribution of the bead along a line which crosses the bead. From the graph a high signal/background ratio and an nearly constant volume of the intensity across the bead is visualized

6.3 Results/Discussion

Velocity Measurements of Beads using Fourier Analysis

The optical output of a bead moving through the microfluidic channel enables us to track the path of the bead shown in fig 6. The waveforms recorded of a single bead shifts from a fluorescent peak intensity as the beads pass through the detection regions excited by the light source whereas the beads passing through the metal grids block the light path resulting in a stable baseline. This shows a periodic emission patterns as the bead moves along the channel. The frequency component is proportional to the bead velocities by performing the Fourier analysis. To test this system a single bead was tracked. The

center frequency of the fundamental peak in figure 5 was 9.67 x 10^{-4} KHz. The velocity of the bead is (0.967 Hz x 50μm)=48.35 μm/sec. In this case the velocity (v)
and the periodicity of the metal slits (d), and the frequency of the fundamental peak (f) from equation 6.1 can be rewritten.

$$v = d\,f$$

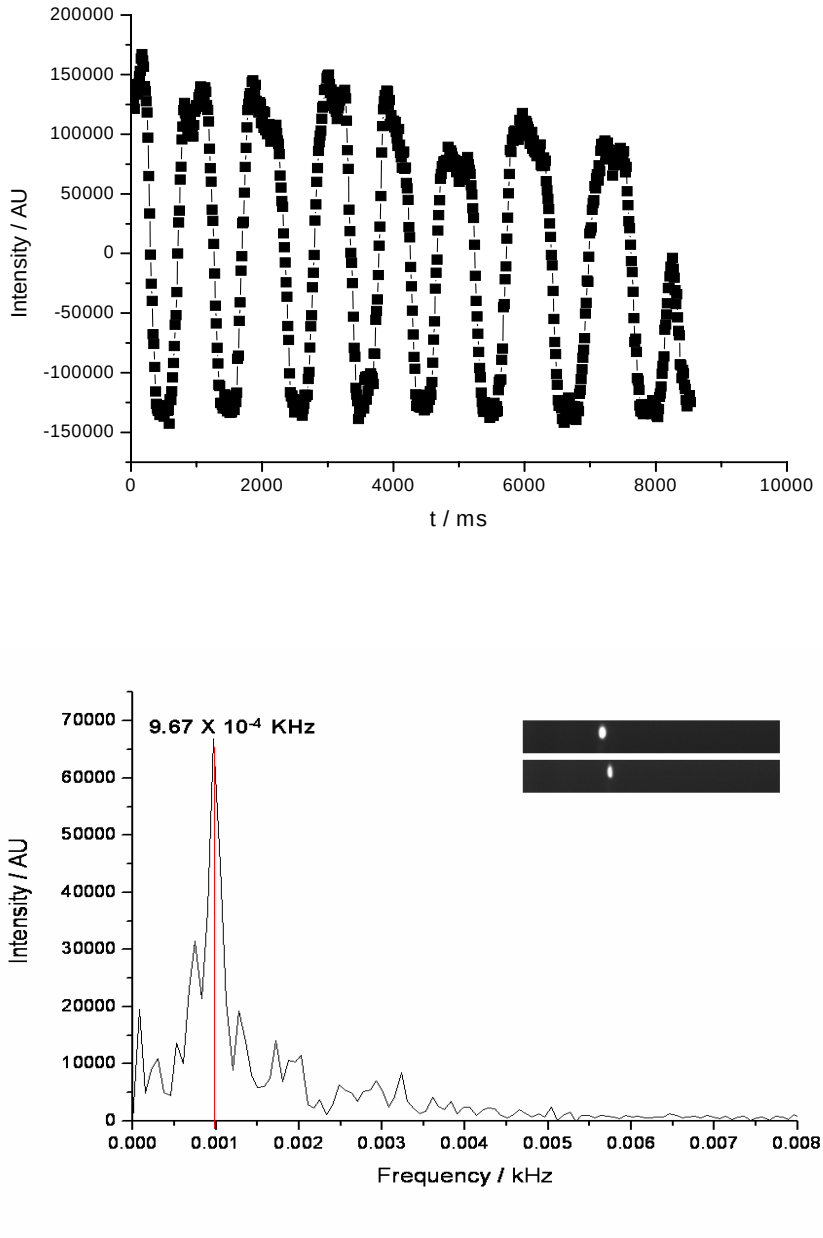

Fig 6: A time domain detection of the periodic fluorescent intensity distribution as a single bead flows through the metal slit detection region (8 slits) of the channel. The time scales for a bead to move across the channel was about 9000 milliseconds. The Fourier analysis of this periodic signal is shown in the lower graph and display a peak of 9.67 * 10^{-4} kHz which corresponds to the velocity of the bead. Fourier transform was performed with an FFT algorithm.

To demonstrate the applicability of our method onto multiple beads, in the next set of studies two beads moving at similar velocities were analyzed. The fluorescent intensity distribution of the periodic signals of the two beads as shown in fig 7 when transformed has a fundamental peak (1.3 Hz) which signifies the velocity of the first bead at 64.9 μm/sec and the peak (2.5 Hz) which corresponds to a velocity of the second bead of 64 μm/sec. By inspecting the graph a little closer one can see the harmonics of higher order. Especially the signal of the first and fourth harmonics is well above the noise background. This clearly demonstrates the applicability of this system to accurately track two beads flowing at similar velocities.

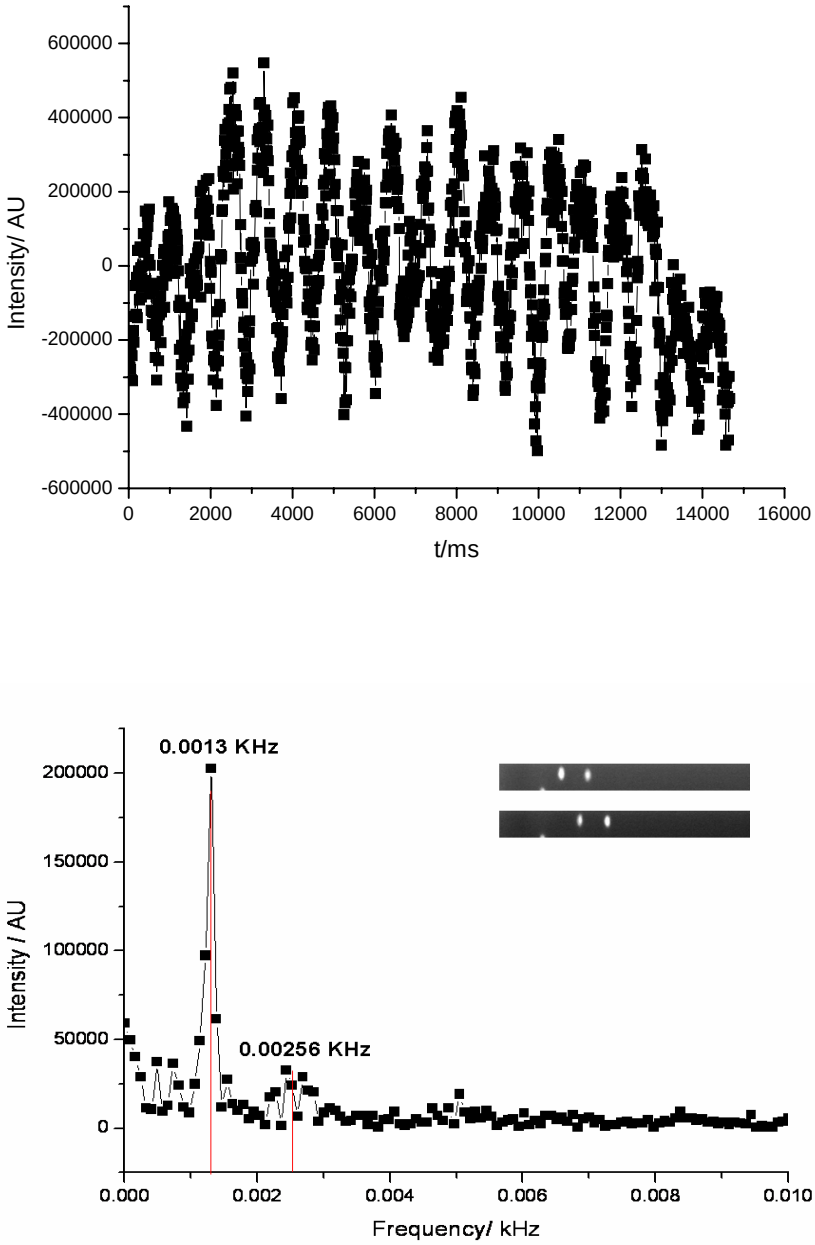

Fig 7: a) A periodic intensity distribution of two beads moving at similar velocities through the microchannel, and the Fourier transformation of the periodic intensities.

Finally to take it one step further, we tracked two beads with different velocities. In fig 8 again the intensity profile against time is plotted. Usually you can see 9 periods of the slow bead moving at 9000 ms through the grid. Superposed to the previous point, one can observe a signal of much higher frequency in the time range for about 1000 -2,500 ms. The signal corresponds to another fast moving bead which enters the grid at about 100 ms after the first bead and passes the grid within 1500 ms. The values when transformed have two distinct fundamental peaks which fits to the velocities of the two beads. The velocities measured accurately corresponds to the fundamental peaks at 0.826 Hz a velocity of bead was 60.5μm/sec, while at a peak of 8.03 Hz a faster velocity of 416 μm/sec was measured. In these studies the response of the Fourier transformation to detect changes to velocities of more than 1 bead gives us the capability to test multiple beads of varying velocities.

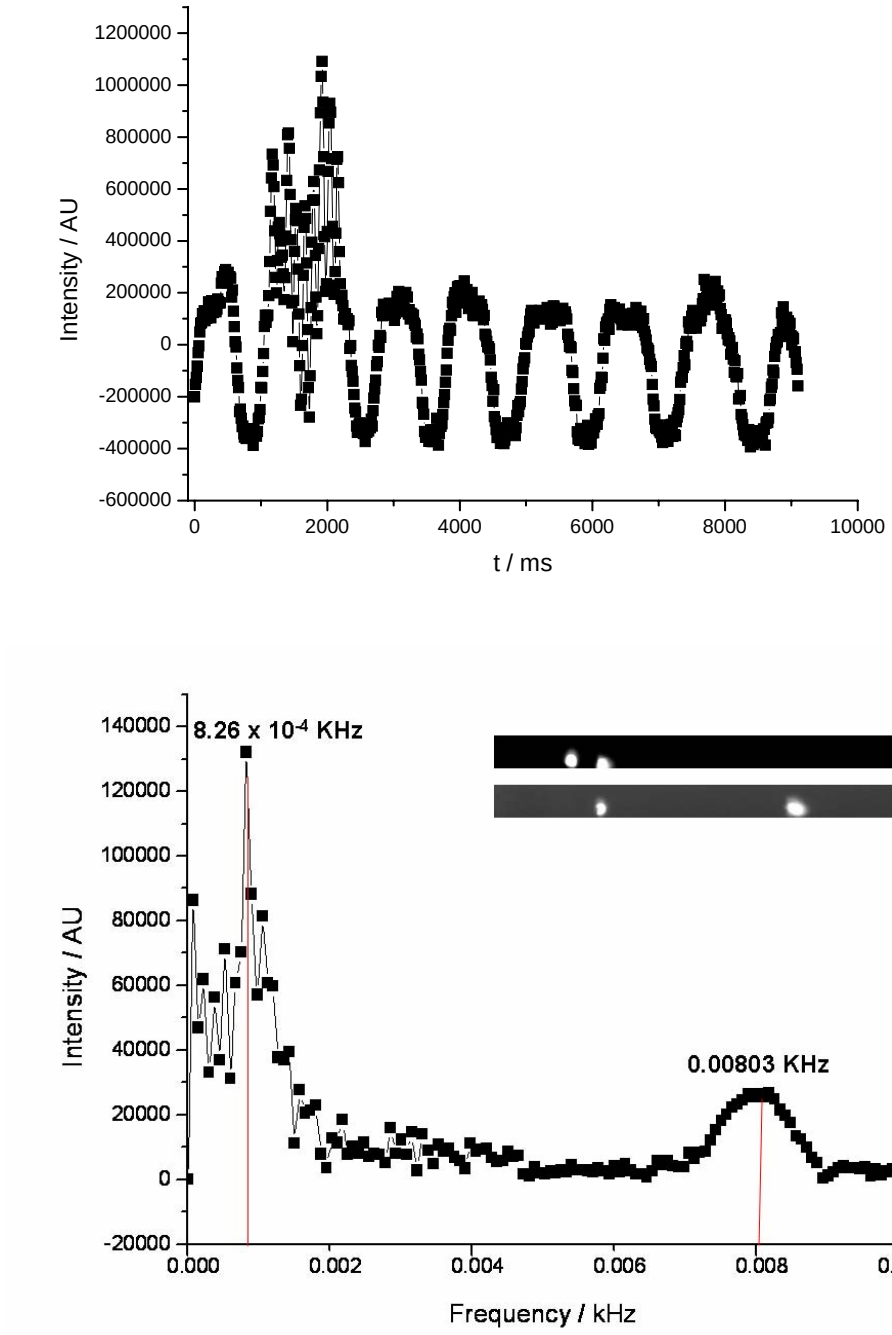

Fig 8: a) An intensity distribution of the two beads flowing at different velocities show two superposed periodic signals. The FFT accordingly shows two fundamental peaks at 0.826 Hz and 8.03 Hz which again reflects the velocities.

In addition to the frequency analysis of the moving bead, we now analyze the "shape" of the signal in the following set of experiments. In fig 5 we showed that the intensity across the channel and bead is constant in our experiments. Therefore it is the area of the bead which corresponds to the intensity. The shaded region shows a segment of a circle (stripped area) as it enters the region of the metal grid (fig 9). The area (A_{seg}) can be calculated by simple geometry as:

$$A_{seg} = r^2 \arccos\frac{r-h}{r} - (r-h)\sqrt{2rh-h^2}$$

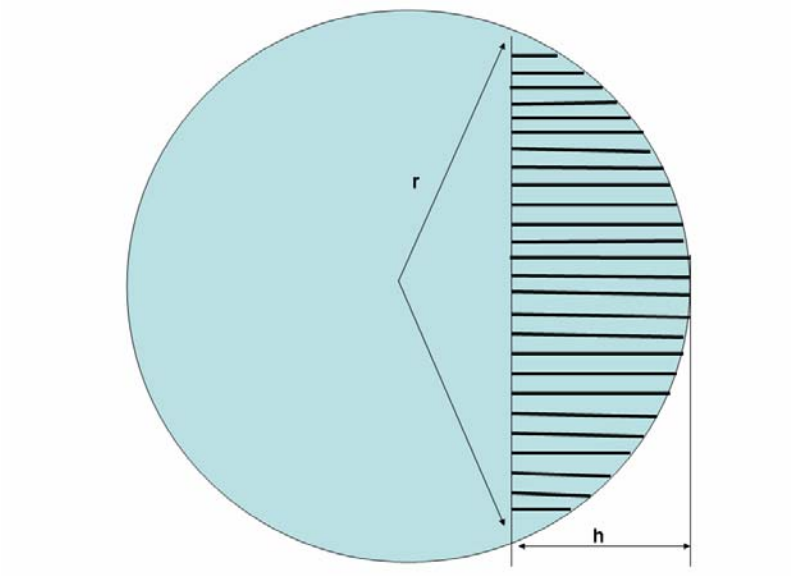

Fig 9: A schematic representation of a bead size entering the metal grid (striped area) as shown by the height (h) and the radius (r).

As already demonstrated, the fluorescence intensity during the analysis is a periodic function. The plotted graph (fig 10) shows the intensity distribution of the bead area (A_{seg}) as its tracked leaving the metal slit (shaded region) entering the open channel and as it approaches the next metal slit as a function of time over one period. The ascending

(red) and descending (blue) theoretical curves were calculated according to the parameters of the system which matched the experimental data confirming the validity of the technique.

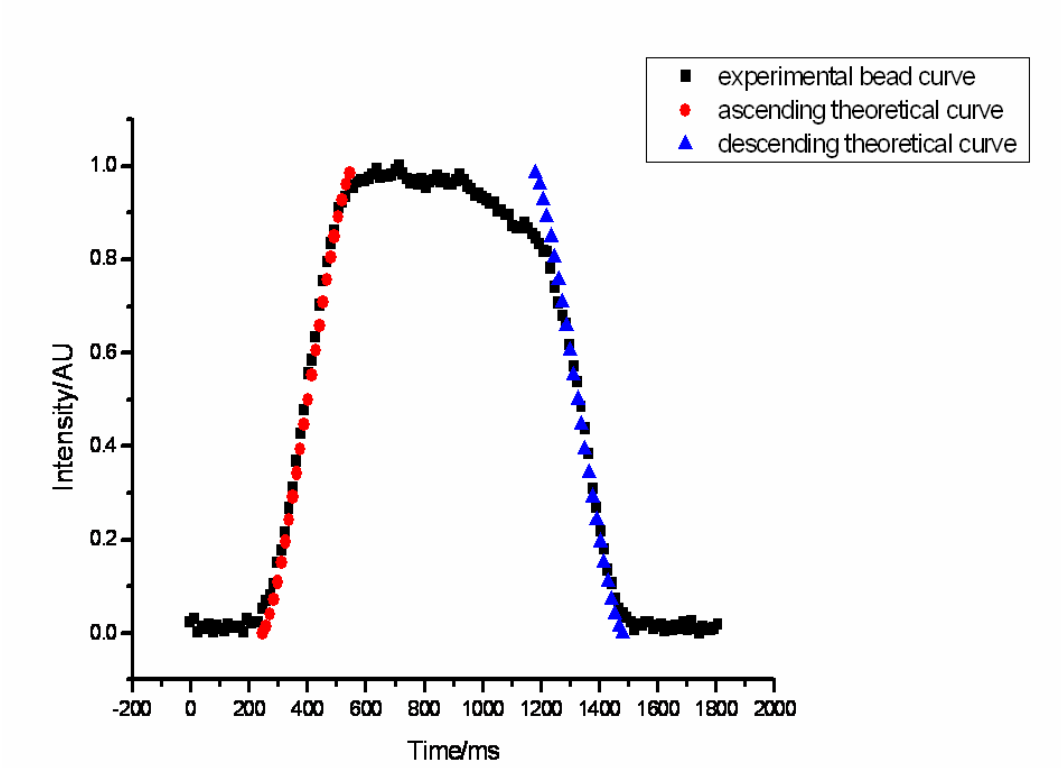

Fig 10: A line plot showing the intensity distribution of the fluorescent bead as a function of time as it leaves the grid where the peak intensity is normalized to 1 and then the intensity decreases as it enters the next grid. The red and the blue lines are the theoretical curves obtained from equation 1.

5.4 Summary

We have successfully employed Fourier analysis as a method of detection on our SAW induced microfluidic flow chamber formed by using spatially distributed metal grids. The frequency of the fundamental peaks is sensitive to changes in the net velocity of fluorescent beads. We accurately measured changes in velocity of a single bead, two beads with same velocities and two beads with different velocities moving through the channel, enabling us to analyze the flow profile of particles. Particles can represent object

like red blood cells and changes to the response of a cell under flow is detected by Fourier analysis. A non-invasive technique for the velocity measurement of particles in a SAW driven microfluidic chip has been clearly demonstrated. Also we have shown the applicability of our detection system to measure the size of a particle. This can enable us to track particles of different sizes and shapes as it flows through these grids.

Chapter 7

Quantification of Melanoma Cell Adhesion to VWF

7.1 Introduction

The adhesion of melanoma cells to VWF using the SAW microfluidic flow chamber gave insight into the initial events of melanoma cell arrest and stabilization. During this process melanoma cells which travel through the blood stream must have the ability to attach themselves to VWF and resist fluid detachment. As we have shown from our studies (chp 4 and 5) that conformational changes to VWF after an applied shear is critical for melanoma cell adhesion to VWF protein and upon endothelial cell secretion of VWF. In order to quantify the mechanical and molecular mechanisms of melanoma cell adhesion to VWF conformations after an applied shear, the combination of SAW microfluidic flow chamber and micropipette aspiration was employed.

7.1.1 Background on Cell Adhesion Molecules

In blood flow conditions a number of proteins function in mechanically stressful environments. Since cells and proteins are deformable bodies, the interaction under mechanical forces affect the biochemical processes of living cells. In our studies we have shown that melanoma cells stay firmly attached at high shear rates over a long period of time which indicates the strong adhesion potential of VWF. The force a melanoma cell is exposed to is estimated using the following equation (7):

$$F \approx 32\, R^2 \eta \dot{\gamma}$$

where η is the fluid viscosity, R is the cell radius and $\dot{\gamma}$ is the shear rate (up to $6000s^{-1}$). The rupture force between melanoma cell to the stretched VWF is significantly higher since no detachment between low and high rates is observed, this results in an average adhesion strength $\sim 10^{-8}$ N. In other studies, the binding of selectins to carbohydrate

ligands mediates the leukocyte to roll on the endothelium in shear flow, which may exert a force high as hundreds of piconewtons onto selectin-ligand bonds (62).

As cells come in contact with another cell or protein substrate there is a reorganization of the cytoskeleton which influences not only the cell shape, but also other cellular functions including cell spreading, crawling, polarity, and cytokinesis. Although the deformation of a cell depend on the cytoskeleton, other factors such as mechanical and biochemical interactions between cell and the extracellular matrix also play a big role. Recent evidence has shown that melanoma cell adhesion to the ECM has been mediated by integrins (39). Integrins are diverse group and large group of heterodimers containing both alpha and beta subunits. The isoforms depend on the the combination of α and β subunits which are constitutively upregulated and can actively bind to the ligand (25, 26). In blood flow conditions rapid integrin $\alpha_v\beta_3$ ligand interaction break the flow of circulating melanoma cells, and the receptor immediately co-localized with polymerizing actin to promote cell spreading (39). In our studies we speculate when VWF is subjected to mechanical forces the unrolling of VWF may expose binding domains which are specific to integrins.

7.1.2 Cell Adhesion (receptor-ligand interactions)

The membrane of a cell has specific receptors which can interact with a ligand on the ECM or another cell surface, which results in a lock and key bond. The idea here is that for a firm adhesion a conformational match between the receptor and ligand must occur to result in a strong and long-lasting bond. A poor conformational match however will not lead to such a result. The specific lock and key forces depend on 10 to 20 different single weak bonds (bogan and thorn 1998), the number of hydrogen bond interactions is the key for a strong binding between the receptor and ligand. However, other interactions such as Vander-Waals forces, electrostatic forces and hydrophobic interactions are all responsible for the interplay between the lock and key forces (43). The 3-D conformational structure of the binding pocket between the receptor and ligand has become an important paradigm when investigating cell adhesion because it dictates the

characteristics of the bond (43, 62). In blood flow conditions the circulating cells must have the ability to find the appropriate ligand for adhesion to the blood vessel wall. The ligand binding may lead to a number of biochemical reactions which affects the contact area of the cell surface and bond distribution.

7.1.3 Cell Adhesion as a Wetting Principle

In order to differentiate between specific and non-specific interactions the rate of adhesion needs to be analyzed carefully. Typically cells have the ability to flatten in most surfaces where outgrowth of lamelopodia or filapodia instigates the spreading phenomenon. However if there are specific interactions between the receptor of the cell and the substrate a more rapid cell spreading due to the chemical binding kinetics between the receptor and ligand would be expected. The plasma membrane can regulate the interaction of the cell to the extracellular environment during the cell adhesion process (1). It consists mainly of lipids, cholesterol, steroids, fatty acids and proteins. These compositions vary according to the cell type and the most abundant lipid is the phospholipid. The phopsholipid bilayer is considered a semi-permeable membrane arranged in a double layer where the hydrophilic phosphate heads are exposed to the water both within the cell and within the exterior region, while the hydrophobic fatty acid tail groups are hidden inside the membrane bilayer (1). The proteins float through the phospholipids according to the fluid mosaic model introduced by singer and Nicholson (1972)(20). In order to analyze the nature of cell adhesion, the elasticity of the membrane defines the changes in the cell shape during adhesion with another substrate or cell (43). Similarly when a liquid droplet is placed on a solid surface depending on the surface tension of the droplet (the internal bonds) and the surface energy of the solid, the shape of the droplet will result in different wetting conditions. A liquid with a high surface tension will remain a droplet with low wettability whereas a liquid with low surface tension will easily spread throughout the surface.

These principles can be applied when analyzing cell adhesion. The key concept is the adhesion energy Δg_{ad} defined as the mechanical work required to separate a unit area of

the adherent surface. Since the receptor-ligand interactions occur close to the surface, the adhesion energy can be determined on the basis of the elastic boundary conditions. In our mechanical analysis, the adhesion energy Δg_{ad} is related to the work done by external forces and the energy stored in and dissipated by the deformed cell (43, 61).

$$\Delta g_{ad}=\gamma(1-\cos\theta) \qquad (7.1)$$

Where γ (in nN/μm) is the membrane tension and θ is the contact angle between the direction of the applied tension and the contact plane.

Our experiments were designed for a two-fold investingation. First, to determine whether VWF in the stretched conformation after a critical shear can enhance melanoma cell adhesion compared to the globular or collapsed state. This is followed by the study of the mechanical properties of melanoma cell spreading, specifically whether the spreading rate of melanoma cell membrane is a result of specific or non-specific interactions to biologically modified surfaces. By employing the micropipette technique we can directly analyze the mechanical and molecular components of melanoma cell adhesion to VWF. We show for the first time that the conformational changes to VWF under an applied shear from it's coiled to stretched conformation plays a significant role in melanoma cell adhesion. A ~40% increase in the adhesion energies of melanoma cells to VWF in the stretched configuration compared to it's coiled state was observed. Once VWF is stretched the number of binding sites exposed to melanoma cells increases as a result of integrin-VWF interactions. This is confirmed by blocking the $\alpha_v\beta_3$ receptor expressed in melanoma cells as well as applying the VWF-ab directed against the stretched-fiber like VWF conformations.

7.2 Materials and Methods

7.2.1 Cell culture

A7 melanoma cells were grown in MEM medium (PAA, Munich, Germany)) supplemented with 10% fetal calf serum (Biochrom, Munich, Germany) and 1% penicillin/streptomycin (Biochrom, Munich, Germany) in a 95% air-5% CO_2 incubator at 37°C. For adhesion experiments, cells were detached by adding 500µl trypsin ($c = 0.05\%/0.2\% EDTA\ (w/v)$, then centrifuged and the pellet was resuspended in MEM medium without fetal calf serum for the experiments.

7.2.2 Preparation of coverslips

The glass coverslips were cleaned with ethanol and distilled water prior to coating the surface with either collagen or poly-L-lysine. Type 1 collagen purified from rat tail (Courtsey Stefan W Schneidere) was diluted with PBS++ (1:5). The cleaned coverslips were either coated with 100 µl of collagen solution and were allowed to polymerize for 5 min at 37^0C, or they were coated with poly-L-lysine. Therefore, the poly-L-lysine was diluted in dH_2O for a final concentration of 0.1 mg/ml and then added to the glass slide. After 5 min the poly-L-lysine was removed and was left to dry prior to administering the VWF. The human VWF purified from blood (50µg/µl) was added to both collagen and poly-L-lysine coated substrates and then used for experiments.

7.2.3 Immunostaining/Immunofluorescence

Fluorescence microscopy was used to analyze the unrolling and stretching phenomena of the von Willebrand factor (vWF) under surface acoustic wave (SAW) induced streaming and to study the adhesion of melanoma cells to vWF.
For immunofluorescence staining purified anti-human polyclonal antibody (host rabbit, $c = 1.3 mg/ml$) (Herford, Germany)) and a rhodamine-conjugated goat anti-rabbit secondary antibody (Herford, Germany)) were used. The VWF sample was fixed and

permeabilized with ice-cold methanol at 4^0C. The methanol was removed by washing the sample with PBS++ and was subsequently blocked with 1% BSA. After washing with PBS++, the primary antibody ($c = 0{,}0013 mg/ml$) was added for 1h incubation time at room temperature. The secondary antibody ($c = 0{,}001 mg/ml$) was added after washing the sample with 1% BSA and incubated for 1h at room temperature. Following the washing step, Diazabicyclooctane "Dabco" was added for preservation of the fluorescence dye and a glass slide was put on top of the sample.

7.2.4 Coverslips coupled to SAW device

To study the response of VWF to hydrodynamic stress, the surface acoustic wave technology was used. The glass slide functionalized with either collagen or poly-L-lysine was coupled to the SAW slide booster. The VWF immersed in a droplet of PBS++ was exposed to a strong shear for 2 minutes (Fig. 1b). The slide with the sheared VWF was then directly utilized for adhesion studies and/or for immunostaining.

a)

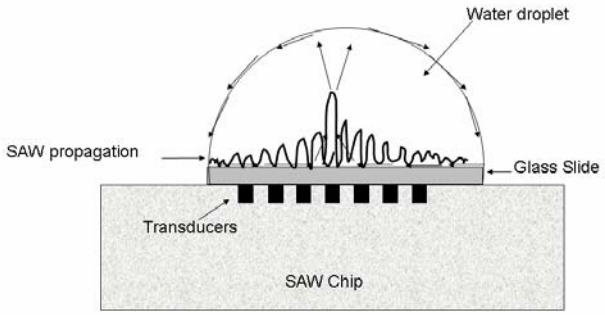

b)

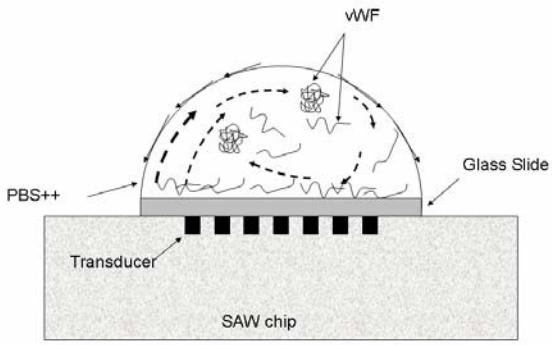

Fig. 1: a) Sketch of a surface acoustic wave which is excited on a piezoelectric material and, thus, inducing an acoustic streaming into a water droplet on a slide (arrows). b) Acoustic streaming unrolls the protein vWF immersed in a droplet of PBS++.

7.2.5 Micropipette Aspiration Experiments

To qualitatively assess shear related conformational changes of VWF to melanoma cell adhesion, single melanoma cells were suctioned by the micropipette and the spreading ability of the cell were anayzed (27). The micropipette aspiration technique was adopted to quantify the free adhesion energy of A7 melanoma cells to von Willebrand factor (VWF). A coverslip was bio functionalized with either poly-L-lysine or collagen. Adhesion experiments with VWF (50µg/µl) were done on both the globular and stretched conformation to determine whether the changes in VWF conformation can impact melanoma cell adhesion. Furthermore, specific blocking experiments were performed using integrin antibody (Chemicon) to target the integrin $\alpha_v\beta_3$ on the melanoma cell membrane as well as VWF antibody (Herford) to block the activity of the VWF. Melanoma cells were incubated with the integrin antibody for 15min in MEM medium prior to the experiments. The antibody was added to the melanoma cells in a concentration of $c = 0{,}05 mg/ml$. The VWF antibody was directly added to the biofunctionalized surface in a concentration of $c = 0{,}0013 mg/ml$ and incubated for 15min. Melanoma cell adhesion experiments were performed at room temperature (23-26°C). The cells were aspirated onto the tip of a micropipette with a pressure of 80Pa and were micromanipulated towards the biofunctionalized surface until there was contact. The contact area for each cell was kept constant. The adhesion process of the melanoma cell was monitored for five minutes using video microscopy.

Theory

From classical wetting it is known that cell adhesion can be regarded as a water droplet wetting a surface (Fig. 2a). The free adhesion energy can then be calculated with the Young-Dupré equation

$$\Delta g_{ad} = \gamma(1 - \cos\alpha) \qquad (7.1)$$

α is the contact angle between the flat surface of the wall and the curved cell membrane. γ is the lateral membrane tension, which can easily be determined with the micropipette aspiration technique.

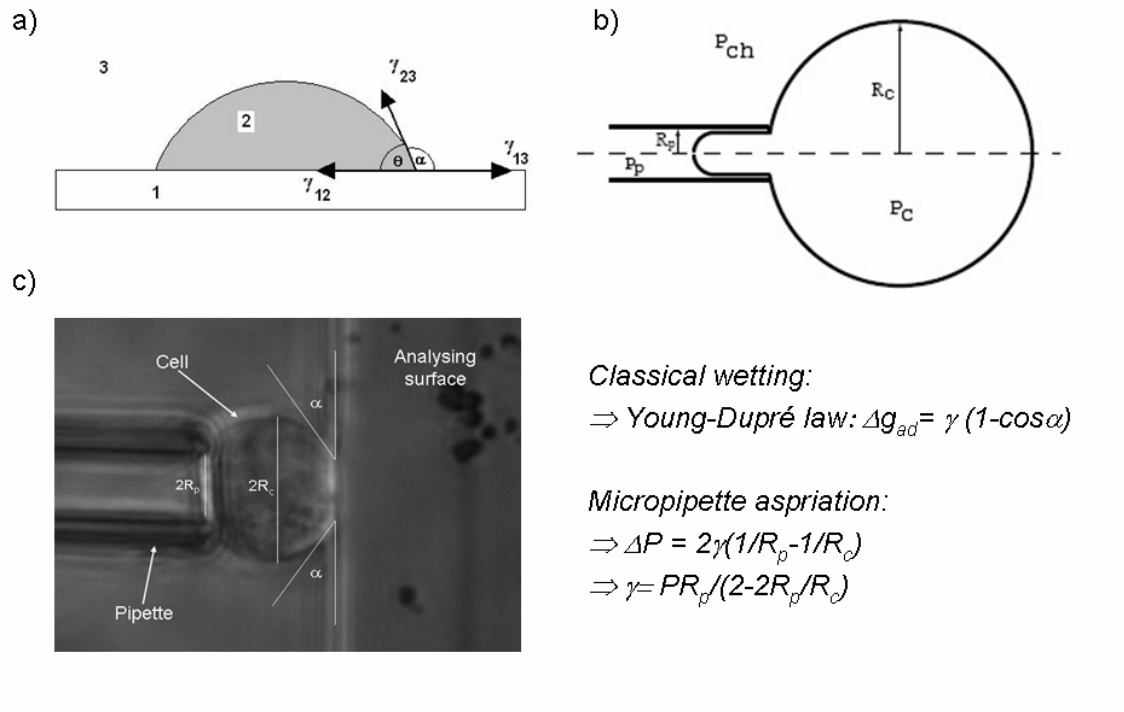

Fig. 2: a) Schematic representation of a wetting process. Three media, a cell/droplet (1) is deposited on a surface (2) surrounded by media (3). The arrows indicate the direction of the forces acting on the contact line of the cell/droplet. The contact angle α is determined by the balance of the tensions between the three media. b) Schematic diagram of an aspirated cell with the cell radius R_c, the meniscus radius R_p inside the pipette and the three existing pressures in the chamber P_{ch}, inside the cell P_c and inside the pipette P_p. c) Light microscope image of the adhesion process of a cell on a surface. Note that we can measure the contact angeļ α on both sides of the cell, the cell radius R_c and the pipette radius R_p.

By aspirating a cell with a micropipette, a cylindrical tube with a small meniscus at its end emerges inside the pipette (Fig. 2b). The applied external pressure $\Delta P = P_{ch} - P_p$ between the chamber and the pipette induces the isotropic membrane tension γ. Adopting

the Laplace-equation for the aspirated part inside the pipette with the radius R_p and the outer part with the radius R_c leads to an equation for the membrane tension:

$$\gamma = \frac{R_p}{2\left(1 - \frac{R_p}{R_c}\right)} \Delta P \qquad (7.2)$$

By measuring the contact angle, the cell radius and the radius of the meniscus in the pipette, it is possible to combine equation (2) with the Young-Dupré equation (1) and, thus, to calculate the free adhesion energy. Consequently it is possible with this technique to determine the difference in adhesion of melanoma cells to glass, collagen, poly-L-lysine and von Willebrand Factor (Fig. 2c)(35).

Analysis

The adhesion process was recorded with a CCD camera in order to analyse the adhesion process. Each picture taken was analyzed with Jörg Schilling's analyzing software Open Box and the free software ImageTool. Each experiment comprised the results of four or five cells and was repeated at least once under the same conditions. By averaging the results of those experiments the adhesion of melanoma cells to a specific surface could be analyzed.

7.3 Results and Discussion

7.3.1 VWF Network Formation and Melanoma Cell Binding under Acoustic Streaming

To investigate the formation of VWF fiber like networks were analyzed by superfusing VWF on biofunctionalized substrates under SAW induced acoustic streaming. Under a high shear rate (>1000s^{-1}) the VWF fibers have the ability to specifically bind to a collagen coated surface and non-specifically to a poly-L-lysine coated surface (Fig.3a).

However, under static conditions, the VWF globular clusters were identified on both collagen and poly-L-lysine coated surfaces (Fig.3b). As a control, on an untreated glass surface there was no detection of VWF with and without an applied shear (data not shown).

Our main goal was to identify the adhesive behaviour of VWF and melanoma cells under a constant shear flow. The unrolling of VWF forms fibers which extend in the direction of the flow and become immobilized on collagen or poly-L-lysine coated substrates. These VWF fibers can cross-link with other fibers of different lengths resulting in an assembly of a multimeric complex. The VWF multimers can not only bind to platelets, but also to melanoma cells in a similar way. The immobilized VWF multimeric fibers bind to multiple melanoma cells which have been superfused at a high shear rate of $1000s^{-1}$ (Fig.3c). The VWF multimeric fibers bound to melanoma cells are thick enough to be detected under phase contrast (Fig.3d). These results led to the quantification of the adhesion energies that exist in melanoma cell adhesion to VWF by employing the micropipette aspiration technique.

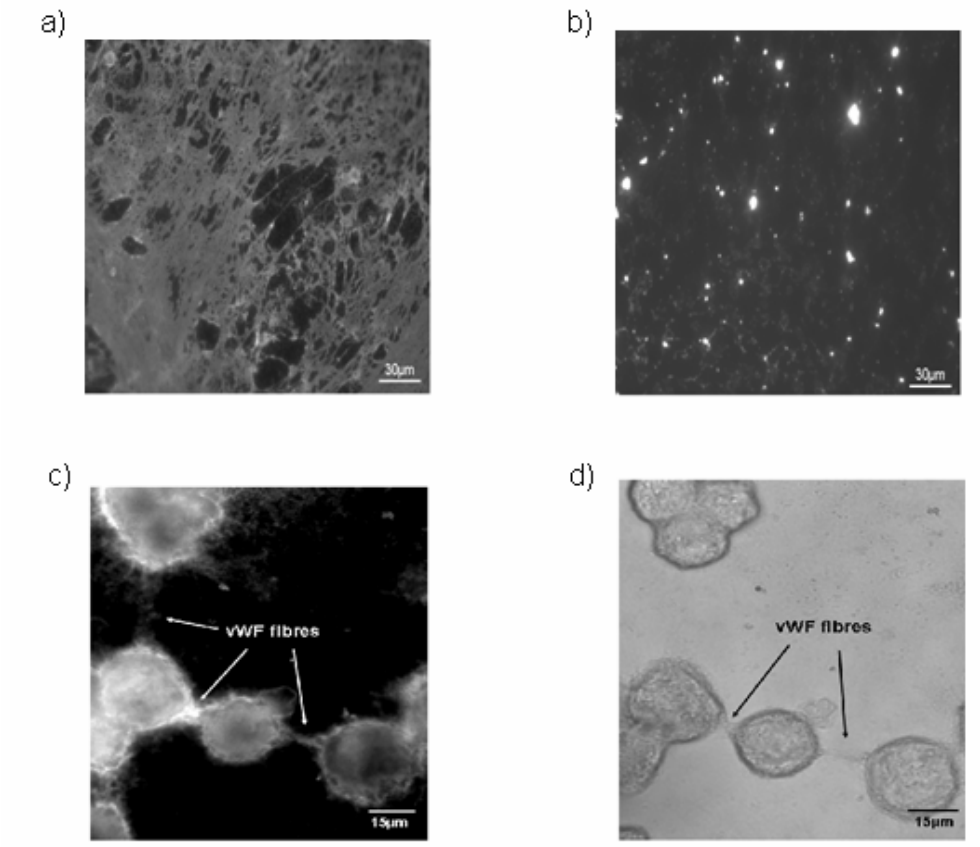

Fig 3: a) An immunofluorescent image of unrolled vWF after applying a shear by surface acoustic waves or b) of globular vWF under static conditions (no shear applied). c) Melanoma cells aligned along immunostained vWF fibers and d) a phase contrast image of vWF fibers attached to the melanoma cells. Note that the multimeric strands are thick enough to be visualized under phase contrast.

7.3.2 Adhesion energies of Melanoma Cells to different VWF Conformations

To quantify whether these VWF network like fibers can enhance melanoma cell adhesion a combination of both SAW and micropipette technique were employed. Using our SAW microfluidic system, VWF was added to collagen or poly-L-lysine coated glass surfaces coupled to the SAW device, where a shear flow was applied to stretch the VWF. The adhesion of melanoma cells to the unfolded VWF surface was then directly measured using the micropipette aspiration technique. Under static conditions, the VWF protein was applied to both the collagen and poly-L-lysine coated surfaces and the adhesion energies were measured. Our results show that conformational changes to VWF have a

significant influence on the binding characteristics of melanoma cells (Fig. 4a). When a high shear flow is applied the VWF it is unrolled and forms a network. These networks are presumably repeating units of stretched α and β helices of the secondary structure of VWF where collagen binding domains attach to the collagen substrate and other exposed domains which bind to melanoma cells. Melanoma cells can adhere more effectively to the stretched VWF ($8.04 \cdot 10^{-5}\,J/m^2$) than to the globular conformation ($5.79 \cdot 10^{-5}\,J/m^2$). However, the collagen coated surfaces without VWF also showed a similar adhesion energy value ($7.86 \cdot 10^{-5}\,J/m^2$) compared to the unfolded VWF.

The entropic spring theory could play a role in the dramatic changes in the adhesion values of melanoma cell adhesion to VWF. By changing the environmental conditions, in this case the shear rate, result in a stretching phenomenon of VWF causing long fiber-like extensions. When the VWF protein stretches it could result in the fibers orientating themselves in a preferable state thus reducing the entropy of the system. The hydrophobic residues of VWF fibers get exposed so the water molecules become ordered resulting in an increase in melanoma cell adhesion to VWF. In comparison, under static conditions, the VWF is in the globular form where the protein is in entropic equilibrium. As the melanoma cell is brought into contact with globular VWF protein, the coiled VWF protein acts as a spring leading to entropic repulsion which results in a lower adhesion energy.

If there are specific interactions between VWF and melanoma cells, we then take a closer look at lock and key forces. In melanoma cells various receptors expressed in the cell membrane are recognized to be promiscuous, which means the same receptor could bind to different ligands. Our results show that the common binding domains of melanoma cells to both collagen and VWF result in similar adhesion energies, which could be due to the high expression of integrin receptors on the plasma membrane. Recent reports have shown that both collagen and VWF share binding domains to the integrin isoforms expressed in melanoma cells.

The rate of melanoma cell adhesion to VWF gives insight into the possible spreading characteristics of the melanoma cell membrane to the blood vessel wall. We show that the adhesion energies measured for all substrates is a function of time and is constant. The equilibrium time to completely deform the cell may take longer than 20 min (data not shown). An increase in the rate of adhesion of the unfolded VWF and collagen occurs within seconds of melanoma cell contact and surface coverage compared to the other samples. The amount of binding domains of VWF and the ligand density of melanoma cells initiate the first binding followed by subsequent binding events, to promote strong adhesion over a 5 minute period (Fig 4b).

Adhesion energies of sheared vWF on poly-L-lysine and collagen substrates

a)

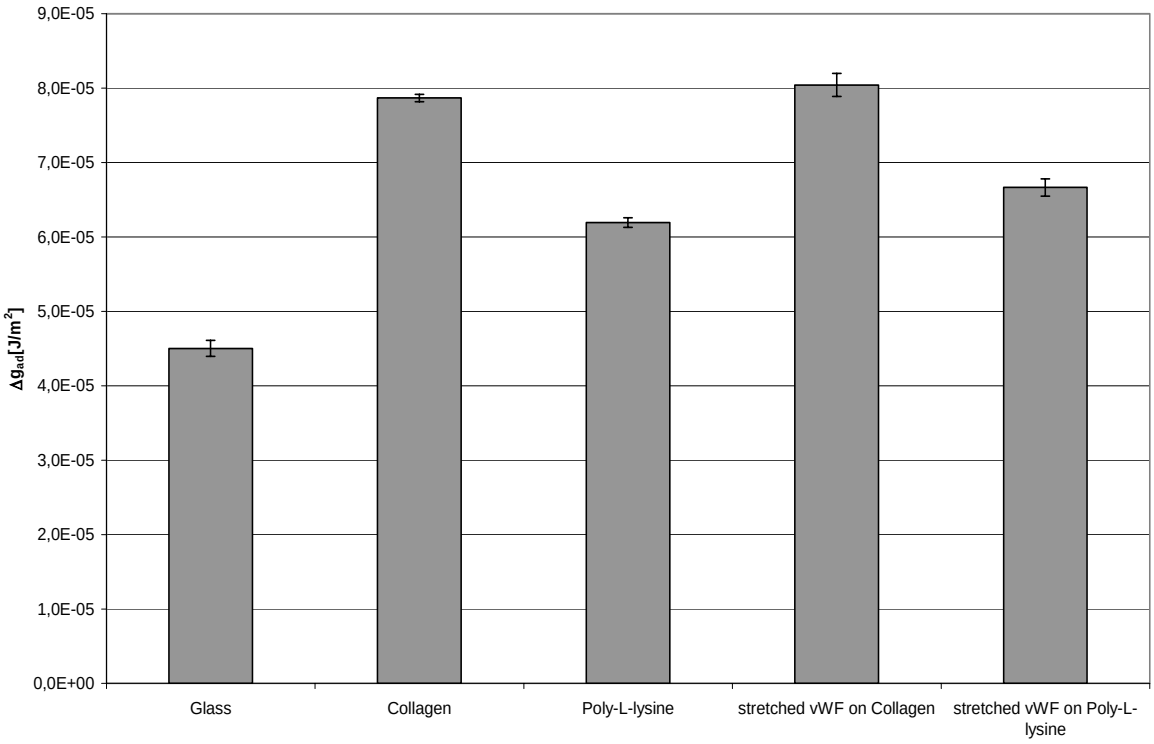

b)

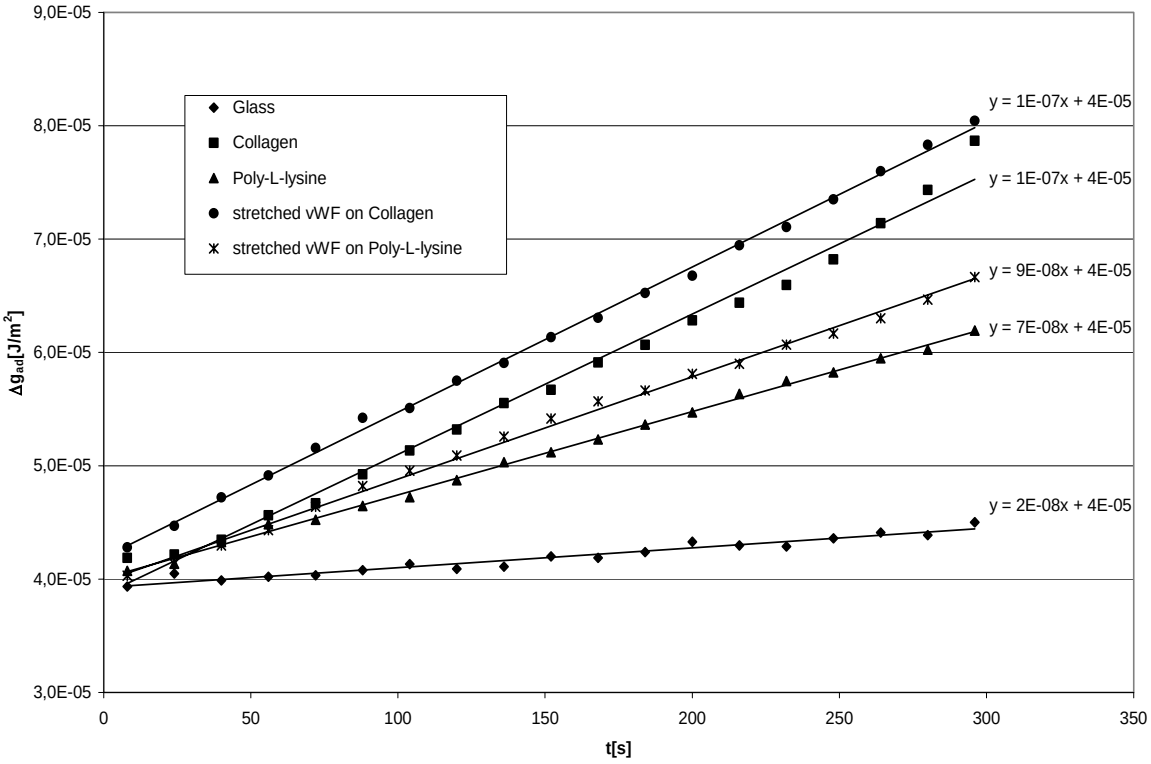

c)

Surfaces	**Free adhesion energy [J/m^2]**	**Slope**
Glass	4.5027E-05	2.00E-08
Collagen	7.8682E-05	1.00E-07
poly-L-lysine	6.1923E-05	7.00E-08
vWF stretched on collagen	8.0430E-05	1.00E-07
vWF stretched on poly-L-lysine	6.6657E-05	9.00E-08

Fig 4: a) Free adhesion energies were quantified for melanoma cell adhesion to glass, collagen, poly-L-lysine, unfolded VWF on collagen substrate and poly-L-lysine substrate after a 5 min adhesion process. Each column represents the mean (5 cells) $\pm$ SEM (vertical bar). b) The rate of adhesion of the five substrates was measured by taking the slopes of the free adhesion energies of melanoma cells from the initial cell contact till 5 min. The collagen coated substrate and the unfolded VWF on collagen substrate yielded the highest adhesion energy of melanoma cells. c) Table summarizing free adhesion energy and rate of adhesion (slope).

Since collagen and collagen + VWF coated surfaces adhered most strongly to the melanoma cells, the specificity of VWF binding to melanoma cells remains in question. Therefore another protein, poly-l-lysine, was chosen as substrate to immobilize VWF. Poly-l-lysine is a polycationic polymer which bears a net positive charge and has been previously used to attach cells for cell culturing purposes, as well as a drug delivery vehicle. As the overall charge of VWF is negative, VWF was able to attach effectively through an electrostatic interaction to poly-l-lysine with and without an applied shear. The unfolded VWF shows a greater adhesion of melanoma cells compared to poly-L-lysine alone, thereby confirming our expectations of a specific interaction. A common pattern observed is less adhesion of melanoma cells to the globular clusters of VWF identified on both poly-L-lysine and collagen coated surfaces (Fig. 5a). Another possibility is when VWF is in its coiled conformation less binding domains are exposed, so the rate of melanoma cell adhesion is lessened compared to its stretched conformation.

Adhesion energies of unfolded and folded vWF on poly-L-lysine and collagen coated substrates.

a)

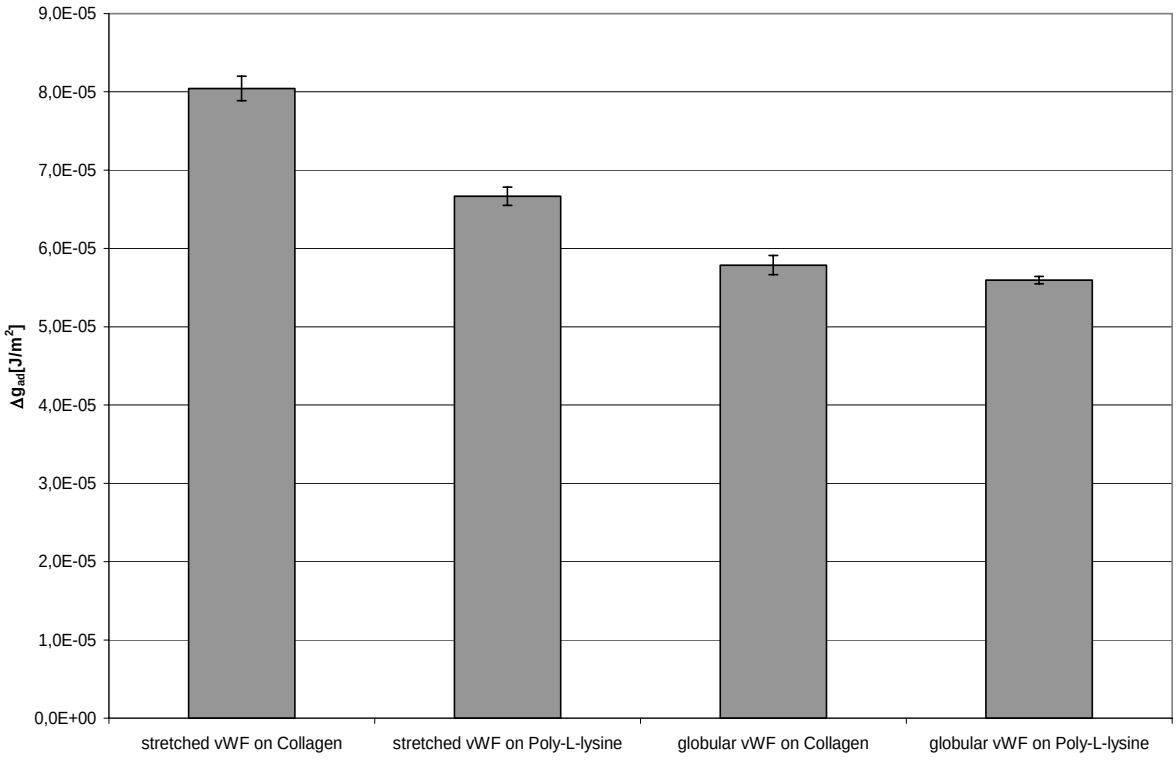

b)

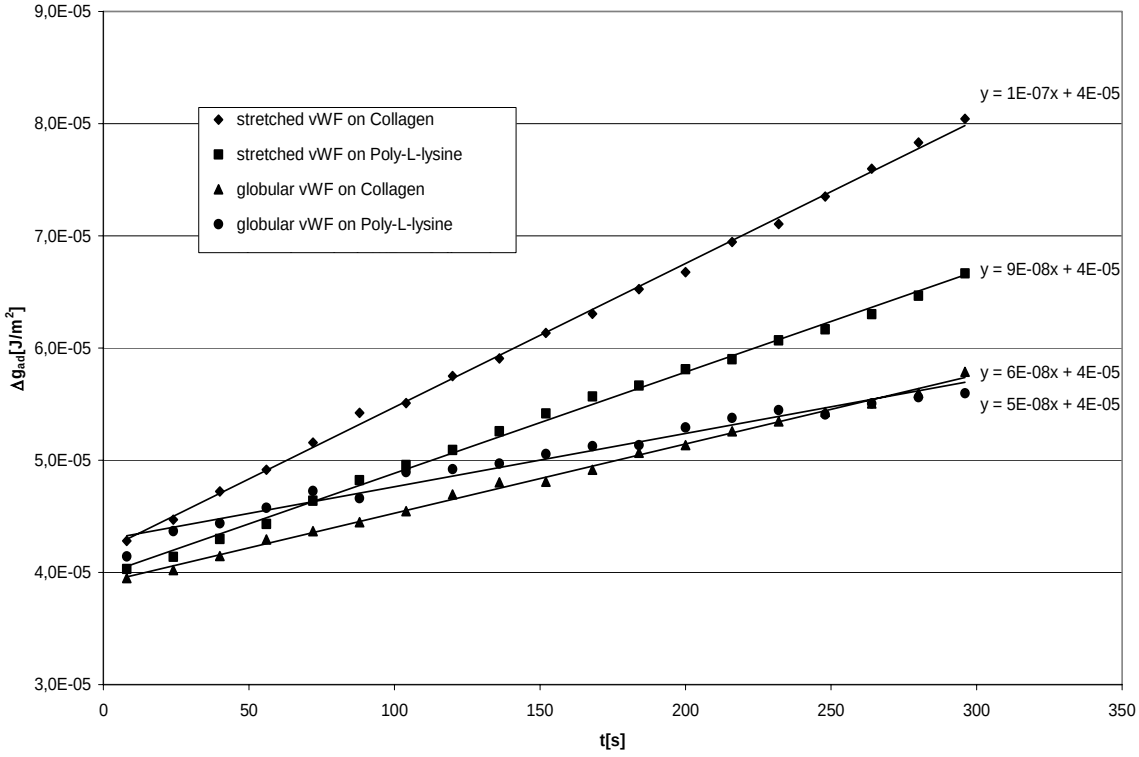

c)

Surfaces	**Free adhesion energy [J/m^2]**	**Slope**
vWF stretched on collagen	8.0430E-05	1.00E-07
vWF stretched on poly-L-lysine	6.6657E-05	9.00E-08
vWF glob on collagen	5.7878E-05	6.00E-08
vWF glob on poly-L-lysine	5.5957E-05	5.00E-08

Fig 5: a) The augmentation of VWF after an applied shear flow enhances melanoma cell adhesion compared to the native globular conformation on both collagen and poly-L-lysine substrates shown by bar graphs. b) Compared to unfolded VWF, the rate of adhesion of melanoma cells is significantly decreased in case of globular VWF. c) Summary of the free adhesion energy and the rate of adhesion of melanoma cell adhesion to the unfolded vWF and globular VWF.

7.3.3 Blockage roles of VWF Antibody in the adhesion of Melanoma Cells to VWF

To ascertain whether there are specific binding events of melanoma cells to unfolded VWF, the von Willebrand Factor antibody was applied to block the activity of VWF. The VWF antibody is targeted against the full-length sequence of the protein to fully inactivate the adhesive potential of VWF. Our results show a decrease in the adhesion energies of melanoma cells which were measured on both poly-L-lysine and collagen coated substrates, suggesting that specific receptors expressed on melanoma cells could play a role in adhesion. The free adhesion energy of VWF stretched on a poly-L-lysine substrate was reduced from $6.67 \cdot 10^{-5}\,J/m^2$ to $5.35 \cdot 10^{-5}\,J/m^2$ once the antibody was added. On a collagen coated substrate, the adhesion energy of the unfolded VWF was inhibited from $8.04 \cdot 10^{-5}\,J/m^2$ to $6.4 \cdot 10^{-5}\,J/m^2$ (Fig. 6a).

Surprisingly, there was no change in the adhesion energies when the VWF antibody was applied to the globular VWF (data not shown). A possible explanation could be that the antibody works effectively when the proteins are stretched which expresses more binding regions to the antibody compared to the globular conformation. Almost no melanoma cells adhered strongly to the stretched VWF substrate after pre-treatment with the VWF antibody as shown by the decrease in melanoma cell adhesion rates (Fig. 6b).

Adhesion energies of unfolded VWF on poly-L-lysine and collagen substrate blocked with VWF antibody

a)

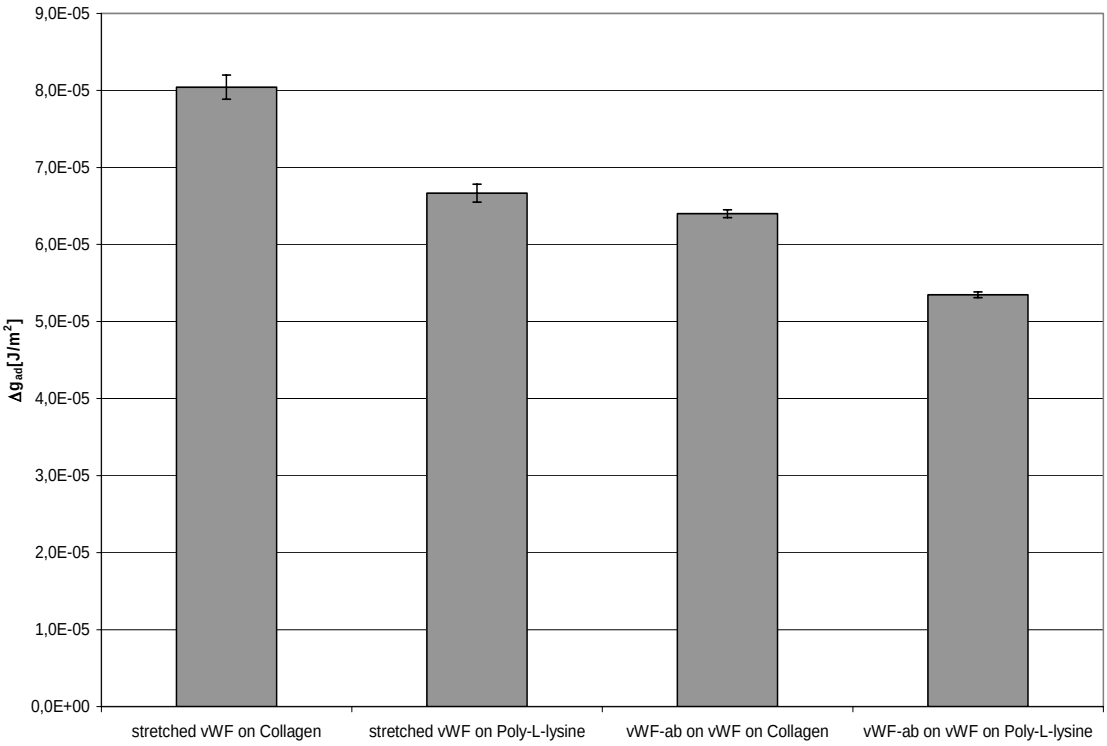

b)

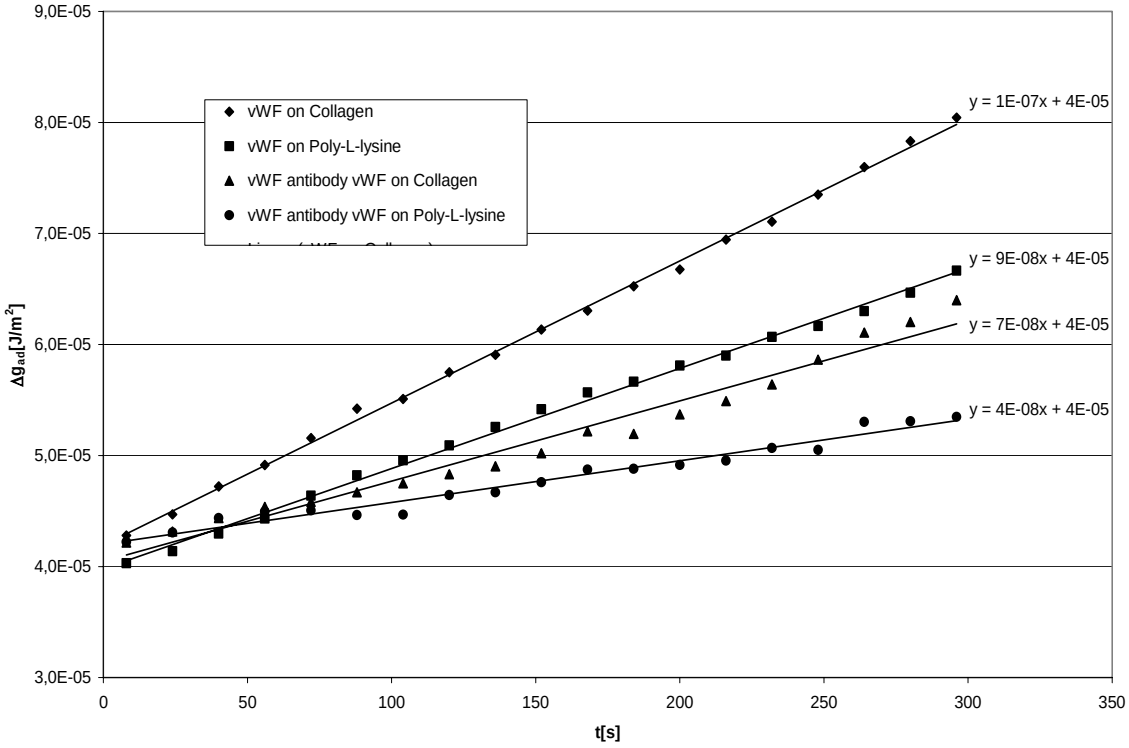

c)

Surfaces	**Free adhesion energy [J/m^2]**	**Slope**
Collagen	7.8682E-05	1.00E-07
poly-L-lysine	6.1923E-05	7.00E-08
vWF ab on vWF on collagen	6.4005E-05	7.00E-08
vWF ab on vWF on poly-L-lysine	5.3476E-05	4.00E-08

Fig 6: a) Bar graph showing an inhibition of melanoma cell adhesion with VWF antibody applied to an unfolded VWF on collagen and poly-L-lysine substrate. b) Decrease in melanoma cell adhesion rates once the antibody is applied to block the activity of vWF. c) Table summarizing the free adhesion energy and the rate of adhesion (slope) once the vWF antibody is applied to unfolded VWF.

7.3.4 Role of Integrins in Melanoma Cell Adhesion to VWF

As noted before, the most expressed receptors on melanoma cells are integrins. The relevant integrin in melanoma cell arrest and adhesion is the $\alpha_v\beta_3$. The $\alpha_v\beta_3$ has been implicated in binding to fibronectin, von Willebrand factor, and collagen. Both fibronectin, and collagen which are extracellular matrix proteins of the blood vessel play a dual role in which fibronectin connects cells to collagen fibers to allow cells to move through the extracellular matrix. However, the promiscuity of the integrins which play multiple roles in melanoma cell adhesion and migration has not been clearly elucidated. In these set of studies, the importance of the integrin $\alpha_v\beta_3$ and its role in the adhesion process of melanoma cells was examined.

To show that integrin $\alpha_v\beta_3$ plays a role in melanoma cell adhesion, we obtained the antibody to integrin $\alpha_v\beta_3$ to block the activity of the receptor. The melanoma cells were blocked with anti-integrin $\alpha_v\beta_3$, the adhesion energies were measured on stretched VWF on collagen and a poly-L-lysine coated substrate. There was a similar decrease in the adhesion energy values of melanoma cell interaction to VWF on both surfaces. The value of the free adhesion energy for melanoma cells incubated with integrin antibody on unfolded VWF surface coated with poly-L-lysine was $5.18 \cdot 10^{-5}\,J/m^2$, compared to $5.11 \cdot 10^{-5}\,J/m^2$ of stretched VWF on a collagen coated surface. The free adhesion energy of melanoma cells incubated with integrin antibody on surfaces coated with only poly-L-lysine was $6.24 \cdot 10^{-5}\,J/m^2$ compared to a decrease in free adhesion energy of melanoma cells on a collagen coated substrate to $5.211 \cdot 10^{-5}\,J/m^2$ (Fig.7a). This suggests that a common binding domain for integrins on collagen and VWF substrate initiates a strong surface adhesion of melanoma cells. The blockage of melanoma cell adhesion by antibodies directed against VWF and integrin $\alpha_v\beta_3$ clearly results in a decrease in the adhesion energies. The antibodies serve as a repeller molecule to the melanoma cell-VWF interaction. This confirms our theory that specific interactions are necessary to achieve maximum adhesion of melanoma cells to VWF.

a)

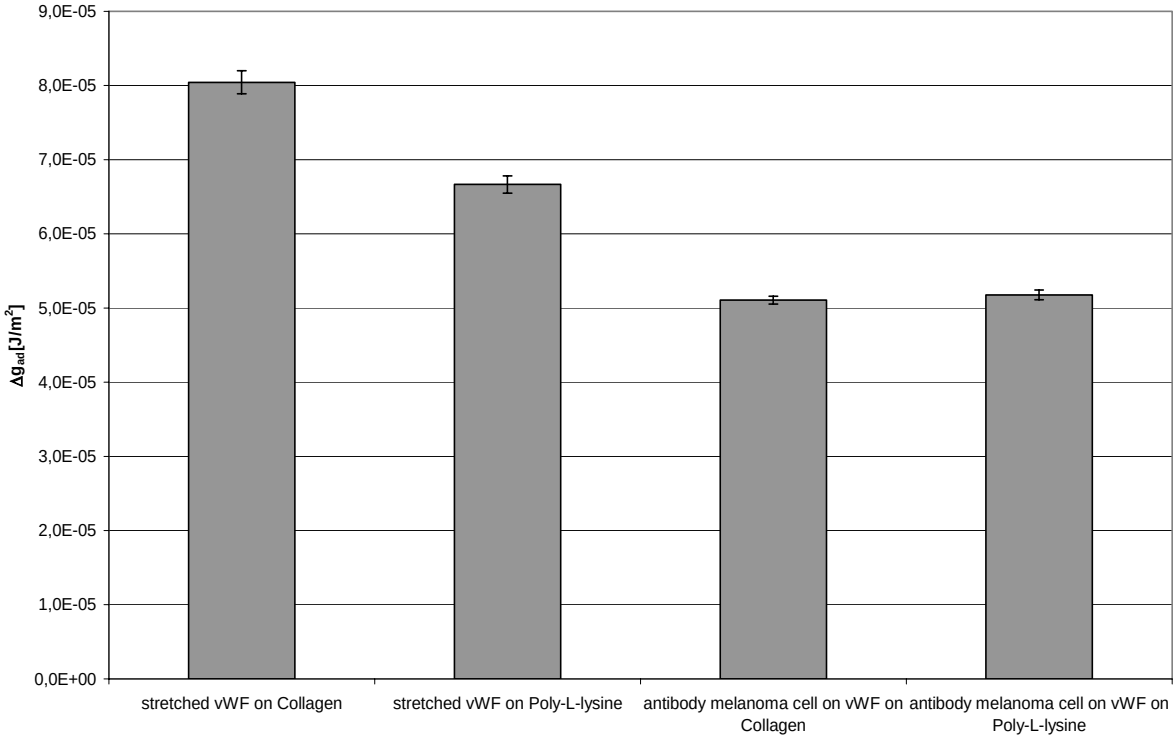
9,0E-05
8,0E-05
7,0E-05
6,0E-05
5,0E-05
4,0E-05
3,0E-05
2,0E-05
1,0E-05
0,0E+00
Δg_ad [J/m²]
stretched vWF on Collagen
stretched vWF on Poly-L-lysine
antibody melanoma cell on vWF on Collagen
antibody melanoma cell on vWF on Poly-L-lysine

b)

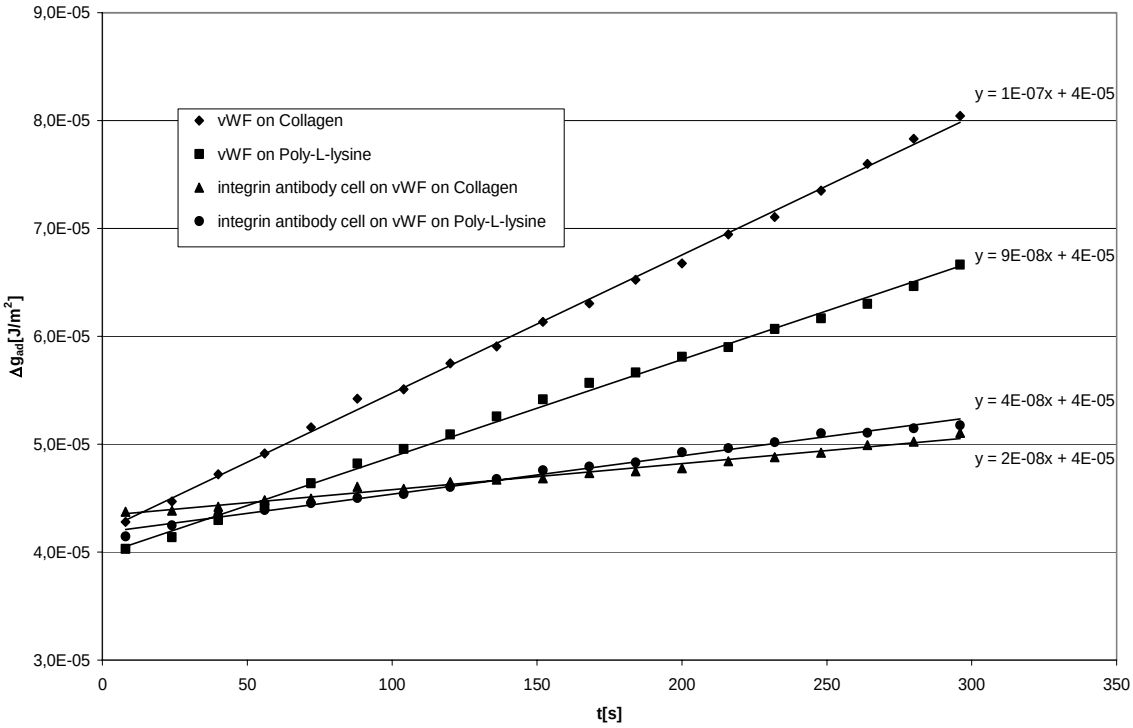

c)

Surfaces	**Free adhesion energy [J/m^2]**	**Slope**
collagen	7.8682E-05	1.00E-07
poly-L-lysine	6.1923E-05	7.00E-08
antibody melanoma cell on vWF collagen	5.1063E-05	2.00E-08
antibody melanoma cell on vWF poly-L-lysine	5.1770E-05	4.00E-08

Fig 7: a) Bar graph showing an inhibition of melanoma cell adhesion to unfolded vWF on a collagen and poly-L-lysine substrate once the integrin $\alpha_v\beta_3$ antibody is applied to the melanoma cells. b) Decrease in the rate of melanoma cell adhesion once the integrin $\alpha_v\beta_3$ is applied. c) Table summarizing free adhesion energy and rates of adhesion.

7.4 Summary

The unique combination of SAW and micropipette aspiration enables us to quantify the conformational changes to VWF under a defined shear flow (1000 s^{-1}), which enhances melanoma cell adhesion as directly analyzed. Under static conditions, the unfolded state or globular VWF shows less adhesion, due to a combination of entropic repulsion effects and a lack of binding domains. Once VWF is stretched after an applied shear it presumably results in the exposure of the secondary structure of VWF, which is involved in the binding mechanisms of blood platelets. We show that binding domains to integrins enhances melanoma cell adhesion under hydrodynamic flow, however collagen which immobilizes VWF to maintain the stretched conformation can also bind to melanoma cells. To show the specificity of VWF binding to melanoma cell a poly-l-lysine substrate was utilized. An increase in adhesion energy to the unfolded VWF confirms our theory that specific interactions can promote melanoma adhesion. The amount of receptors on the melanoma cells and the amount of binding domains of the stretched VWF initiates the spreading rate (deformation), in our analysis the spreading rate depends on these parameters. A rapid spreading rate of melanoma cells to VWF that is initiated by integrins is observed, which through some complex signaling events rearranges actin fibers within the melanoma cells to deform or flatten the plasma membrane to avoid detachment within the blood vessel.

Concluding Remaks and Recommendations

Through this research we have demonstrated the applicability of SAW to mix and pump fluids in microfabricated systems. It has been proven that SAW can be utilized as a multifaceted tool (micropump or micromixer) in microfluidic systems. Using different photolithographic techniques, we can effectively create a 3-dimensional to 2 dimensional channel design which is incorporated into our SAW chip to form a hybrid system such as a SAW based flow chamber or micromixer. In this thesis we discuss the successful employment of our SAW driven microfluidic system to analyze the following:

- To expedite the mixing process of two fluid streams in microchannels by applying SAW
- The usage of a thermoresponsive polymer, to create synthetic microvalves in microchannels with the aid of a heating unit and SAW as a nanopump. A convenient method to pump and mix fluids without cumbersome geometries or pumps.
- Using our SAW driven microfluidic system, we are able to analyze a mechanically activated protein called von Willebrand Factor (VWF). As VWF changes its conformation from a coiled to stretch configuration when a critical shear (1000 s^{-1}) is applied. Once VWF is stretched it becomes an adhesive protein to bind tumor cell (melanoma) adhesion within our blood vessel.
- We have also optimized the velocity measurements of particles based on Fourier analysis detection on a SAW based microfluidic chip.
- The combination of SAW and micropipette aspiration is utilized to quantify the adhesive potential of melanoma cells to VWF as it undergoes conformational changes after an applied shear.

Our SAW driven microfluidc system in conjunction with video microscopy allows us to capture the dynamic effects of microfluidics such as micromixing, analyzing blood flow, tumor cell adhesion and viscosity. The use of photolithography for micro and

nano structuring of channels can enable us to understand the physics of flow in low Reynolds numbers as a helpful tool for biological and chemical applications.

Impact of SAW In Microfluidics

The development of the SAW based microfluidic systems has enabled us to analyze biological and chemical material using low volumes. The performance of SAW in a variety of microfluidic applications serves as a breakthrough in some of the complex issues in microfluidics such as mixing and pumping of fluids. Some of the several challenges of scientists working in the field of lab on a chip technology or microfluidics are to find ways to optimize these conditions. For our applications we present a unique combination of solid state physics and microfluidics to enable us to significantly progress in these fields. By incorporating a SAW based system, we have established a motor that can be used for a variety of applications in the fields of microfluidics and lab on a chip technology.

References

1. Alberts B, Bray D, Lewis J, Raff M, Roberts K, Watson JD (1994) Molecular Biology of The Cell. Garland Publishing, Inc., New York & London
2. Alexander-Katz A, Schneider MF, Schneider SW, Wixforth A, Netz RR (2006) Shear-flow-induced unfolding of polymeric globules. Physical Review Letters 97:138101/138101-138104
3. Barakat AI (1999) Responsiveness of vascular endothelium to shear stress: potential role of ion channels and cellular cytoskeleton (review). Int J Mol Med 4:323-332
4. Barg A, Ossig R, Goerge T, Schneider MF, Schillers H, Oberleithner H, Schneider SW (2006) Soluble plasma-derived von Willebrand factor assembles to a hemostatically active filamentous network. Thrombosis and Haemostasis 97:501-684
5. Beebe D, Mensing G, GM W (2002) Physics and Applications of Microfluidics in Biology. Annu Rev Biomed Eng 4:261-286
6. Bernardo A, Ball C, Nolasco L, Moake JF, Dong JF (2004) Effects of inflammatory cytokines on the release and cleavage of the endothelial cell-derived ultralarge von Willebrand factor multimers under flow. Blood 104:100-106. Epub 2004 Mar 2016.
7. Bongrand P (1988) Physical Basis of Cell-Cell Adhesion. CRC Press, Boca Raton, FL
8. Brizard M, Megaharfi M, Verdier C (2005) Absolute falling-ball viscometer evaluation of measuremnt uncertainty. Metrologia 42:298-303
9. Chandaroy P, Sen A, Hui SW (2001) Temperature-controlled content release from liposomes encapsulating Pluronic F127. J Control Release 76:27-37
10. Cheresh DA (1987) Human endothelial cells synthesize and express an Arg-Gly-Asp-directed adhesion receptor involved in attachment to fibrinogen and von Willebrand factor. Proc Natl Acad Sci U S A 84:6471-6475.
11. Dong JF (2005) Cleavage of ultra-large von Willebrand factor by ADAMTS-13 under flow conditions. J Thromb Haemost 3:1710-1716.
12. Eijkel J, Kwok Y, Manz A (2001) Wavelet transform foe Shah convolution velocity measurements of single particles and solutes in a microfluidic chip. Lab on a Chip 1:122-126

13. England JL (2004) Stabilization and Release Effects of Pluronic F127 in Protein Drug Delivery. Journal of Undergraduate Sciences:Biochemistry 5:17-24
14. Erickson D, Dongquing l (2004) Integrated microfluidic devices. Analytica Chimica Acta 507:11-26
15. Frommelt T (January 2007) Mischen and Sortieren mit SAW-Fluidik in Simulation und Experiment. PhD Thesis
16. Giavazzi R, Foppolo M, Dossi R, Remuzzi A (1993) Rolling and adhesion of human tumor cells on vascular endothelium under physiological flow conditions. J Clin Invest 92:3038-3044
17. Goerge T, Barg A, Schnaeker EM, Poppelmann B, Shpacovitch V, Rattenholl A, Maaser C, Luger TA, Steinhoff M, Schneider SW (2006) Tumor-derived matrix metalloproteinase-1 targets endothelial proteinase-activated receptor 1 promoting endothelial cell activation. Cancer Res 66:7766-7774
18. Goerge T, Kleinerüschkamp F, Barg A, Schnaecker E, Huck V, Schneider MF, Steinhoff M, Schneider SW (2007) Microfluidic reveals generation of platelet-strings on tumoractivated endothelium. Thrombosis and Haemostasis 98:283-286
19. Goerge T, Kleineruschkamp F, Barg A, Schnaeker EM, Huck V, Schneider MF, Steinhoff M, Schneider SW (2007) Microfluidic reveals generation of platelet-strings on tumor-activated endothelium. Thromb Haemost 98:283-286
20. Gonnenwein S (2003) Generic and Specific Cell Adhesion: Investigations of a Model System by Micro-Interferometry. PhD Thesis
21. Gravesen P, Branebjug J, Jenson O (1993) Microfluidics-a review. J Micromech Microeng 3:168-182
22. Guttenberg Z, Muller H, Habermuller H, Geisbauer A, Pipper J, Felbel J, Kielpinski M, Scriba J, Wixforth A (2005) Planar chip device for PCR and hybridization with surface acoustic wave pump. Lab Chip 5:308-317. Epub 2004 Dec 2016.
23. Guttenberg Z, Rathgeber A, Keller S, Radler JO, Wixforth A, Kostur M, Schindler M, Talkner P (2004) Flow profiling of a surface-acoustic-wave nanopump. Phys Rev E Stat Nonlin Soft Matter Phys 70:056311. Epub 052004 Nov 056323.
24. Haass NK, Smalley KS, Li L, Herlyn M (2005) Adhesion, migration and communication in melanocytes and melanoma. Pigment Cell Res 18:150-159

25. Haier J, Nicolson GL (2000) Tumor cell adhesion of human colon carcinoma cells with different metastatic properties to extracellular matrix under dynamic conditions of laminar flow. J Cancer Res Clin Oncol 126:699-706
26. Haier J, Nicolson GL (2001) Tumor cell adhesion under hydrodynamic conditions of fluid flow. Apmis 109:241-262.
27. Hochmuth RM (2000) Micropipette aspiration of living cells. J Biomech 33:15-22
28. Holden MA, Cremer PS (2005) Microfluidic tools for studying the specific binding, adsorption, and displacement of proteins at interfaces. Annu Rev Phys Chem 56:369-387
29. Kasemo B (2002) Biological surface science. Surface Science 500:656-677
30. Knight JB, Vishwanath A, Brody JP, Austin RH (1998) Hydrodynamic Focusing on a Silicon Chip: Mixing Nanoliters in Microseconds. Physical Review Letters 80:3863
31. Kwok Y, NT J, A M (2001) Velocity Measurement of Particles Flowing in a Microfluidic Chip Using Shah Convolution Fourier Transform Detection. Anal Chem 73:1748-1753
32. Ludwig T, Ossig R, Graessel S, Wilhelmi M, Oberleithner H, Schneider SW (2002) The electrical resistance breakdown assay determines the role of proteinases in tumor cell invasion. Am J Physiol Renal Physiol 283:F319-327.
33. Luo CP (2004) Detection of Antibody-Antigen Reactions using Surface Acoustic Wave and Electrochemical Immunosensors. PhD Thesis:1-131
34. Menter DG, Fitzgerald L, Patton JT, McIntire LV, Nicolson GL (1995) Human melanoma integrins contribute to arrest and stabilization potential while flowing over extracellular matrix. Immunol Cell Biol 73:575-583
35. Neumaier T (2006) Mechanical Forces of Cell Adhesion-Physical Perspective of Cell Adhesion. Diplomarbeit
36. Nianzhen L, Tourovskaia A, Folch A (2003) Biology on a Chip: Microfabrication for Studying the Behaviour of Cultured Cells. Critical Reviews in Biomedical Engineering 31(5&6):423-488
37. Nuygen N, Wu Z (2005) Micromixers-a review. Journal of micromechanicsmicroengineering 15:R1-R16
38. Nyborg W (1965) Acoustic Streaming. Academic press Inc, New York

39. Pilch J, Habermann R, Felding-Habermann B (2002) Unique ability of integrin alpha(v)beta 3 to support tumor cell arrest under dynamic flow conditions. J Biol Chem 277:21930-21938
40. Reyes D.R, Lossifidis D, Auroux P-A, Manz A (2002) Micro-Total Analysis Systems.1. Introduction,Theory and Technology. Analytical Chemistry 74:2623-2636
41. Ruggeri ZM (1997) von Willebrand factor. J Clin Invest 99:559-564.
42. Ruggeri ZM (2003) Von Willebrand factor, platelets and endothelial cell interactions. J Thromb Haemost 1:1335-1342.
43. Sackmann E, Bruinsma RF (2002) Cell adhesion as wetting transition? Chemphyschem 3:262-269
44. Sadler JE (2005) von Willebrand factor: two sides of a coin. J Thromb Haemost 3:1702-1709.
45. Schneider SW, Nuschele S, Wixforth A, Gorzelanny C, Alexander-Katz A, Netz RR, Schneider MF (2007) Shear-induced unfolding triggers adhesion of von Willebrand factor fibers. Proc Natl Acad Sci U S A 104:7899-7903
46. Shankaran H, Alexandridis P, Neelamegham S (2003) Aspects of hydrodynamic shear regulating shear-induced platelet activation and self-association of von Willebrand factor in suspension. Blood 101:2637-2645. Epub 2002 Nov 2627.
47. Sia SK, Whitesides GM (2003) Microfluidic devices fabricated in poly(dimethylsiloxane) for biological studies. Electrophoresis 24:3563-3576
48. Springer TA (1995) Traffic signals on endothelium for lymphocyte recirculation and leukocyte emigration. Annu Rev Physiol 57:827-872.
49. Squires Todd M, Quake S. R (2005) Microfluidics:Fluid physics at the nanometer scale. Review of Modern Physics 77:977-1022
50. Sritharan K, Strobl CJ, Schneider MF, Wixforth A, Guttenberg Z (2006) Acoustic mixing at low Reynold's numbers. Applied Physics Letters 88:054102
51. Stoeber B, Liepmann D, Muller SJ (2005) A Planar 2-Stage Micromixer. Digest of Technical Papers of Transducers'05, the 13th International Conference on Solid State Sensors, Actuators and Microsystems, Seoul, Korea, June 5-9,2005:368-371
52. Strobel CJ (Marz 2005) Mikro-und Nanofluidik auf piezoelektrischen Substratum. PhD Thesis

53. Takayama S, Mcdonald JC, Ostuni E, Liang MN, Kenis PJA, F.Ismagilov R, Whitesides GM (1999) Patterning cells and their environment using multiple laminar flows in capillary networks. PNAS 96:5545-5548
54. Tegenfeldt JO, Prinz C, Cao H, Huang RL, Austin RH, Chou SY, Cox EC, Sturm JC (2004) Micro-and nanofluidics for DNA analysis. Anal Bioanal Chem 378:1678-1692
55. Terraube V, Pendu R, Baruch D, Gebbink MF, Meyer D, Lenting PJ, Denis CV (2006) Increased metastatic potential of tumor cells in von Willebrand factor-deficient mice. J Thromb Haemost 4:519-526
56. Uchida T, Suzuki T, Shiokawa S (1995) Investigation of acoustic streaming excited by surface acousticwaves. IEEE ULTRASONICS SYMPOSIUM 2:1081
57. Wixforth A (2006) Acoustically Driven Programmable Microfluidics for Biological and Chemical Applications. Journal of the Association for Laboratory Automation 11:399
58. Wixforth A, Strobl C, Gauer C, Toegl A, Scriba J, v Guttenberg Z (2004) Acoustic manipulation of small droplets. Anal Bioanal Chem 379:982-991. Epub 2004 Jul 2015.
59. Wurtsel C (2006) Quantisierter akustoelektrischer Strom durch Kohlenstoffnanorohren. PhD Thesis
60. Xiong X, Tam K, Gan L (2005) Synthesis and thermal responsiveness properties of P(LA-b-EO-b-PO-b-EO-b-LA) block coploymers with short hydrophobic poly(lactic acid) (PLA) segemnts. Polymer 46:1841-1850
61. Zhu C (2000) Kinetics and mechanics of cell adhesion. Journal of Biomechanics 33:23-33
62. Zhu C, Bao G, Wang N (2000) Cell Mechanics: Mechanical Response, Cell Adhesion, and Moleucular Deformation. Ann Rev Biomed Eng 2:189-226

Appendix A

Microscopy

The phase contrast microscopy that is used for visualising cella relies on the evaluation of the diffraction pattern of the rear objective focal plane. The illuminant is imaged by a collector on a ring aperture in the front condenser focal plane. Every beam passing the ring aperture is a parallel light beam which then passes the objective plane. As a result, the characteristic Frauenhofer diffraction pattern occurs in the rear objective focal plane. There, the zero-order image is sharp and the images of higher orders are distributed over the whole plane. Moreover, it is also possible to exploit diffracted and non-diffracted beams for image generation. This is usually done by employing a circular phase-disc, the so called λ/4-disc (35).

Fluorescent microscopes (Zeiss Axiovert 200M) enable scientists to observe fluorescent samples. Fluorescence is the property of some atoms and molecules to absorb light of a particular wavelength and after a brief interval, to re-emit light at longer wavelengths. In our experiments, we made use of fluorescein (FITC) labeled microbeads (Sigma-Aldrich Co, St. Louis, MO) and Rhodamine labeled secondary antibodies (Invitrogen, Karlsruhe, Germany), whose excitation maximums were 490 nm and 542 nm and their emission maximums were 520 nm and 612 nm respectively. Due to their emission and adsorption behaviour fluorescent dyes such as rhodamine and fluorescent are employed for this kind of microscopy. During fluorescence, electrons are excited into a higher energetical state by the irradiation with light. They return into the ground state by emitting a photon; it usually has a lower frequency than the exciting photon. This leads to a red-shift of the outgoing light with respect to the incoming light, known as Stokes shift. It is the basis of fluorescent-microscopy. The Zeiss microscope is equipped with an Hg-vapour-lamp HBO 100 which provides light with several intensive spectral lines. For our samples stained with rhodamine, a beam splitter at 580nm and a blocking filter at 590nm were used.

The illumination radiation is filtered in order to achieve almost monochrome light. This short wavelength light is reflected to the objective by a dichroic mirror or a beam splitter. The Stokes-shifted fluorescent light, however, is almost completely transmitted. At the same time, the beam splitter filters the reflected excitation light from the sample. Consequently, the formation of a temporary image is not disturbed and an additional emission filter filters the remaining nonfluorescent light (Fig.1).

Recording movies during the experiments was done with a CCD camera which was controlled by the computer program “Open Box”. This program was also used for analysing the movies as well as the program ImageTool.

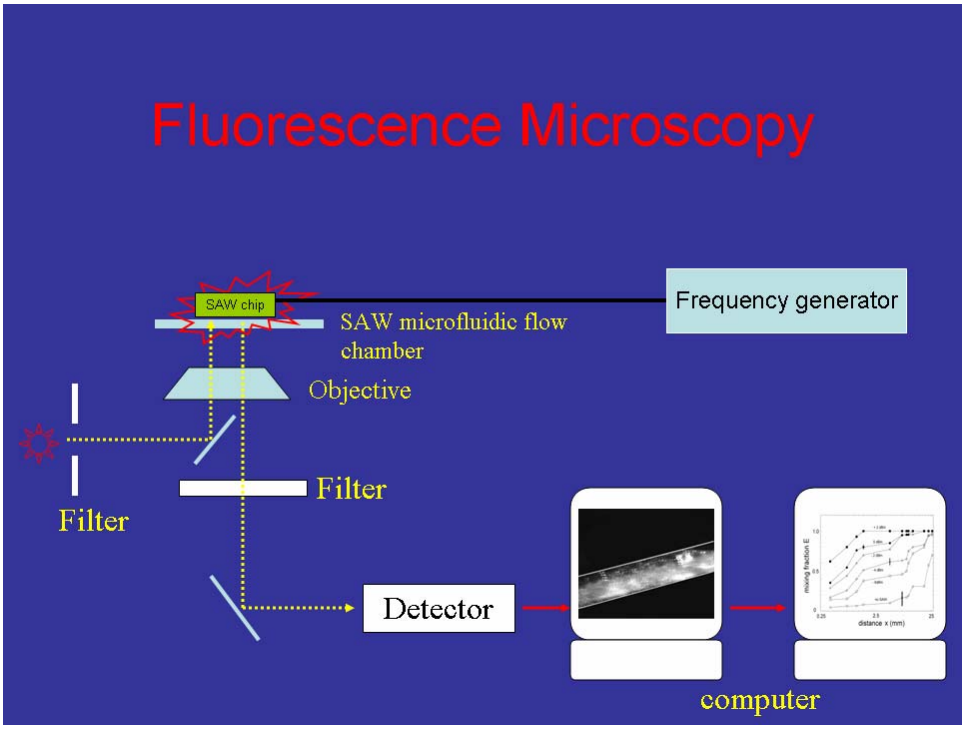

Fig 1: A schematic diagram showing the SAW microfluidic flow chamber connected to the fluorescent microscope stage. A CCD camera picks up the fluorescent signal to be viewed and analyzed by the computer.

Appendix B

Photolithography

The use of photolithography is an important technique for microfabricating structures on a chip surface which is utilized for lab on a chip or microfluidics technology.
Photolithography is the process of transferring geometric shapes on a mask to the surface of a silicon or piezoelectric wafer . The types of masks which are used are either transparencies made out of high resolution photographic film (3600 dpi) or opaque plates to allow light to pass through a defined pattern. For the microfluidic studies the use of photolithography is essential in designing a two dimensional channel or a three dimensional channel structures. An important step in the development of SAW chips is the deposition of the interdigital tranducers onto a piezoelectric substrate using photolithography. The typical steps involved in the photolithographic process are wafer cleaning; barrier layer formation; photoresist application; soft baking; mask alignment; exposure and development; and plasma etching.

Optical Lithography for manufacturing of SAW chips

Lithium Niobate Wafer Cleaning, and Photoresist Application

In the first step, the Lithium Niobate ($LiNbO_3$) wafer samples are chemically cleaned to remove particulate matter on the surface as well as any traces of organic, ionic, and metallic impurities. A layer of photoresist is applied to the wafer and a high-speed centrifugal spin coating at 5000rpm for about 30 sec to produce a thin uniform photoresist layer on the surface. The sample is kept at 80^0C for half an hour to remove the solvent from the photoresist. Soft-baking plays a very critical role in photoimaging, the photoresist coatings become photosensitive, or imageable, only after softbaking.
Once the mask has been accurately aligned with the pattern on the wafer's surface, the photoresist is exposed through the pattern on the mask with a single layer of ordered molecules adsorbed on the glass surface bonding between the surface and

molecular head groups photoilluminates the structure of the interdigital transducers onto the $LiNbO_3$ wafer. This creates a positive photoresist so the exposed structure gets washed away by the developer while rest of the resist remains.

Metallisation

The titan and gold layers were deposited onto the $LiNbO_3$ wafer substrate as conducting metarial. Titan, as binding substrate, was first deposited (20 nm) on to $LiNbO_3$ wafer followed by gold (200 nm) and another layer of titan is added to protect the deposited gold. In order to either construct channels on the chip or to couple glass microchannels, 100 nm of silicom monoxide was deposited onto the $LiNbO_3$ wafer.

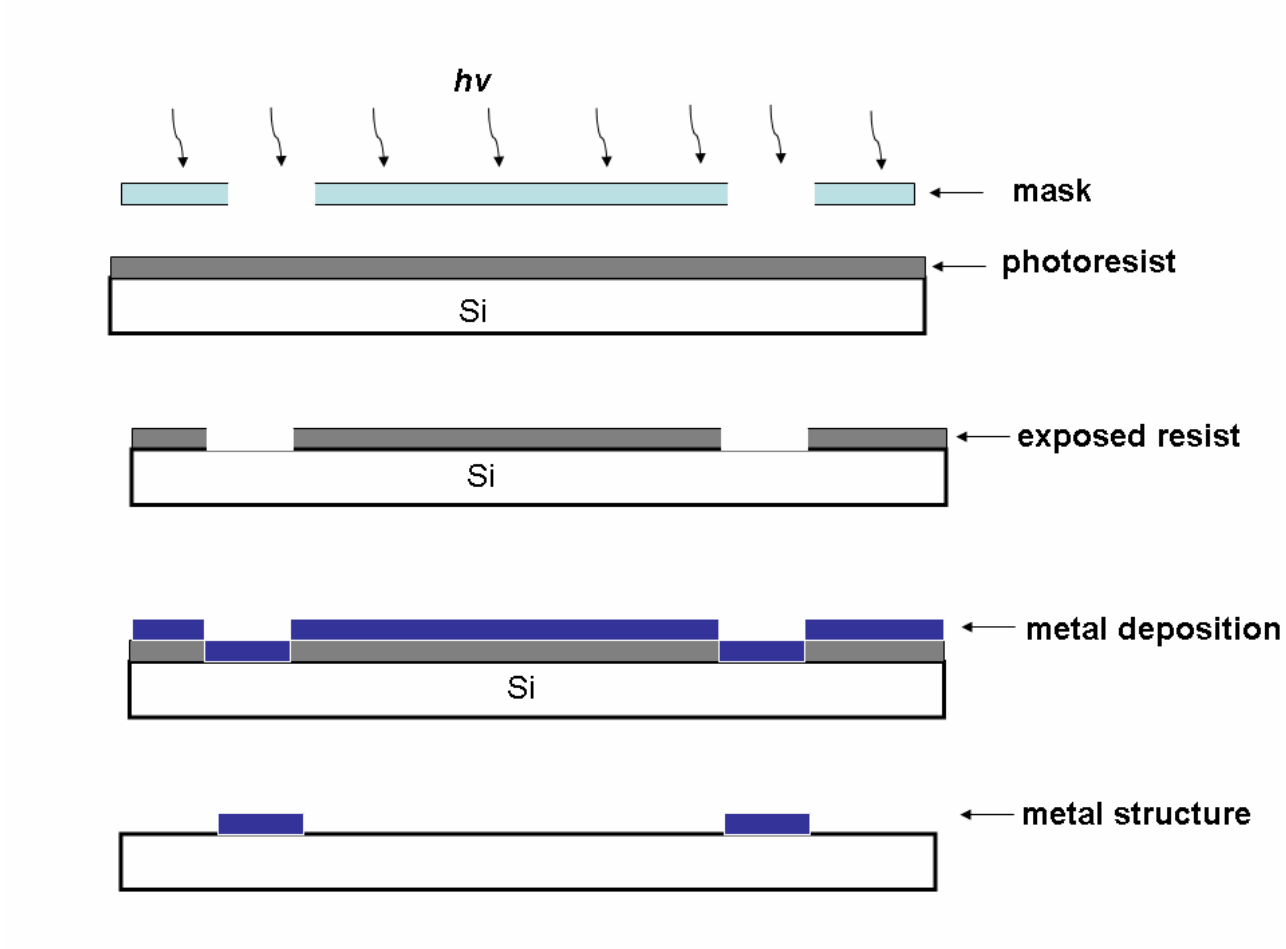

Fig 1:Schematics of photolithography sequence: (1). Etch a structure manifold on the substrate by using ultraviolet illumination 2) The developing process to take off the exposed photoresist. 3) Deposition of the metal layers. (4) Liftoff the non-attached metal layers so the etched deisgn stays intact.

Acknowledgements

I would like to thank Achim Wixforth for his encouragement and motivation to help me pursue this PhD. Along with his insight and discussions on all the topics covered in this thesis, especially in helping me to understand the physics of SAW.

Thomas Franke for his help and input into the pluronic, quantification of melanoma cell adhesion and Fourier analysis experiments. The fruitful discussions on these topics helped me with the analysis

Matthias Schneider and Stefan Schneider for their ideas on the biophysical and biochemical properties of melanoma cell adhesion to VWF. Matthias Schneider in his thoughts for the development of SAW microfluidic flow chamber for the analysis of VWF protein stretching, melanoma cell adhesion and quantification studies.

Thomas Frommelt for his discussions on microfluidics and helping me with the FEM lab simulations

Teresa Nuemaier for her help and analysis on the quantification of melanoma cell adhesion experiments

Daniel Steppich and Stefan Nuschele on their assistance with the melanoma cell adhesion to VWF studies.

The technical staff of EP1 for helping me with the technical assistance to pursue these studies

Curriculum Vitae

Personal information
Kumudesh Sritharan

Born in Colombo (Sri Lanka), 27th September 1967
U.S. citizen
Married, one child

Lilienthalstraße 20 86159 Augsburg
Telephone 0821 / 2093043
E-Mail: kumudeshs@hotmail.com

Education

University of Augsburg (Augsburg, Germany) since 2004
PhD Dissertation

University of New Haven (New Haven, Connecticut, USA) 09/1999–03/2003
MS Molecular and Cell Biology

University of New Haven (New Haven, Connecticut, USA) 09/1993–12/1996
BA Sociology/Biology

Work experience

Postgraduate research student since 7/2004
Experimental Physics 1
University of Augsburg (Augsburg, Germany)

Research Associate 05/1997–05/2004.
Department of Surgery (Gastroenterology)
Yale University (New Haven, Connecticut, USA)

Research Internship 09/1995-04/1997
Department of Surgery (Gastroenterology)
Yale University (New Haven, Connecticut, USA)